TECHNISCHE UNIVERSITÄT WIEN
Vienna University of Technology

DIPLOMARBEIT

Quantitative Bestimmung von Kräften auf den Nukleus während der Zellmigration

Quantitative evaluation of nucleus strains during confined cell migration

---

Ausgeführt am Institut für

Angewandte Physik

der Teschnischen Universität Wien

unter der Anleitung von Univ.Prof. Dipl.Ing. Dr.techn. Gerhard SCHÜTZ

durch

Solenne DEVRAUX (1327763)

17 cours Franklin Roosevelt, 69006 Lyon, FRANKREICH

Abstract

Cell migration in confined environments is a burning topic, since it is one of the main biological processes ruling embryo-genesis, cancer metastasis or an organism immune system. Based on a previously developed cell confined migration model and the observation of micro-channels experiments, we decided to focus on two main aspects during this thesis. First, the evidence that the nucleus was capable of breaking its lamina to pass through narrow sub-nuclear constrictions led us to reconsider the way it was defined: we decided to use two different rheological models for the lamina and the nucleoplasm. While the latter is modeled as a viscoelastic medium, the first is defined as a viscoelastoplastic medium. Indeed the introduction of plasticity in the lamina could account for its ability to break down. We tested this new model in a compression test and then implemented it in the previous confined migration model. During confined migration, we highlighted the rate-limiting role of the nucleus and the effect of plasticity on the model. Our confined migration model relied on an adhesion-based migration mode, while all the recent interest in cell migration through confined environments featured a compression-based migration mode in which the cell would not need to form any focal adhesions with the substrate. We thus decided to focus on improving our migration mode to describe this adhesion-free mode that mostly occurs during three-dimensional confined migration and is referred to as 'chimneying', since it mimics the behaviour of a rock climber in a chimney. During chimneying, the cell rear contraction triggers an increase in internal hydrostatic pressure, which then leads to the nucleation of a bleb – a herniation of the cell membrane – at the leading edge. When the bleb expands and touches the surface in which the cell is confined, it 'pushes' against it, creating a perpendicular force that acts as an anchor for the cell to move forward. The cycle repeats and the cell migrates. We developed a first simple and deterministic model in which the cell has frontal and rear blebs that cyclically expand and retract and that push on the walls of the micro-channel to migrate through it. In this model, we ensure the synchronization between adhesion forces and active strains. A second model kept the same motion cycle but introduced the notion of self-regulation. Indeed, the cell is given conditions, and depending on whether they are met or not, the cell governs the migration steps. Eventually, we began developing a model with a motion that more closely resembles how chimneying looks like in live cells, with the rear contraction governing the bleb expansion. The model presented here is still preliminary and will be improved in the future.

Acknowledgements

First and foremost, I would like to express my special appreciation and thanks to my thesis supervisors Professors Denis Aubry and Rachele Allena. They offered me a real opportunity to work and research in the very best conditions on such an interesting topic. Thank you for the clear and valuable advice you both gave me, for your patience with my many questions and for continuously pushing me to give my best. I would like to specifically thank you both for proof-reading this report. I also thank all the people from the MSSMAT laboratory, who offered me a very warm welcome and were always there to help me when I needed. I thank particularly the PhD and Post-Doctoral students who helped me blend in and with whom I spent a wonderful time.

Contents

1. General introduction

It might be hard to see what embryogenesis, tumor metastasis and wound healing have in common. Be that as it may, the underlying process of these three phenomena is the very same: the ability cells have to migrate. If cell migration might be observed in unicellular organisms, muticellular organisms are particular since the migration will often take place in a confined three-dimensional environment. Therefore, the cell needs to adapt to its surrounding and to develop strategies to migrate to the right place in order to perform its mission within the organism. This capacity is a crucial property of multicellular organisms to ensure their development and their homeostasis. Cell migration can indeed occur in response to various situations, such as a mere need to feed, or a stimulus that could be chemical or mechanical. These stimuli may originate from larger vital biological processes that govern the activity of the organism : morphogenesis of embryos, which requires cells to be able to migrate to a very specific and potentially distant location, or homeostasis of adult organisms. Therefore, a pathologically impaired cell migration can have disastrous effects on the development of the organism, resulting in birth defects, auto-immune syndrome, ineffective wound healing or tumor metastasis.

Depending on cell type, on its environment and on the force ratio between adhesion, contraction and actin-network polymerization, the cell can adopt various modes of migration and is able to rapidly switch from one to the other [Lämmermann and Sixt, 2009]. Migration can occur collectively as a group of cells moving to a specific location, or individually as an immune cell translocate to the inflammation site for instance. Rapid single cell crawling is usually referred to as 'amoeboid' migration. It regroups various cell and migration types that all have in common the cyclic protrusion and retraction of cellular extensions that lead to active cell deformation during the migration process.

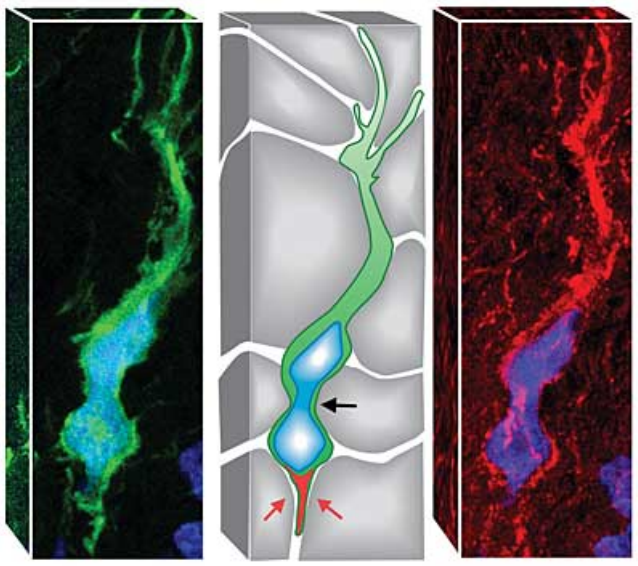

Figure 1.1: Glioma cells need a push from behind to invade the brain. This image of a transplanted human glioblastoma cell squeezing through rat brain cortex shows that cancer cells use special machinery (myosin II, labeled red in the right image) to migrate through the brain's tight spaces. The center image illustrates a model of how glioma cells migrate through brain tissue: First, the cell extends a long leading process followed by forward movement of the nucleus and cell body. To get the cell body through narrow points in the extracellular space, the nucleus deforms into an hourglass shape (black arrow). Actomyosin contraction at the rear (red arrows) generates force to push the cell forward. [Columbia University Medical Center, 2009]

Migration in healthy organisms

Migration takes place in healthy organisms during the development of the embryo and later on to assure homeostasis of the adult organism. During gastrulation – the morphogenetic movement that shapes the embryo – large groups of cells migrate to form embryonic layers. They then undergo a differentiation and can afterwards migrate to their final location where they experience final differentiation to form a limb or an organ. The embryonic cells hence need to translocate various times and to very specific locations to ensure the healthy development of the embryo. Some homeostatic processes in which cell migration plays a prominent role are wound healing and immune responses. Skin cells from the basal layer proliferate and migrate closer to the wound in order to close it. Other cells will migrate there and inflammatory signals will be emitted, triggering the recruitment of immune cells to combat the possible infection. Leukocytes will thus translocate through the blood vessel and the tissue to the wound healing site to perform their immune function. Some other cells, like macrophages, do the inverse process: they collect sample of the infectious agent and move to the lymph nodes to trigger the reaction of other immune cells.

Migration in diseased organisms

The migration process is so complex it can easily be deregulated and this can can have from trivial to much more serious consequences. If the deregulation occurs during embryo development, the aftermath might directly concern limb or organ formation, which could be fatal to the embryo. Defective migration in homeostasis would result in a delayed wound healing and possibly an incomplete immune response. Another major field of study for cell migration is tumor metastasis. Tumor cells have indeed defective mechanical properties that enhance cell motility and some cells can hence detach from the initial tumor and migrate much more easily – usually collectively – through the tissues and eventually blood vessels to form a new tumor. To migrate through tight spaces such as the brain, cancer cells, which have a decreased stiffness, can significantly squeeze and deform, as Fig 1.1 illustrates.

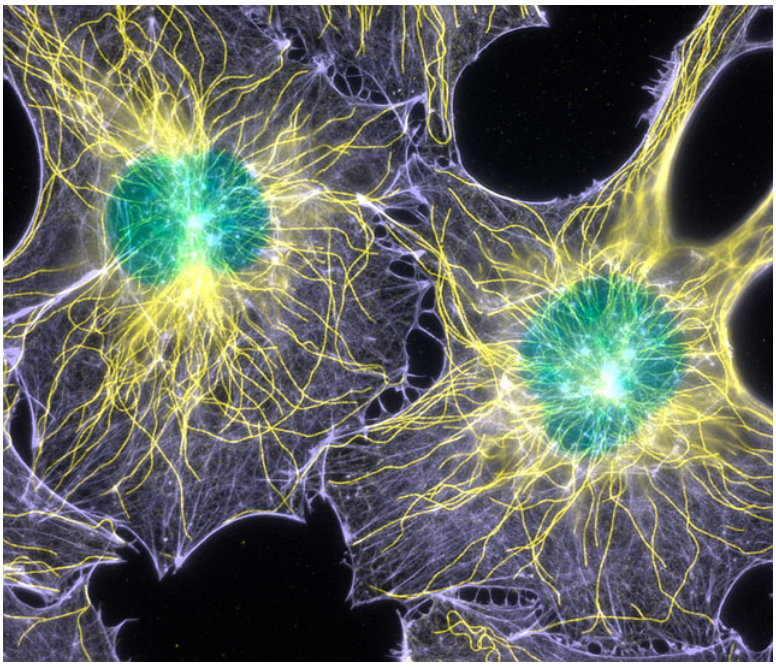

Figure 1.2: In this digitally colored picture of a mouse fibroblasts, actin filaments appear light purple, microtubules yellow, and nuclei greenish blue. By Dr. Torsten Wittmann, First place in 2003 Nikon Small World competition.

If the cell's environment is a major factor for migration, the cell's mechanical properties also play an essential role in this process. Indeed, the cell cytoskeleton, as well as its nucleus, contain different types of filaments which ensure a tight connexion with the environment but also between the cytoskeleton and the nucleus. Figure 1.2 wonderfully illustrates the complexity of the filament network inside cells. As the largest and stiffest organelle inside the cell, the nucleus appears to have a critical role in the migration process. Since it was found to be much stiffer than the surrounding cytoplasm, it is a rate-limiting factor that needs to be taken into account when studying migration.

The relevance of cell migration among vital biological processes and the use of mechanical modeling are the underlying ideas under this whole study, which comes as an extension of previous work[Allena and Aubry, 2012] [Allena, 2013] [Allena et al., 2013] [Aubry et al., 2014] [Allena, 2014]. Our research will first focus on the critical role of the nucleus that leads us to reconsider and refine its mechanical model to address the plasticity that can be observed during experiments. This refined model will first be tested during a compression test and then be implemented into the previously developed confined migration models. The second axis of our study is the improvement of the migration behaviour of the cell in confined environments through the implementation of a bleb-based migration mode, also referred to as "chimneying". The models presented here are based on mechanics of continuous media and are numerically approximated by Finite Elements Modeling (FEM).

2. Experimental data on cell migration and nuclear mechanics

This chapter presents experimental data that offer an insight into two topics of interest. First, cell migration will be reviewed, with the possible migrations strategies a cell may adopt depending on its environment. Then, we will focus on the cell nucleus and unravel its structural components and interactions with the cytoplasm that may play a part in its mechanical behaviour and thus during confined migration. Eventually, we introduce the experimental method for micro-channel assays, since we will try to reproduce such experiments of cell confined migration.

2.1 Cell migration

Amoeboid migration commonly refers to rapid cell crawling thanks to pseudopods, which comprises a wide range of biophysical modes of cell motility [Lämmermann and Sixt, 2009]. At one end of this spectrum, we find actin-polymerization-based gliding, which relies on the coupling of protrusion through actin-filaments polymerization and adhesion of the cell to the substrate [Hawkins et al., 2009] [Lämmermann and Sixt, 2009] [Wilson et al., 2013]. This mode of migration has been preferably studied in the past decades in comparison to blebbing motility, that can be found at the other end of the spectrum, in which the contraction of the actomyosin-network at the rear of the cell generates the formation of an actin-free bleb due to hydrostatic pressure. While actin-polymerization-based crawling requires adhesion and protrusion forces to move forward, blebbing motility is an adhesion-free locomotion mode, based on contraction forces [Lämmermann and Sixt, 2009] [Charras and Paluch, 2008].

2.1.1 Overview of the possible migration strategies

Although some cells display an exclusive mode of protrusion formation, some other cells are able to switch from actin-polymerization to blebbing protrusions and vice versa in response to properties of their environment [Paluch and Raz, 2013]. Three main forces that are at stake during migration have been proposed to control which mode of protrusion the cell may use: substrate adhesiveness, actomyosin contractility and actin polymerization. The equilibrium between these forces, that may evolve during migration, will determine which mode of migration the cell will adopt (see Figure 2.1). On two-dimensional (2D) surfaces, cell adhesion to the substrate is essential to ensure the transduction of internal contraction forces to the substrate, whereas cell migration in three-dimensional (3D) or confined environments does not necessarily require adhesions forces since the cell will be able to "push" perpendicularly to at least two surfaces, thus using them as fixation points.

2.1.1.1 2D migration

A first category of cells can use all three forces to generate movement. In Figure 2.1 (I), we see that the actin network will 'push' the membrane to the front while the rest of the cell undergoes a traction force which is myosin-II-generated and that is transduced to the substrate via the focal adhesions. On high adhesive surfaces, the cell needs rear contraction forces to detach the focal adhesions and allow the cell to glide forward, whereas on low adhesive surfaces, trailing edge contraction is not necessary. Figure 2.1 (II) illustrates the case in which myosin-II contraction is impaired: in that case, it was found that actin polymerization alone is capable of creating a traction force that is transduced through focal adhesions, and that enables migration. On the other hand, myosin-II contraction alone

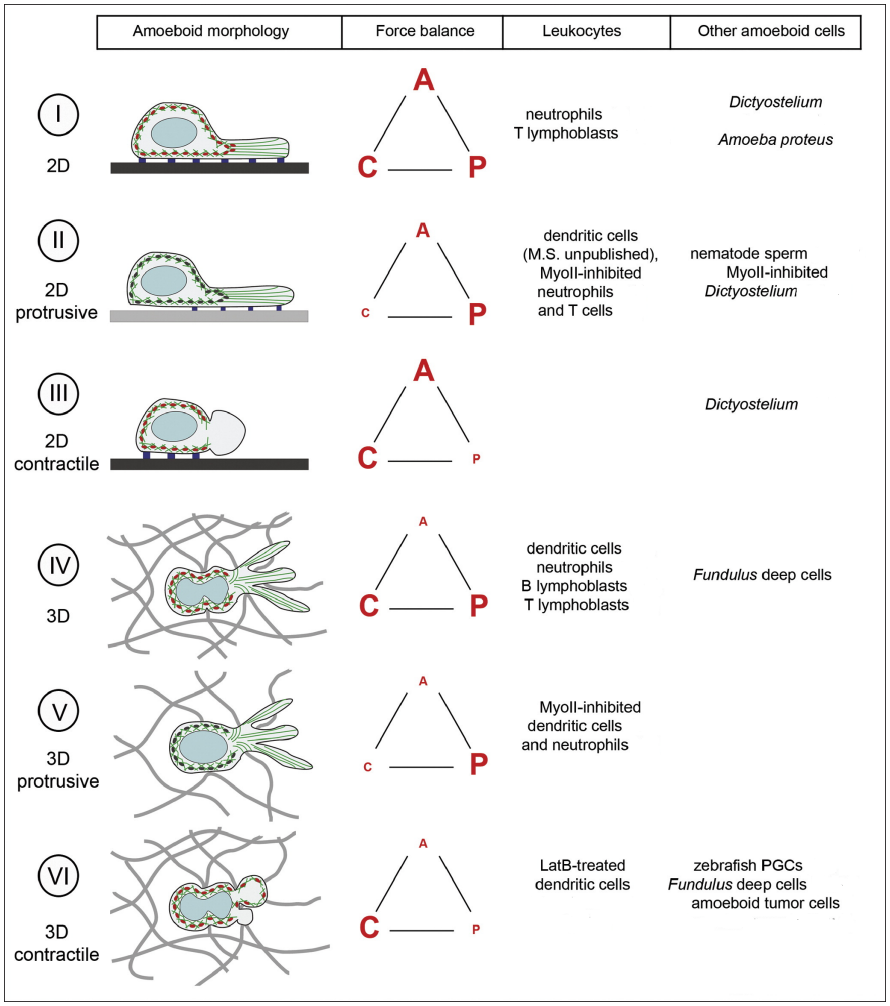

Figure 2.1: The force-relationship between adhesion, contraction and polymer-network expansion determines the 'amoeboid' phenotype. The three major forces in cell migration are adhesion (A), contraction (C) and polymer-network expansion (P). The color code is the following: actin filaments in green, Myosin-II as red ellipses (black ellipses if this function is impaired), adhesions points in blue, fibrillar network in gray and cell nucleus in light blue. Thick black lines represents high adhesive surfaces while thick gray lines stand for low adhesive surfaces [Lämmermann and Sixt, 2009].

can generate migration (see Figure 2.1 (III)): rear contraction increases the hydrostatic pressure inside the cell that will lead to herniation of the plasma membrane, creating a bleb. Blebs have been observed during 2D migration but it is still not clear whether they have the ability to transduce traction forces on the surface, which would require adhesion between the bleb and the surface.

2.1.1.2 3D migration

In a 3D environment, the cell no longer needs so much adhesive forces to migrate since it can build on the surrounding fiber network and generate a force perpendicular to the surface that is high enough to prevent 'sliding' against it, hence enabling migration. For actin-polymerization based migration in a dense fibrous network, the migration process may require some contraction forces when the cell has to squeeze its nucleus through narrow constrictions (see Figure 2.1 (IV)). If the fibrous network is less dense, the contraction will not be necessary (see Figure 2.1 (V)) because the nucleus does not need to deform to fit through the fibres. As for 2D migration, there also is a contraction-based strategy in 3D migration: blebbing (see Figure 2.1 (IV)). During blebbing motility, the increase in

the internal hydrostatic pressure of the cell due to rear contraction leads to a bleb formation at the leading edge. In confined migration, blebbing motility offers an interesting alternative to actin polymerization, since no adhesions forces are required for the cell to move forward. Indeed, the adhesion needed for the cell to move forward is provided by the sheer force of actin filaments polymerizing and pushing perpendicularly to the outer surface: this mode of migration is often referred to as 'chimneying' [Hawkins et al., 2009][Charras and Paluch, 2008] [Malawista et al., 2000] [Lim et al., 2013]. Interestingly, blebbing seems to be faster than actin polymerization and less energy-consuming, since there are no adhesions to detach in the forward movement. This mode of migration is further explained in the following section.

2.1.2 Bleb-based migration: Chimneying

Blebs are spherical extensions of the cell membrane that are driven by an increased hydrostatic pressure in the cell. Initially, they are mere cytoplasmic protrusions and are thus deprived of filamentous actin. The formation of blebs at the cell membrane has long been considered to be the sign of cell apoptosis – which refers to programmed cell death – but the last decades have also seen the emergence of studies about bleb-based migration, also referred to as chimneying. Indeed, blebbing has been observed in cell moving over a 2D substrate, even though it is more usually found during migration in 3D environments. Some cells use specifically blebbing-based or actin polymerization-based migration [Paluch and Raz, 2013], but other cells, such as metastatic cancer cells, have the ability to change protrusion type to optimize their migration with the environment.

2.1.2.1 The life cycle of a bleb

The life cycle of a bleb consists of three step: initiation (or nucleation), expansion and retraction (see Figure 2.2). These steps have been observed in non-motile cells, but it is believed that they are very similar for motile cells [Charras and Paluch, 2008].

Bleb initiation, also referred to as bleb nucleation, can follow two different mechanisms: a local rupture of the cortex – a layer of actin, myosin and associated proteins underneath the plasma membrane – or a local detachment of the membrane from the cortex [Lämmermann and Sixt, 2009] [Paluch and Raz, 2013]. Both mechanisms are the result of an increased global or local pressure in the cell, generated by actomyosin contraction, leading to herniation and thus bleb formation.

Bleb expansion follows bleb nucleation. It is driven by the pressure generated by actomyosin contraction and lasts for 5-30s [Charras and Paluch, 2008]. Growing blebs are deprived of an actin cortex but would possess a spectrin-based cytoskeleton underneath the membrane. The size of the bleb seems to be determined by the initial growth rate of the bleb and by the time the cortex will need to reform beneath the membrane.

Bleb retraction occurs once the cortex has re-polymerized. Then, a slow retraction is induced by myosin-driven contraction: it can last for 60-120 seconds. For migrating cells, it is thought that bleb retraction does not have time to fully take place before a new bleb is nucleated over thee old one.

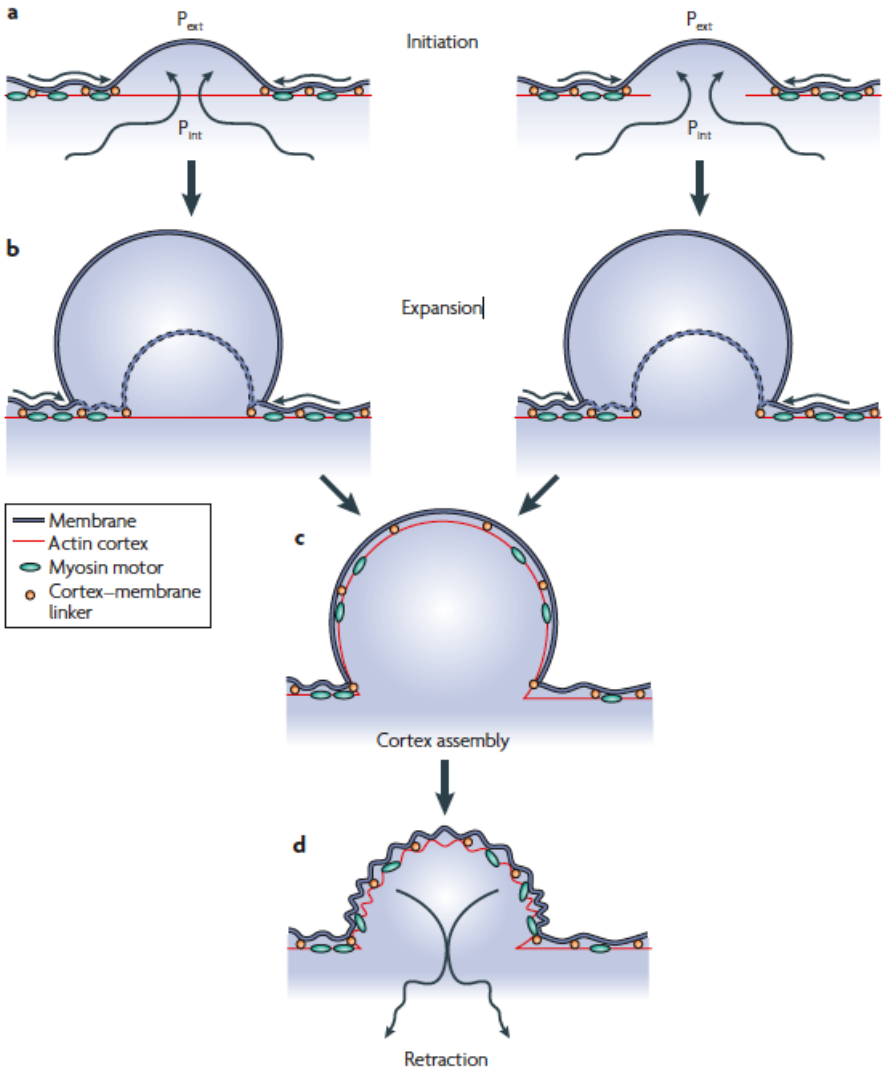

Figure 2.2: The life cycle of a bleb can fall into three phases: bleb nucleation, expansion and retraction. **a.** Bleb initiation can result from a local detachment of the cortex from the membrane (left model) or from a local rupture of the cortex (right model). **b.** Hydrostatic pressure in the cytoplasm (P_{int}) then drives membrane expansion by propelling cytoplasmic fluid through the remaining cortex (left model) or through the cortex hole (right model). concomitantly, the membrane can detach further from the cortex, increasing the diameter of the bleb base (dashed line). **c.** As bleb expansion slows down, a new actin cortex reforms under the bleb membrane. **d.** recruitment of myosin to the new cortex is followed by bleb retraction. P_{ext}, extracellular hydrostatic pressure. [Charras and Paluch, 2008].

2.1.2.2 Bleb-based migration

Bleb-based migration relies upon the cell contractility, but this property is not enough to generate forward movement of the cell by itself. The cytoplasmic flows into the bleb during its expansion moves the center of mass of the cell in the direction of the bleb and is thus a first step towards migration. In order for the migration to be in the right direction, the cell needs to be polarized and the bleb must form at the leading edge. Eventually, the most interesting part in chimneying is that the cell generates forces perpendicular to the surrounding surfaces and use them as an anchoring point to then translocate, just like a rock climber would when mounting a chimney [Malawista et al., 2000] (see Figure 2.3). These forces are triggered by the polymerization of actin filaments directly perpendicular. It was found that such polymerization can yield a migration speed that is higher than the speed of

polymerization; it is thus a very effective migration strategy [Hawkins et al., 2009] .

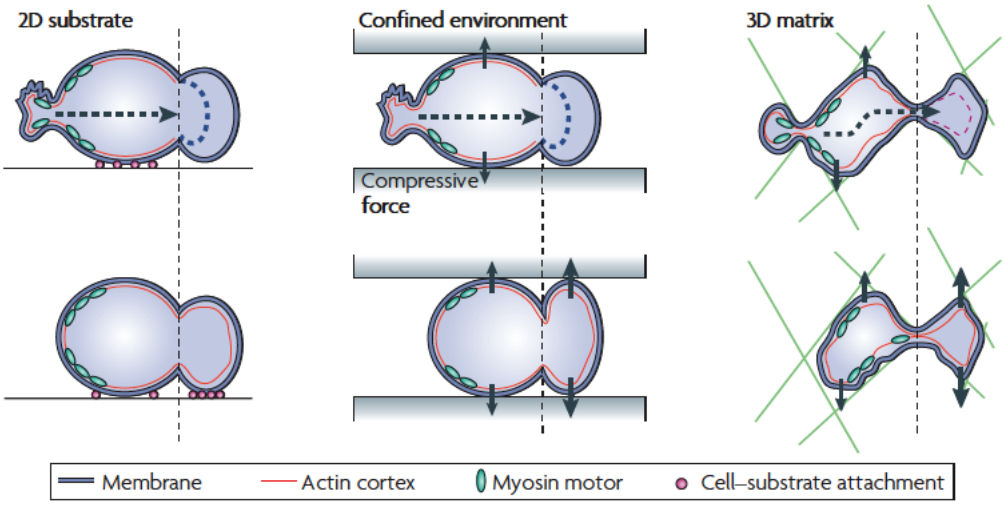

Figure 2.3: In two-dimensional (2D) cultures, in order to translate polarized blebbing into movement, the cell must adhere to the substrate. When a new bleb is formed and comes in contact with the substrate, new cell–substrate adhesions are formed and the cell mass can stream forward. the pink dots indicate cell–substrate attachment points. When the cell is in a confined environment (for example, between two glass coverslips or in a thin microfluidic channel), it can move in the absence of cell–substrate adhesions. Instead, the cell exerts forces perpendicularly to the substrate and can squeeze itself forward; this mechanism is known as chimneying. When the cell is migrating in an extracellular matrix gel (3D matrix), it can move by a combination of the mechanisms described. the fluid nature of growing blebs enables the cell to squeeze through the ECM network mesh. the dashed line indicates the position of the leading edge before bleb nucleation, arrows indicate the forces that are exerted by the cells on the extracellular environment and dashed arrows indicate the streaming of cytoplasm. [Charras and Paluch, 2008].

Cell polarization – the differentiation of the cell front from the cell rear – is essential for cell migration and particularly for chimneying, since the edge where blebbing occurs determines the direction of migration. The mechanism by which the first bleb is formed in the right direction is still unclear but once the first bleb is created, the cell is more prone to blebbing at the leading edge than at the trailing edge because the cortex is younger and more fragile there. A recent study demonstrated the existence of an ezrin-rich region at the cell rear of specific melanoma cells, forming a uropod-like region in which membrane blebbing would be reduced [Lorentzen et al., 2011]. The chimneying cycle starts with the nucleation of a bleb at the leading edge. Then, the cell rear – the uropod – contracts, giving rise to a higher intracellular pressure and hence a simultaneous bleb growth, until the bleb gets into contact with the surface and the confinement keeps it steady. The cycle can then start again and the cell will have a forward movement thanks to the forces pushing up against the walls confining the cell [Charras and Paluch, 2008].

2.2 The cell nucleus

The nucleus, the largest and stiffest organelle of the cell, can adopt various shapes and sizes depending on the cell type and on its environment. The nucleus contains the DNA, the genetic information contained in every eukaryote cell. As the cell's information center, any disruption of the nucleus can be deadly to the cell, and it can be easily imagined that any modification of it – may it be chemical or mechanical – could have an impact on the DNA and potentially trigger gene-related modifications in the cell. Understanding how the cell nucleus undergoes mechanical stresses and strains is thus a crucial branch of research.

2.2.1 Structural components of the nucleus

The nucleus is most commonly ovoid or spherical shaped with diameters ranging from 5 to 15 μm and it generally occupied around 10 percent of the cell's volume, making it one of the largest components of the cell [MBI - National University of Singapore, 2014]. The nucleus, as can be seen on Figure 2.4, have two separate regions [Nava et al., 2014] [Dahl et al., 2008].

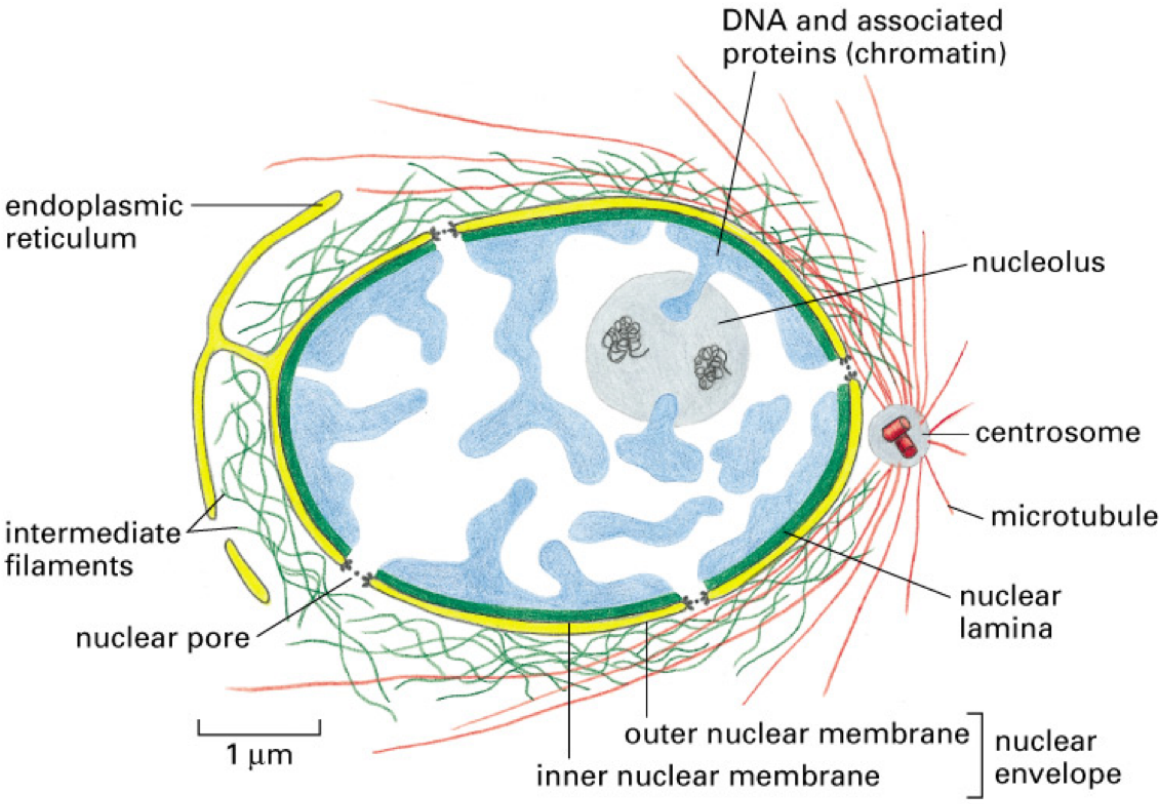

Figure 2.4: A cross-sectional view of a typical cell nucleus [Alberts B., 2002]

2.2.1.1 The nuclear interior: nucleoplasm

If the nuclear envelope is rather well defined, it is not the case for the nuclear interior, whose fluid viscosity has been measured and found to be five times higher than that of water. Some molecules are however known to be found inside the nucleus and these will be discussed here.

Chromatin

The nucleus can be seen as the "brain" of the cell since it contains its genetic information. If DNA is often studied when it is packed in chromosomes, it is usually found in its unpacked form in the nucleus, which is called chromatin. Chromatin is not merely composed of DNA but it also contains histone proteins, around which DNA winds, therefore packing it in structures called nucleosomes [MBI - National University of Singapore, 2014]. This process allows roughly 2 meters of DNA to be packed in a 5-20 μm large nucleus. Two types of chromatin can be found : euchromatin and heterochromatin [Dahl et al., 2008]. Euchromatin corresponds to gene rich regions with thus a high transcriptional activity, it is to be found in the interior of the nucleus and presents open structures and is more deformable than heterochromatin. The latter is densely packed and found more at the

periphery of the nucleus or close to the nucleolus and transcriptionally inactive with a low activity in gene expression.

Nuclear bodies

Along with chromatin, the nuclear interior is filled with nuclear bodies [Dahl et al., 2008] [Nava et al., 2014]:

Nucleoli are the region of the biogenesis of the ribosomes – the organelles responsible for the translation of mRNA into proteins. Atomic Force Microscope (AFM) testing showed that the nucleolus appears to be stiffer than the nucleus, while pipette aspiration experiments showed that it has a fluid-like behavior with a permanent deformation under high stress.

Cajal bodies ("coiled bodies") are dynamic structures that associate with nucleoli and snRNPs (small nuclear ribonucleoproteins). Their translocation within the nucleoplasm can be the result of numerous stimuli. For instance, they would feel cellular stresses and respond to it accordingly.

Promyelocytic leukaemia (PML) bodies are located close to transcriptionally active genes, involved in the regulation of transcription and respond to chemical stresses. They are also thought to be stress-responsive structures since they increase in number and size in response to mechanical stress.

Structural proteins

Besides genetic information and various nuclear bodies, structural proteins exist inside the nucleus [Dahl et al., 2008]. First, lamin A/C, that partially forms the lamina, can form stable structures inside the nucleus. Nuclear actin can also be found: although its structure inside the nucleus is uncertain, it would exist both as filamentous and globular and would be able to bind lamins. As an intra-nuclear component, the question remains whether it would be involved in the process of transcription or not. Along with it, actin-associated proteins are present inside the nucleus, such as nuclear myosin and nuclear alpha-II spectrin [Nava et al., 2014]. Since these are associated with the generation of movement when inside the cytoplasm, their presence inside the nucleus raises the question of a possible influence of the DNA on the locomotion.

2.2.1.2 The nuclear envelope

The nuclear envelope is made of a double membrane constituted by an inner and outer part. As the cell membrane, both inner and outer nuclear membranes are lipid bilayers in which diverse proteins are engulfed. The outer membrane is continuous with the endoplasmic reticulum and both membranes join at the nuclear pore complexes, multi-protein complexes that allows various molecules to get in or out the nucleus. A closer representation of the nucleus is illustrated by Figure 2.5. The stability of the nucleus is however mainly governed by the lamina, a dense protein network located just beneath the nuclear membrane and made of lamins, type V intermediate filaments, and lamin-associated proteins that give the lamin-network its structure by stabilizing it. Some of these proteins usually have one transmembrane domain and a lamin binding one, connecting the lamina to the inner nuclear membrane, while others establish connexions between lamins and chromatin, as well as gene regulatory components. The lamina is a very dynamic network: it is indeed thought to be the main stress-sensing component of the nucleus and it is able to adapt the nucleus stiffness to the one required by the surrounding tissue [Pederson and Marko, 2014] [Swift and Discher, 2014] [Deguchi et al., 2005]. If lamins are mostly found in the lamina, it should be reminded that stable lamin structures are also to be found inside the nucleus [Nava et al., 2014] [Dahl et al., 2008].

Lamins structure

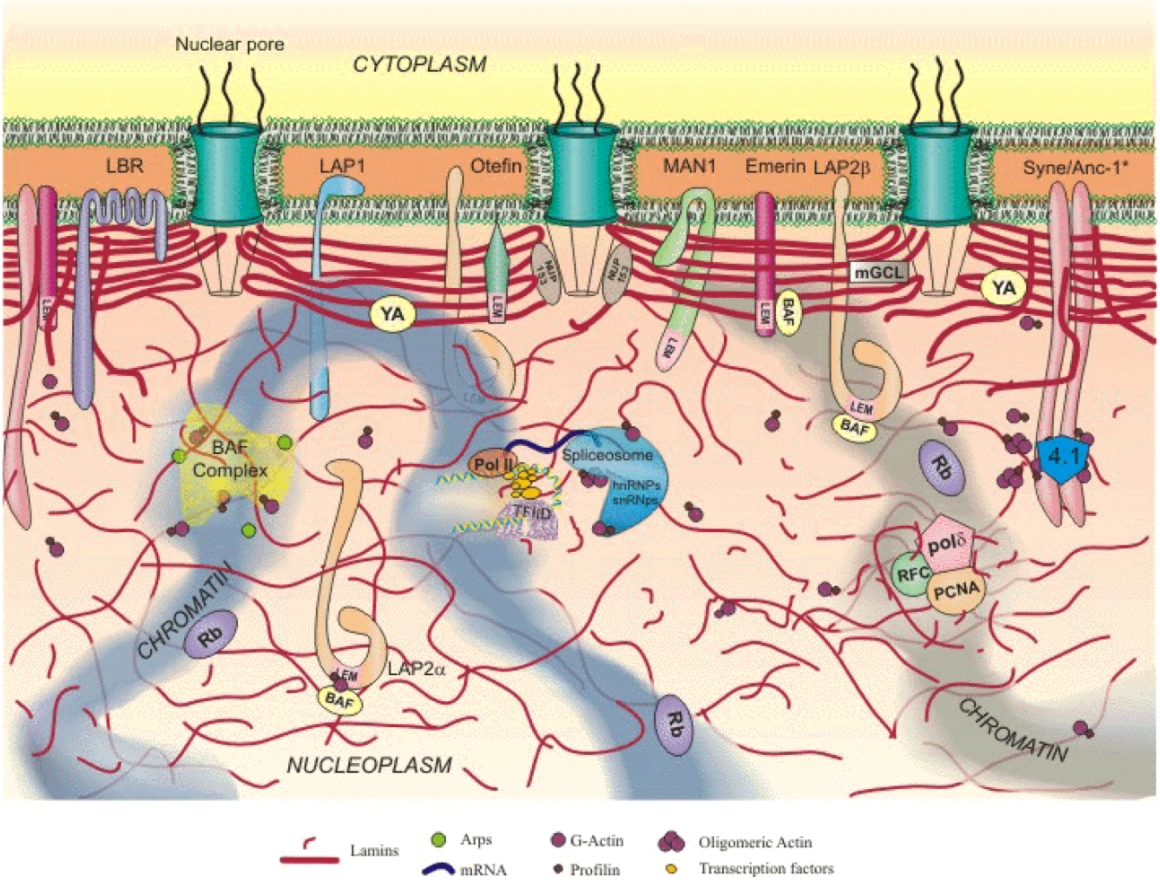

Figure 2.5: Representation of the nuclear envelope, lamina and nuclear interior [Goldman Lab, 2014].

Lamins are type V intermediate filaments with two subtypes :

A-type lamin are lamin A and lamin C, which result from alternative splicing from the LMNA gene [Dahl et al., 2008]. They are present within the nucleus only after cells begin differentiation and they form a thick network (up to 100 nm) that provides nuclear stiffness. Their role in the maintenance of the nuclear structure, stability and shape is major.

B-type lamin are lamin B1 and B2, which are encoded by two separate genes (*LMNB1* and *LMNB2*) [Dahl et al., 2008]. They form a thin fibrous meshwork that is closely associated with the inner nuclear membrane. The lamin B1/B2 network is most likely separate from the lamin A/C network but they are overlapping. The role of B-type lamin is less obvious than the one of A-type lamin but it has been observed that a mutation in B-type lamin is embryonic lethal and that the loss of lamin B1 causes the appearance of nuclear blebbing.

Although the precise structure of lamins is still under study, [Patricia M Davidson, 2013] proposed a structure based on new findings. Lamins are monomers, mostly made of a alpha-helicoidal central rod domain along with a short N-terminal head and a long tail domain with the presence of globular immunoglobulin (Ig) motif. These monomers form dimers through coiled-coil interactions within the rod domain and then polymers through supramolecular assembly which is driven by interactions within lamin rod domains and N-terminal head domains [Goldman Lab, 2014] [Rowat et al., 2005].

2.2.2 Basic nuclear mechanics

2.2.2.1 Mechanical properties

As the stiffest organelle in the cell, the nucleus has a major speed-limiting role during confined cell migration [Davidson et al., 2014]. It is therefore specifically relevant to study the nucleus mechanical properties. Depending on methods and cell types, the nucleus has been found to be 2 to 10 times stiffer [Guilak et al., 2000] than the surrounding cytoplasm with a nuclear stiffness ranging from 0.1 to 10 kPa [Dahl et al., 2008]. Moreover, nuclei exposed to shear stress have an increased stiffness. This specific resistance to shear is vital for the survival of the cell since DNA is particularly sensitive to shear stress and degrades in response to it. The mechanical properties of nucleus do not only emerge from the lamina, but also from the nuclear interior and particularly the chromatin [Rowat et al., 2006]. The latter was proved to provide structure and mechanical stability and showed residual deformation under high mechanical stress, which could be seen as plastic properties or viscoelastic properties if considered on a larger time scale. Indeed, irreversible realignment of chromatin fibers and nucleoli were observed during pipette aspiration tests [Pajerowski et al., 2007]. If chromatin has its part in mechanical properties of the nucleus, the lamina provides a stiff and load-bearing structure that is necessary for the structural integrity of the nucleus. It physically connects the nucleus and the cytoskeleton and contributes to mechanotransduction signaling. Those two parts of the nucleus have an influence depending on the intensity of the deformation: for small deformations, the envelope resists the stress, while the compressibility of the inner nucleus becomes non negligible for large deformations [Rowat et al., 2006].

Lamin stretching The lamina being the prominent element for mechanical stability of the nucleus, its structure has been particularly investigated. Lamin filaments appear to be very deformable and can be stretched several times their initial length. As it was developed earlier, the lamina has a hierarchical structure and therefore responds to different levels of strain [Patricia M Davidson, 2013]: Initially, as they are strained, the coupled alpha-helices of unit-length filaments start uncoiling. Then, as the strain increases, there is a change in configuration and the alpha-helices transition into beta-sheets. Eventually, further increase of the strain lead the hydrogen bonds between beta-sheets to be broken and the monomers slide along each other.

2.2.2.2 Existing models for the nucleus

If the mechanical behavior of cells has been widely studied from an experimental point of view, computational models are being more and more developed to describe cells as well as nuclei. These models allow to predict experimentally observed cell behavior, but will also help getting a better understanding of the behaviour of cells in living systems. The existing computational models can fall into two categories that are further illustrated by Figure 2.6: micro-structural models and continuum models. The method chosen will depend on the length and time scales of interest. The model developed by [Aubry et al., 2014] is a continuum model describing the cell and the nucleus as viscoelastic materials, including active strains to account for the polymerization and depolymerization of actin filaments in the cytosol of the cell. It will be further detailed in the next chapter. Since we developed a continuum approach, we will not elaborate here on micro-structural models, which have been addressed by [Nava et al., 2014].

Continuum methods are generally applicable when the smallest length scale of interest is much larger than the length over which the structure and properties of the cell vary and treat cells as deformable materials with certain continuum material properties [Nava et al., 2014]. These methods are usually accompanied by finite elements computing since it allows a rather simple management of the cell properties and geometry and fast calculations. An extensive review on continuum-based

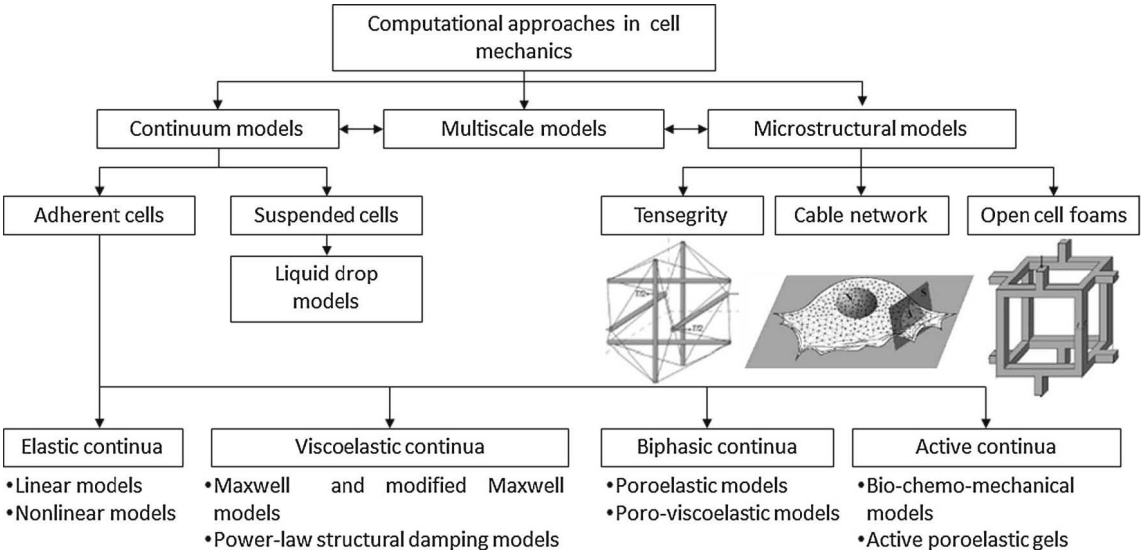

Figure 2.6: Illustration of existing mechanical models for cellular behavior

model was presented by [Vaziri et al., 2007]. Beside active continuum models, most continuum models generally consider the cell materials to be passive and therefore do not take into account the ongoing modifications inside the cell in response to mechanical stress. The materials in the cells being considered as homogeneous, these models do not account for inherent heterogeneities of the cell structure and some aspects, such as distant transduction of forces from focal adhesions, are not reproduced. One interesting and advanced model was presented by [Deshpande, 2006] and proposes a bio-chemo-mechanical modeling of the cell. It is based on the description of stress fibers contractility, which is then used to build a model for the biochemistry of stress fibers remodeling. All the other models are based on elastic or viscoelastic modeling of the cell, often referring to Maxwell models, but only few of them include the nucleus as a separate component (see Table 2.1). Some computational models were even developed for the study of isolated nucleus (see Table 2.2).

As for the nucleus specifically, it is mostly considered as a viscoelastic organelle. Some have shown a particular interest in the nuclear membrane for which a spring elastic model was developed [Ujihara et al., 2011]. The viscoelastic properties of the nucleus are more often associated to the lamina and its overlapping meshworks of A-type lamin and B-type lamin. Indeed, B-type lamin is modeled as immobile, with a solid-like elasticity – thus inducing reversible deformations –, while A-type lamin is considered to be more mobile or "fluid" and would provide a strong non-linear contribution to viscosity, thus inducing irreversible shape changes depending on the LaminA:B ratio [Swift and Discher, 2014].

However, some studies have highlighted its capacity to break its lamina and reform it later in order to pass through very narrow constrictions [Lammerding, 2011] [Aubry et al., 2014] as can be seen on Figure 2.7. This particular property is very interesting since it would be a tremendous asset for the cell during confined migration. It can be seen as a sign of a plastic behaviour of the nucleus, which rose our interest into developing a more complex constitutive model of the nucleus, also accounting for that plasticity.

2.2.3 Nucleo-cytoskeletal coupling

Although our continuum approach does not presently take into account specific molecular processes of mechanotransduction within the cell, having a deeper understanding of the way nucleo-cytoskeleton

Experimental method	Material method
AFM Indentation	Linear elastic Non-linear elastic
Cytoindentation	Linear elastic Poroelastic
Magnetic Twisting Cytometry	Linear elastic Non-linear elastic Maxwell viscoelastic Power law structural damping
Shear Flow	Linear elastic Non-linear elastic
Micro-array/Substrate strain	Linear elastic Modified Maxwell viscoelastic Biochemomechanical
Microplate compression	Non-linear elastic Modified Maxwell viscoelastic
Micropipette Aspiration	Linear elastic Non-linear elastic Maxwell viscoelastic Modified Maxwell viscoelastic Poroelastic Poroviscoelastic
Optical Tweezers	Non-linear elastic Modified Maxwell viscoelastic

Table 2.1: Computational models to study cell deformation in common experiments for cell mechanics [Vaziri et al., 2007] [Nava et al., 2014].

Experimental method	Material method
AFM Indentation	Maxwell viscoelastic
Microplate compression	Non-linear elastic Maxwell viscoelastic
Micropipette Aspiration	Modified Maxwell viscoelastic

Table 2.2: Computational models to study nucleus deformation for isolated nucleus [Vaziri et al., 2007] [Nava et al., 2014].

coupling occurs will be of great interest to be able to adapt our model and refine it. Indeed, besides sheer material properties, modeling the behavior of a cell during confined migration – and particularly its nucleus – requires to understand how and where the active forces due to actin polymerization or myosin contraction, or the mechanical strain induced by the environment might occur so that our model can mimic the experimental observations.

2.2.3.1 LINC complex

The integration of the nucleus into the structural network of the cell is achieved through the LINC complex (LInker of the Nucleoskeleton and Cytoskeleton), which couples the cytoplasm and the nucleoplasm and allows the transmission of forces between the cytoskeleton and the nucleus [MBI - National University of Singapore, 2014]. This proteins complex is essential during cell migration since its disruption prevents a rearward movement of the nucleus, which is crucial for certain cells.

The LINC complex is composed of two families of proteins (see Figure 2.8):

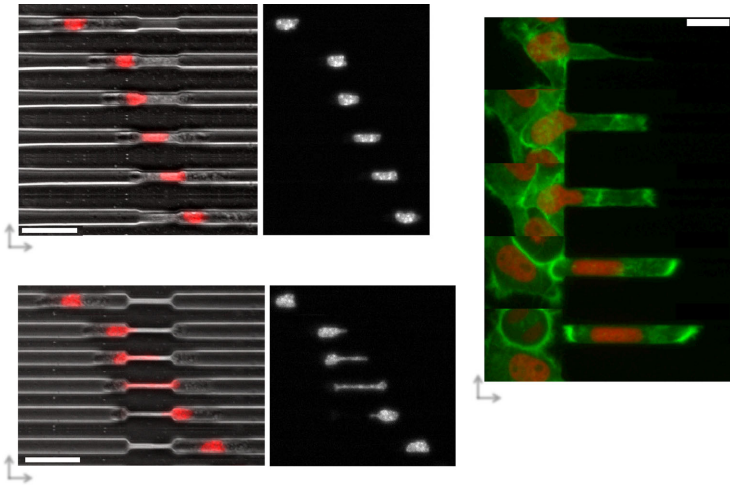

Figure 2.7: **(a:d)** Top view of successive steps of a bone marrow-derived dendritic cell (BMDC) migration (from the left to the right) through a $5\mu m$ **a**–**b** and $1.5\mu m$ **c**–**d** wide micro-channels. Nuclear staining with Hoechst (**a** and **c**) (scale bar: $30\mu m$) **e** Sagittal view of successive steps of a HeLa cell entering (from the left to the right) a $20\mu m$ wide microchannel (HeLa Histone2B-mcherry (nucleus), MyrPalm-GFP (plasma membrane), scale bar: $15\mu m$) [Aubry et al., 2014].

SUN domain proteins are found at the inner nuclear membrane and particularly interact with the nuclear lamina.

KASH domain proteins are found on the outer side of the nuclear membrane and can bind to all major filament networks from the cytoskeleton (actin, microtubules, intermediate filaments)

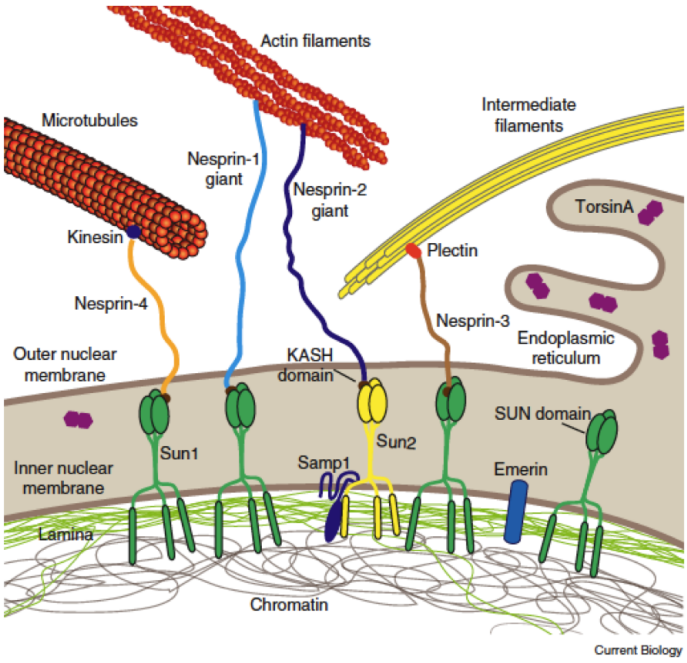

Figure 2.8: Illustration of the coupling between the nucleoskeleton and the cytoskeleton (LINC complex)

2.2.3.2 Potential mechanisms for nuclear mechanosensing

Some modes of cell migration strongly rely on the ability of cells to form focal adhesions with the surrounding environment in order to anchor itself and have an efficient migration. Thanks to these adhesions, the cell can stretch trough polymerization of actin filaments in the cytoplasm and the nucleus within the cell will undergo deformations. The molecular mechanisms triggered by force transmission from the cytoskeleton to the nucleus are still mostly unknown, but the nucleus appears to be able to 'feel' these force and respond to them through transcription regulation [Nava et al., 2014]. Some possible schemes have been proposed and are illustrated in Figure 2.9:

(i) One possible mechanism is that the forces transmitted from focal adhesions to the nucleus induce an opening of the chromatin. The genetic information is thus more easily accessible and the transcriptional regulators can access zones of the DNA that weren't available before.

(ii) Alternatively, we could also consider that under the stretching of the nucleus, the chromatin will locally detach from the lamina. The nuclear periphery being a transcriptionally repressive area, some genes will move out of this zone and become reachable for transcription. This chromatin detachment could also induce changes in the very structure of the chromatin and promote access to transcriptional regulators.

(iii) Eventually, we could imagine that the stretching of the nucleus generates a stretching of the lamina, therefore leading lamins to partially unfold and undergo conformational changes, which would transform the way they interact with transcriptional regulators. Figure 2.9 illustrates how the stretching of the lamina can result in a release of transcription factors, which can then act on target genes.

These potential mechanisms may elucidate how mechanosensing might occur and could possible happen all at once when the cell undergoes mechanical strains. All in all, the straining of the cell triggers a cascade of biochemical reactions and signaling events towards the nucleus that influence the cell function [Nava et al., 2014].

2.2.4 Nuclear mechanics during confined cell migration

During confined migration, the cell has to move through constrictions which are sub-cellular or sub-nuclear. Indeed the stiff extra-cellular matrix (ECM) is a highly complex three dimensional network of fibers that works against cell migration by creating a much restricted environment. The nucleus being much stiffer than the cytoplasm, it is the rate-limiting organelle for migration. The cytosol can indeed deform very easily, but the lamina's higher stiffness acts like a shell and inhibits migration if the deformation is too high. Therefore, depending on the amount of deformation required, the cell can adopt various migration strategies. Some cells show the ability to proteolytically degrade the ECM to widen the gap and decrease the necessary strains while some others squeeze themselves to fit in the available space and thus undergo elastic and plastic deformations. If none of these options can be realized – if the gap is much too small for instance – the cell will retract its protrusion and re-polarize in order to find another route.

As we discussed previously, the mode of migration that has been the most widely studied is adhesion-based. Therefore, it will be the mode considered in this section. Adhesion-based migration can consist of four or five steps depending on the ability of cell to degrade the ECM. Firstly, the cell polarizes and forms protrusions in the direction of migration. These protrusions will then interact with the ECM either by directly forming focal adhesions, or by previously triggering a proteolytic

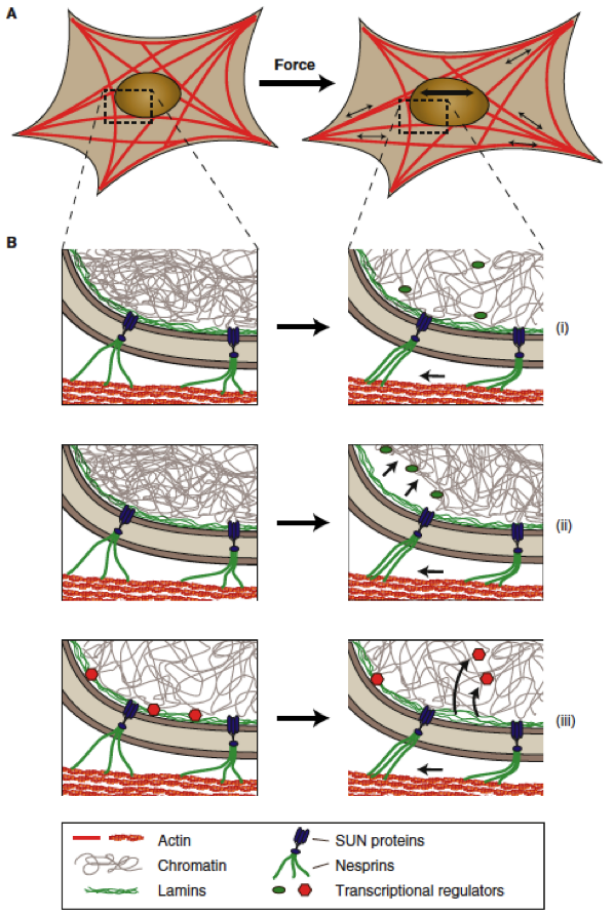

Figure 2.9: Illustration of the possible mechanisms for mechanosensing in the nucleus.

degradation – in proteolytic migration only – and a realignment of the ECM fibers, thus creating or widening the tracks for the cell to move through. A tension is created between the front and the rear of the cell through the myosin-II mediated contraction of the actin filaments network. Eventually, the rear focal adhesions of the cell start detaching and the rear-end can therefore slide forward. Our interest lies particularly in the position of the nucleus during this migration process. After the cell elongation, the nucleus rotates along the length axis of the cell so it might pass more easily through the constrictions. Depending on the cell types, the nucleus then moves either towards the cell rear – for collective migration, epithelial, mesenchymal and neuronal cells – or towards the leading edge – for amoeboid-moving leukocytes – while the rear of the cell remains in place. In the last stage of the migration process, the contraction of the actin filaments pushes the nucleus forward while the leading edge remains anchored to the substrate.

2.3 Micro-channels experiments

Cell migration on 2D flat substrates has been extensively studied and many models have been developed, confirmed by *in vivo* studies. The new emphasis is now on migration in 3D and in confined environments. During confined migration, there are various parameters to take into account that influence the mode of migration, but also the physical parameters of the medium in which the cell moves. Collagen gels were for a long time the reference support used to study cell migration in a

very simplified way, but such gels still give results that depend on so many parameters that they become hard to analyze (gel properties, geometrical confinement, local constrictions due to mesh size). The latest studies have therefore used micro-channels to perform their experimental studies. Indeed, parameters of micro-channels can be tightly controlled and are mostly independent on each other. The simplest assay for the study of confined cell migration consists of straight micro-channels made of silicon rubber. A tremendous advantage of micro-channels is that the geometry can easily be adapted and complexified to fit the needs of the study: once the fabrication technology is implemented, designing new devices is easy and fast. We present here some main steps for the creation on micro-channels assays [Mélina L Heuzé, 2011] [Pablo Vargas, 2014].

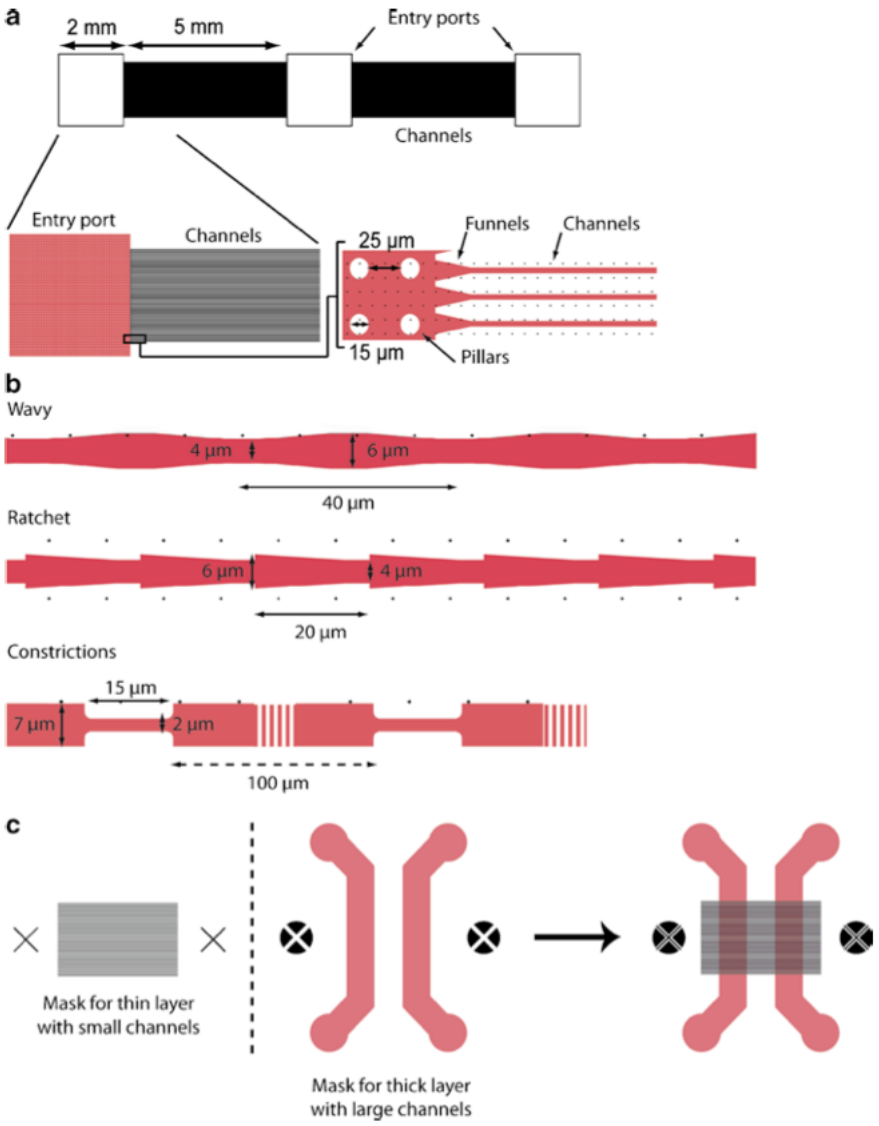

Figure 2.10: Examples of micro-channel designs for migration of dendritic cells. **a.** Multiscale drawing of an entire channel with three entry ports initially designed with 15-mm diameter pillars, linked by two rows of 4-mm large micro-channels. Note the funnel shaped entry of the channels. **b.** Three different examples of micro-channels used in migration assays. **c.** Design for a two-layer micro-channel chamber for immunostaining and drug delivery experiment. The crosses on the side allow the alignment of the two masks during the lithographic process. [Mélina L Heuzé, 2011]

2.3.1 Design of the chamber

The first crucial aspect of the micro-channels array is the design of the geometry of the chamber on which the general behaviour of the cell and their motility depends. Figure 2.10 gives a multiscale representation of a complete chamber. Figure 2.10a presents a design that includes three entry ports in which micro-pillars are included to make sure that the roof of the entry ports will not fall on the bottom coverslip during assembly of the chamber. The distance between these pillars is a major factor, since it must allow the cells to migrate trough the entry port and enter the channel. Another geometric tool to help the cell get into the channel without damages is the funnel structure that can be observed in Figure 2.10a. Two entry ports are bound by hundreds of parallel micro-channels. Their geometry will be chosen depending on the purpose of the study: one can use wavy or ratchet structures for basic migration studies, or use narrow sub-nuclear constrictions in order to highlight the specific rate-limiting role of the nucleus during migration (see Figure 2.10b). Once the design is completed, the corresponding photomask can be ordered for further photolithography. In case one needs some immunostaining or drug delivery for the study, it can be convenient to design a two-layer chamber with short micro-channels direclty delivering the substance (see Figure 2.10c).

2.3.2 Chamber fabrication

Once the design of the chamber is determined, the next step is to create the wafer by photolithography. Photolithography is the process of transferring geometric shapes on a mask to the surface of a silicon wafer. There are several steps involved in this process and some of the most important are wafer cleaning, photoresist application, soft baking, mask alignment and UV exposure, post-exposure baking, development, and rinsing and drying (see Figure 2.12). The complete protocol is exposed in [Mélina L Heuzé, 2011]. After the wafer is produced, it will serve as a base for the PDMS chip fabrication. Indeed, the wafer is a mold for the PDMS chips, it is thus a negative of the final chip (see Figure 2.11). The PDMS chip is then assembled with the glass or plastic substrate and eventually, its upper surface is activated so the chip can be immediately used. The micro-channel assay is compatible with any kind of microscopy if we choose a glass coverslip for the bottom of the device. We can therefore obtain very nice fluorescence images quite easily.

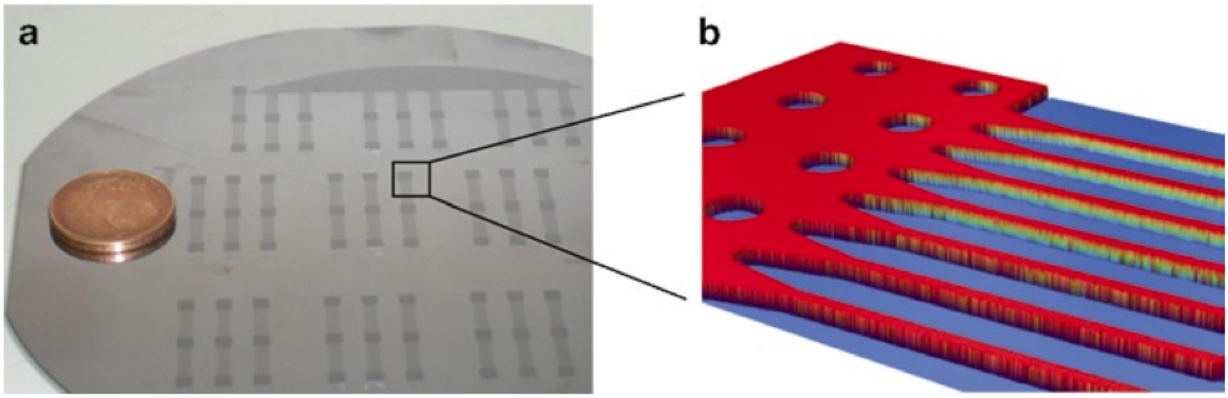

Figure 2.11: Example of a silicon wafer obtained by photolithography. **a.** Wafer obtained by photolithography (a 1 cent coin is shown to compare sizes). **b.** Image of features made of photoresist, obtained by optical interferometry. Color code is set to light blue (ground) to red (5 μmm height) [Mélina L Heuzé, 2011].

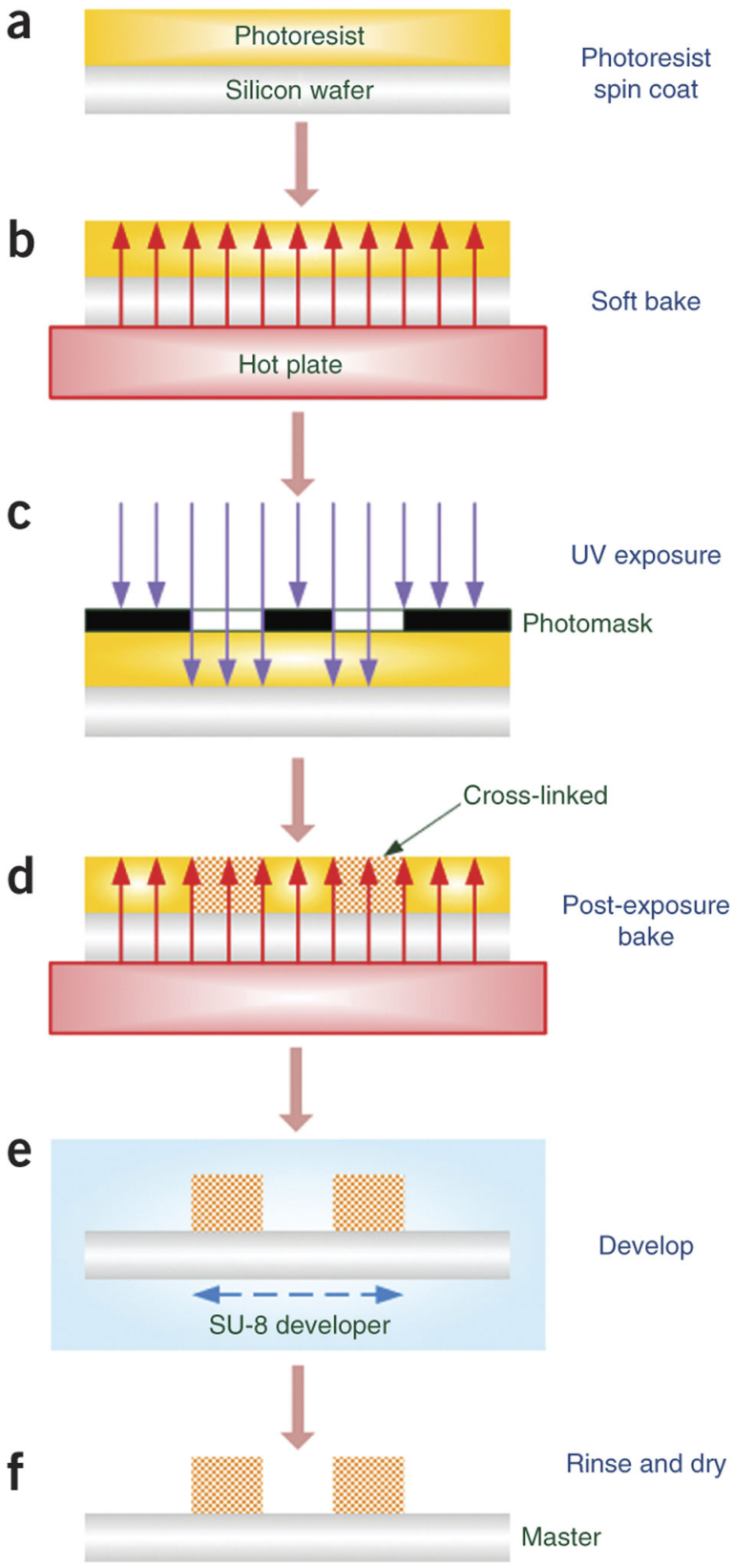

Figure 2.12: Main steps for the creation of a wafer by photolithography [Geng et al., 2011]

To put it in a nutshell, cell migration is a crucial biological phenomenon that occurs during an organism development, its homeostasis, and potentially in diseased tissues. Depending on its environment, the cell adopts its migration strategy as it will more likely use an adhesion-based migration mechanism in 2D and a contraction-based one in 3D. In confined environments, some cells have the ability to use a bleb-based migration mode, often referred to as 'chimneying', that consists in pushing the confining surfaces to create anchor points and thus move forwards. The biggest and the stiffest cell organelle being the nucleus, it has a considerable role during confined migration. Indeed, its lamina is the load-bearing element and the stiff part that acts against confinement and it has also been observed to break to fit through very narrow constrictions, while the chromatin is more compliant. The nucleus Young modulus varies from 0.1 to 10 kPa depending on the cell type and on the measurement technique. During cell migration, it first aligns on the cell polarization axis to minimize strain, and then will either move forward or backward before contraction of the cell rear pushes it forwards along with the cell. The experimental data we work with are obtained thanks to micro-channels arrays. Our simulation models thus imitate such setups.

3. A visco-elasto-plastic model for the cell nucleus

Recent experimental studies have highlighted the ability of certain cells to break their lamina to be able to pass through sub-nuclear constrictions. Such phenomenon may be interpreted by a viscoplastic behaviour of the nucleus. The objective of this section of our work is thus to develop a visco-elasto-plastic finite elements model of the nucleus and to assess its robustness with respect to experimental data from the literature. Such model will constitute a step towards a more realistic representation of the nucleus including the lamina and nucleoplasm, and accounting for a more rigorous constitutive behaviour.

3.1 Description of the model

In this section, we first describe the geometry of the nucleus including the lamina and the nucleoplasm. Then, we will focus on the mechanics of this system, and particularly on the Maxwell models that are used to reproduce the viscoelastic behaviour of the nucleoplasm and the visco-elasto-plastic behaviour of the lamina.

3.1.1 Geometry

The cell nucleus usually has an initial ovoid or spherical shape with a size ranging from 5 to 15 μm in diameter. In our 2D numerical model, the geometry of the nucleus has been simplified by a circular domain $\Omega_{nucleus}$ of radius $r_{nucleus}$ (see Figure 3.1). We consider the nucleus to be made of two regions: the nucleoplasm ($\Omega_{nucleoplasm}$) and the surrounding lamina (Ω_{lamina}). They are defined through two characteristic functions, as in [Aubry et al., 2014] (see Appendix A).

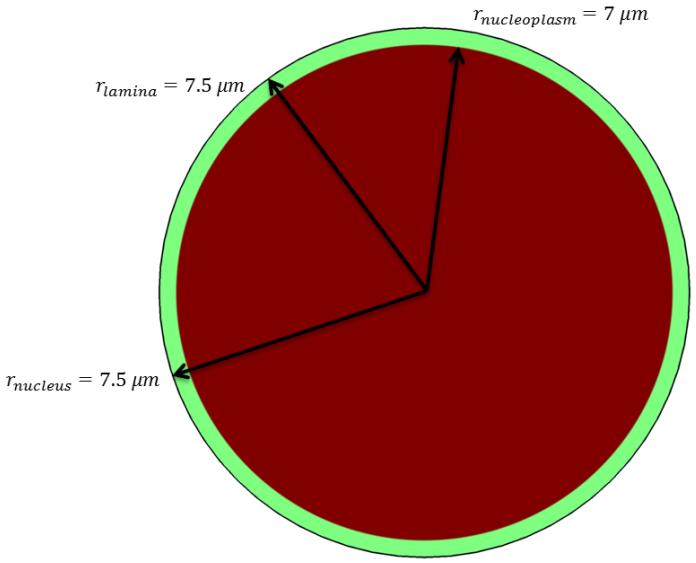

Figure 3.1: Geometry of the nucleus

3.1.2 Constitutive model and mechanics of the nucleus compression

From a rheological point of view, we consider the lamina as the solid phase, and the nucleoplasm as the fluid phase. The latter is thus described with a standard Maxwell model (see Figure B.1a). The lamina is defined as a visco-elasto-plastic material as represented in Figure B.1b (see Appendix B for the detailed equations of the model). This allows to account for the possible reorganization inside the nucleus when submitted to stress, and therefore remaining deformations after relaxation.

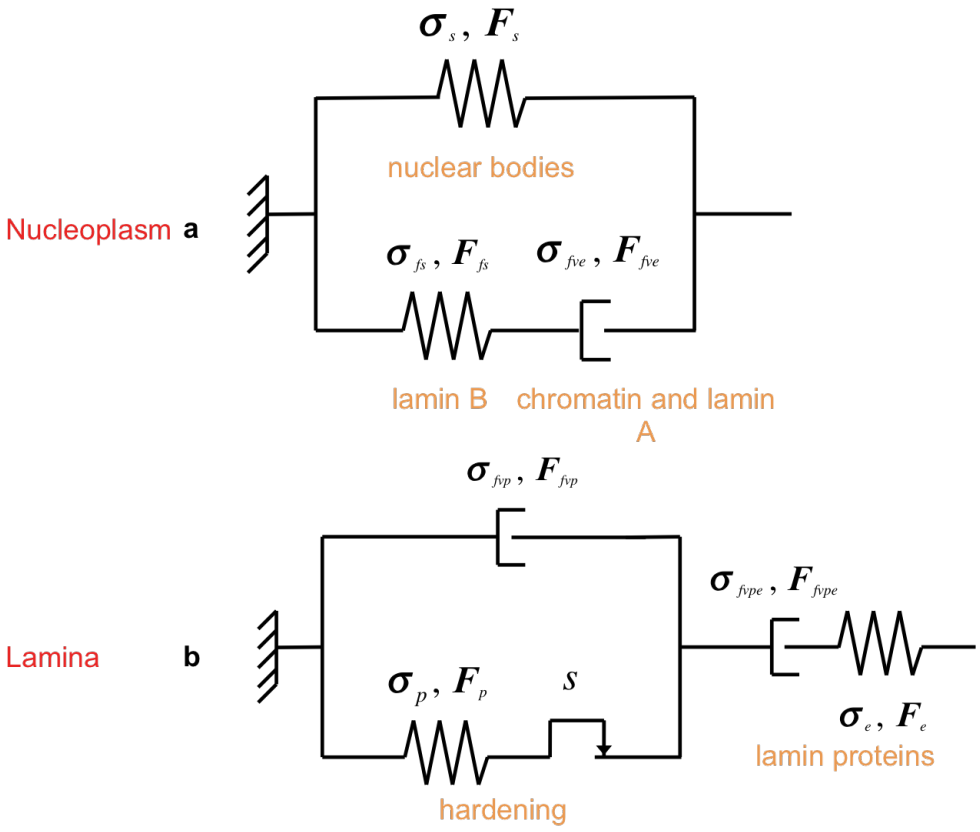

Figure 3.2: Rheological models used to describe the nucleoplasm (**a**) and the lamina (**b**) behaviour

Here, we want to reproduce a simple compression test. Thus, the nucleus is initially places between two parallel horizontal plates (see Figure 3.3). The upper one moves downwards with a speed v_{plate} and progressively squeezes the nucleus with a force $\boldsymbol{f}_{plate}$. The main geometrical and mechanical parameters of the model are reported in Table 3.1.

As described in previous publications [Aubry et al., 2014], the global equilibrium of the system will be expressed as in Equation 3.1

$$\rho \boldsymbol{a} = \boldsymbol{Div}_p(J\boldsymbol{\sigma}\boldsymbol{F}^{-T}) + \boldsymbol{f}_{plate,up} + \boldsymbol{f}_{plate,low} \tag{3.1}$$

where ρ is the nucleus density, considered to be equivalent to the cell density, $\boldsymbol{a}$ is the acceleration, $\boldsymbol{Div}_p$ is the divergence with respect to the initial position $\boldsymbol{p}$, J is the determinant of the deformation gradient $\boldsymbol{F}$ and $\boldsymbol{A}^{-T}$ is the inverse transpose of the matrix $\boldsymbol{A}$. $\boldsymbol{f}_{plate}$ denotes the viscous force exerted by the compression plates on the cell boundaries and is as expressed as

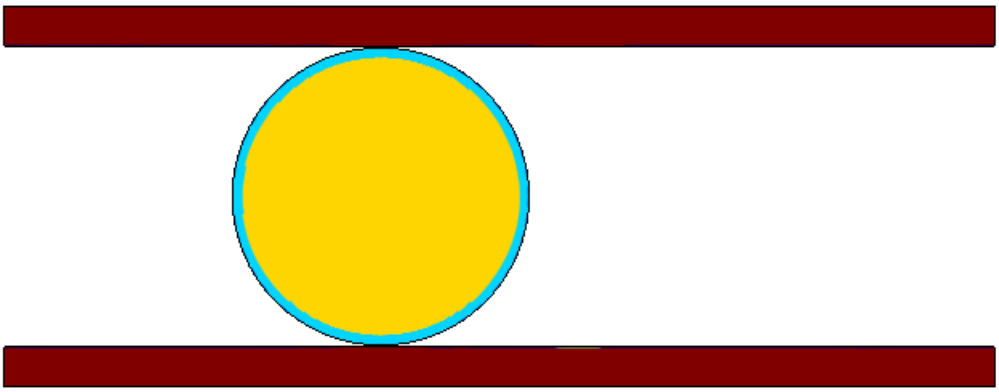

Figure 3.3: Initial situation for the compression test. The compression plates are labeled in dark red, while the lamina is in blue and the nucleoplasm in yellow.

Parameter	Description	Value
E_{lamina}	3000 Pa	Young modulus of the lamina
$E_{nucleoplasm}$	25 Pa	Young modulus of the nucleoplasm
μ_{lamina}	3×10^5 Pa.s	Lamina viscosity
$\mu_{nucleoplasm}$	3×10^5 Pa.s	Nucleoplasm viscosity
ν_{lamina}	0.3	Poison ratio of the lamina
$\nu_{nucleoplasm}$	0.4	Poisson ratio of the nucleoplasm
$(x_0; y_0)$	(0;0)	Initial coordinates of the center of the nucleus
$r_{nucleus}$	7.5 μm Pa	Radius of the nucleus
r_{lamina}	7.5 μm	Outer radius of the lamina
$r_{nucleoplasm}$	7 μm	Radius of the nucleoplasm
$\rho_{nucleus}$	1000 kg/m^3	Nucleus density
h_{plate}	2 μm	Height of the plate
l_{plate}	50 μm	Length of the plate
$d_{plate-nucleus}$	0.1 μm	Initial distance before contact between the cell and the nucleus
v_{plate}	0.5 μm/s	Compression velocity
s	4000 N^2/m^4	Plasticity Threshold

Table 3.1: Main geometrical and material parameters of the nucleus model [Aubry et al., 2014]

$$\boldsymbol{f}_{plate,up}(\boldsymbol{n}_{up}) = -\mu_{up}\frac{1}{(l_{up}+1)^8+\alpha}(\frac{\partial \boldsymbol{u}_{up}}{\partial t}, \boldsymbol{n}_{up})\boldsymbol{n}_{up} \text{ on } \partial\Omega_{up}$$

$$\boldsymbol{f}_{plate,lp}(\boldsymbol{n}_{lp}) = -\mu_{lp}\frac{1}{(l_{lp}+1)^8+\alpha}(\frac{\partial \boldsymbol{u}}{\partial t}, \boldsymbol{n}_{lp})\boldsymbol{n}_{lp} \text{ on } \partial\Omega_{lp} \tag{3.2}$$

where μ_{up} and μ_{lp} are the viscosity of the upper and lower plate, l_{up} and l_{lp} are two level set functions defining the plates (we took here the same functions as the one defining the channel in Appendix A), α is a constant, $\boldsymbol{n}_{up}$ and $\boldsymbol{n}_{up}$ are the outward normal to the boundaries $\partial\Omega_{up}$ and $\partial\Omega_{lp}$ of the upper and lower plate respectively, and $\boldsymbol{u}_{up}$ defines the motion of the upper plate. Finally $(\boldsymbol{a}, \boldsymbol{b})$ defines the scalar product between two vectors. The model implies that the reactive plate force gets larger and larger when the boundary of the cell comes closer to it.

3.2 Results

In this section, we present our results of the compression test on an isolated nucleus. The nucleus has an outer diameter of $7.5\mu m$ and its lamina is 500 nm thick. The nucleus is compressed linearly at a speed of 0.5 $\mu m/s$ until it reaches a degree of compression of 50-70%. Figure 3.4 show the state of the system in the middle and at the end of the compression test.

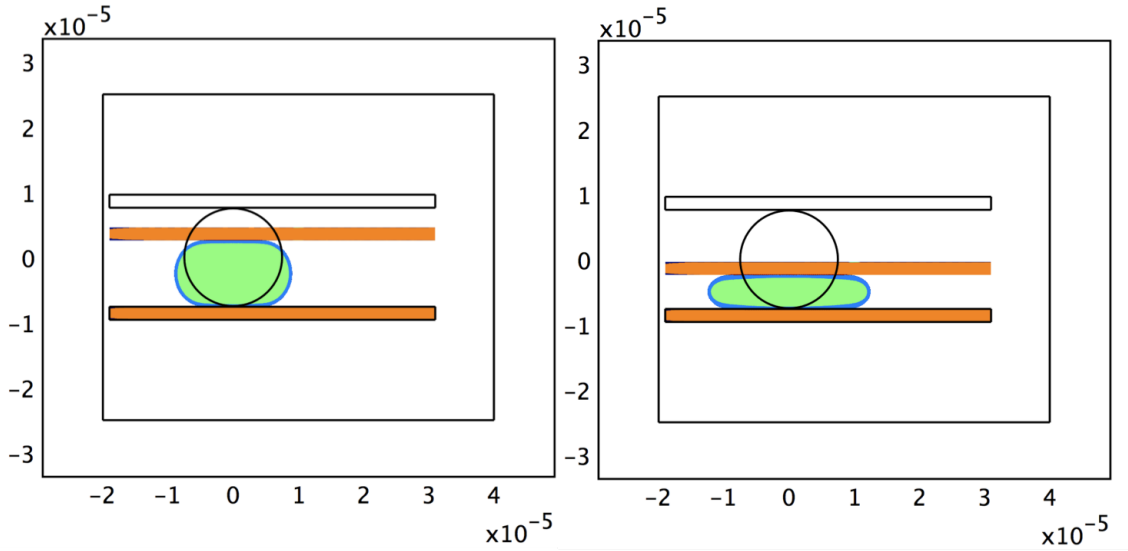

Figure 3.4: State of the system in the middle (Left, t=10s) and at the end (Right, t=20s) of the compression test. The compression plates in orange, the lamina in blue and the nucleoplasm in green.

Then, we can plot the stress and the force against compression rate (see Figure 3.5). The force needed to compress the nucleus up to 50% is around $9 \times 10^{-10} N$.

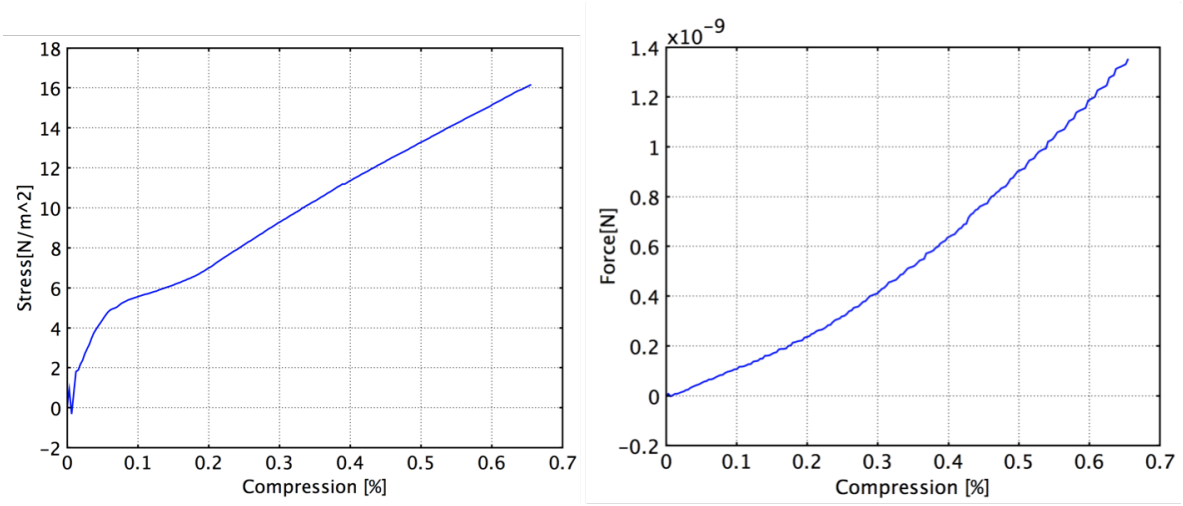

Figure 3.5: Left: Stress/Compression curve, Right: Force/Compression curve during our compression test

3.3 Discussion

The compression test on the nucleus gives a coherent behaviour of the nucleus during compression between two plates. Our test and the experimental setup from [Caille et al., 2002] being slightly different, this can account for the difference between the value of the force needed to compress the cell. Indeed, in the experimental setup, the nucleus has already adhered to the lower compression plate before it gets compressed, and the compression occurs in steps, leaving time for the nucleus to remodel its lamina as well as its chromatin; its mechanical properties would then evolve consequently. Moreover, the Young modulus of the nuclear lamina can range between 0.1 to 10 kPa, this uncertainty thus gives raise to a determining parameter that will need to be adjusted. Once the model is validated, we can safely use it and implement it in already existing confined migration models. It should also be pointed out that for computational reasons, the lamina of our nucleus is thicker than what can be observed in live cells: this is also an area for improvement.

4. Confined migration with a visco-elasto-plastic nucleus

In the previous chapter, we developed a model for the cell nucleus taking into consideration the plastic behaviour of the lamina and tested it in a compression test. The results were coherent with data from the literature, which allows us to use it in further cell models. In this respect, we decided to consider the confined, adhesion-based cell migration model developed in [Aubry et al., 2014] and incorporate our new nucleus model. We first present the main lines of the model that will be tested with four different micro-channels. The results will then be displayed and discussed.

4.1 Model

Based on previous research on modeling of cell confined migration [Allena, 2014] [Aubry et al., 2014], we implemented our visco-elasto-plastic nucleus in the confined migration model with some slight modifications. If the general mechanical equations and the geometry are the same (see Figure 4.1 and @Appendix A for more details), the rheological models used for the different parts of the cell are slightly different. Indeed, in our model, each part of the cell is governed by its own rheological model. The cortex , the cytosol and the nucleoplasm are considered a visco-elastic and the lamina is considered visco-elasto-plastic, with rheological models as in Figure B.1. As was stated previously [Allena, 2014] [Aubry et al., 2014] [Allena et al., 2013], there are four key aspects to our model :

- Newton's law, that provides the governing equations of the model.
- Active strains arising from polymerization of actin filaments and contraction of the actomyosin network, that reflect the cell ability to generate a pulsatile movement triggered by intrinsic signals not considered here.
- Passive contact forces against the channel and adhesion forces generated by focal adhesion complexes between the cell and the substrate, that govern how the cell will squeeze inside the channel and that enables the cell to adhere to the substrate and thus move forward.
- A tight synchronization between adhesion forces and active deformation, giving rise to a coherent motion of the cell.

The global equilibrium of the cell system is given by Equation 4.1

$$\rho \boldsymbol{a} = \boldsymbol{Div}_p(J\boldsymbol{\sigma}\boldsymbol{F}^{-T}) + \boldsymbol{f}_{adh} + \boldsymbol{f}_{channel} \tag{4.1}$$

where ρ is the cell density, $\boldsymbol{a}$ is the acceleration, $\boldsymbol{Div}_p$ is the divergence with respect to the initial position $\boldsymbol{p}$, J is the determinant of the deformation gradient $\boldsymbol{F}$ and $\boldsymbol{A}^{-T}$ is the inverse transpose of the matrix $\boldsymbol{A}$. $\boldsymbol{f}_{adh}$ denotes the viscous adhesive forces on the substrate and $\boldsymbol{f}_{channel}$ refers to the viscous force exerted by the channel on the cell.

Two main assumptions have been made to describe the oscillating movement of the cell that will then be turned into migration:

1. The protrusion and contraction that are governed by the active strains only occur in the cell cytosol. Indeed, we consider that the cyclic protrusion (respectively contraction) motion is

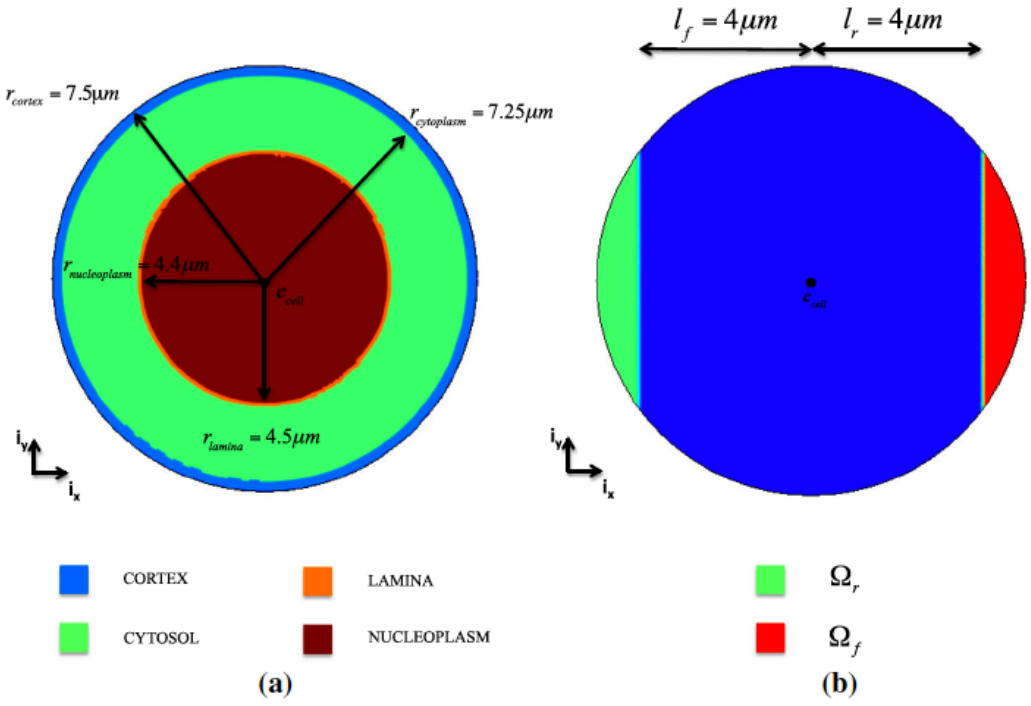

Figure 4.1: Geometry of the cell (**a**) and frontal and rear adhesion surfaces (**b**) [Aubry et al., 2014].

triggered by the polymerization (respectively depolymerization) of the actin filaments that lie in the cell cytosol. Polymarization only takes place at the cell front, while depolymerization takes place from the cell front towards the rear. Hence, except from the protrusion part that is specific to the cytosol, the nucleus will interact with the surrounding cytosol, even though it does not undergo any active strain [Friedl et al., 2011].

2. The cell is considered to form only one pseudopodium in the migration direction. To reproduce experimental setups from [Mélina L Heuzé, 2011], the migration occurs along the micro-channel axis, which is the horizontal axis $\boldsymbol{i}_x$.

The active deformation being triggered by actin filaments, the rheological model that we use for the cytosol thus includes this aspect (see Figure B.2).The solid active deformation tensor can thus be expressed as

$$\boldsymbol{\epsilon}_{cytosol,a} = \begin{cases} e_{a0} sin(2\pi \frac{t}{T}) h_{cytosol,front} \boldsymbol{i}_x \otimes \boldsymbol{i}_x & \text{if } sin(2\pi \frac{t}{T}) > 0 \\ e_{a0} sin(2\pi \frac{t}{T}) h_{cytosol} \boldsymbol{i}_x \otimes \boldsymbol{i}_x & \text{if } sin(2\pi \frac{t}{T}) < 0 \end{cases} \tag{4.2}$$

where e_{a0} is the amplitude of the active strain, t is the time, T is the migration period, $h_{cytosol,front}$ and $h_{cytosol}$ are two characteristic functions (see Appendix A) and $\otimes$ indicates the tensorial product.

For the cell not to oscillate on place, it needs to be able to create adhesion between its frontal and rear zones and the substrate. Moreover, this adhesion has to be tightly synchronized with the active deformation so that the cell can move forward. The adhesion is modeled as a viscous force and can be expressed as a frontal ($\boldsymbol{f}_{adh,f}$) and a rear ($\boldsymbol{f}_{adh,r}$) adhesion force (see Equation 4.3).

$$\boldsymbol{f}_{adh,f} = -\mu_{adh} h_{sync} (-\frac{\partial e_a}{\partial t}) \boldsymbol{v} \text{ on } \Omega_f$$

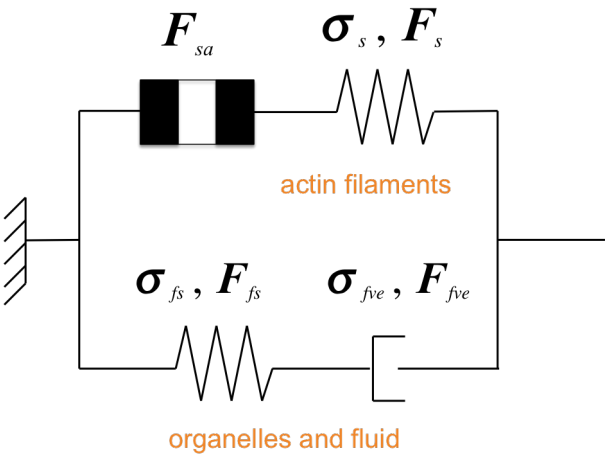

Figure 4.2: Rheological model for the cytosol, comprising active deformation in the actin filaments.

$$\boldsymbol{f}_{adh,r} = -\mu_{adh} h_{sync} (\frac{\partial e_a}{\partial t}) \boldsymbol{v} \text{ on } \Omega_r \tag{4.3}$$

where μ_{adh} is the friction coefficient with the substrate and $\boldsymbol{v}$ is the velocity. h_{sync} is the characteristic function that is the key to synchronization and cell migration since it couples the adhesive forces with the active deformation. Therefore, its action triggers the adhesion at the rear edge during cell protrusion, and the adhesion at the front edge during cell contraction.

To reconstitute micro-channel based assay from [Mélina L Heuzé, 2011], the micro-channel domain $\Omega_{channel}$ in our model is represented by two pseudo-elliptical rigid walls with no top roof. The cell 'feels' a viscous force from the walls once it enters the channel. Each wall (upper and lower) exert a viscous force on the cell that is normal to the wall surface. The detailed expression can be found in Appendix A.

4.2 Results

We present here the results of adhesion-based cell confined migration with the revised rheological model of the cell and particularly of the nucleus. The simulations were run using the finite elements software COMSOL Multiphysics 3.5.a ®. As described in the previous section, the cell is divided into four regions : the cortex, the cytosol and the nucleoplasm, which are modeled as viscoelastic, and the lamina, which is modeled as viscoelastoplastic. The radii of the the cell r_{cortex},$r_{cytosol}$,r_{lamina} and $r_{nucleoplasm}$ have been fixed to 7.5, 7.25, 4.5 and 4.4 μm, respectively. The mechanical properties of the cell areas and various parameters used in the model are the ones presented in Table 1 from Appendix A. The value of the plasticity threshold is taken to 3000 N^2/m^4. The channel is represented by two pseudo-elliptical walls, whose semi-axes a and b are 30 and 2 μm long, respectively. For the simulation, only two-thirds of the total length of the channel are considered, which corresponds to 40 μm. We have tested four different situations of confinement – three different widths of channel – by letting the position the upper and lower walls centers $\boldsymbol{c_{uw,i}}$ and $\boldsymbol{c_{lw,i}}$ vary as presented in Table 4.1. The viscous coefficient of the channel has been set equal to $10^{10} Pa.s/m$.

We have assessed the cell behaviour in the various configurations, its ability to enter the channel and the total covered distance, as expressed in Table 4.1. The total displacement refers to the cell rear total displacement at t-7000s for Channels 16 and 12 an t-4650s for Channel 10. $t_{contact}$ refers to the first contact of the cell with the channel and $t_{penetration}$ refers to time when the cell

body has fully penetrated the channel. For Channel 12, the cell only needs one supplementary protrusion/contraction cycle to fully penetrate the micro-channel compared to Channel 16, where the cell is not confined.

	Channel 16	**Channel 12**	**Channel 10**
Channel width $W_{c,1}$ (μm)	16	12	10
Position of the upper wall $c_{uw,i}$ (μm)	(42.5, 10)	(42.5, 8)	(42.5, 7)
Position of the lower wall $c_{lw,i}$ (μm)	(42.5, -10)	(42.5, -8)	(42.5, -7)
Total displacement (μm)	45	35	15
$t_{contact}$ (s)	–	1,800	1,500
$t_{penetration}$ (s)	3,300	3,900	–

Table 4.1: Main numerical results for confined migrations in the different channels

The cell appears to have a permeative behaviour as long as the channel width is much larger than the nucleus diameter. However, the cell is unable to migrate inside the channel when the channel dimensions become smaller than 10 μm and even more when it is sub-nuclear: the cell is then penetrating (see Figure 4.3). We can see that the cell average migration velocity is about

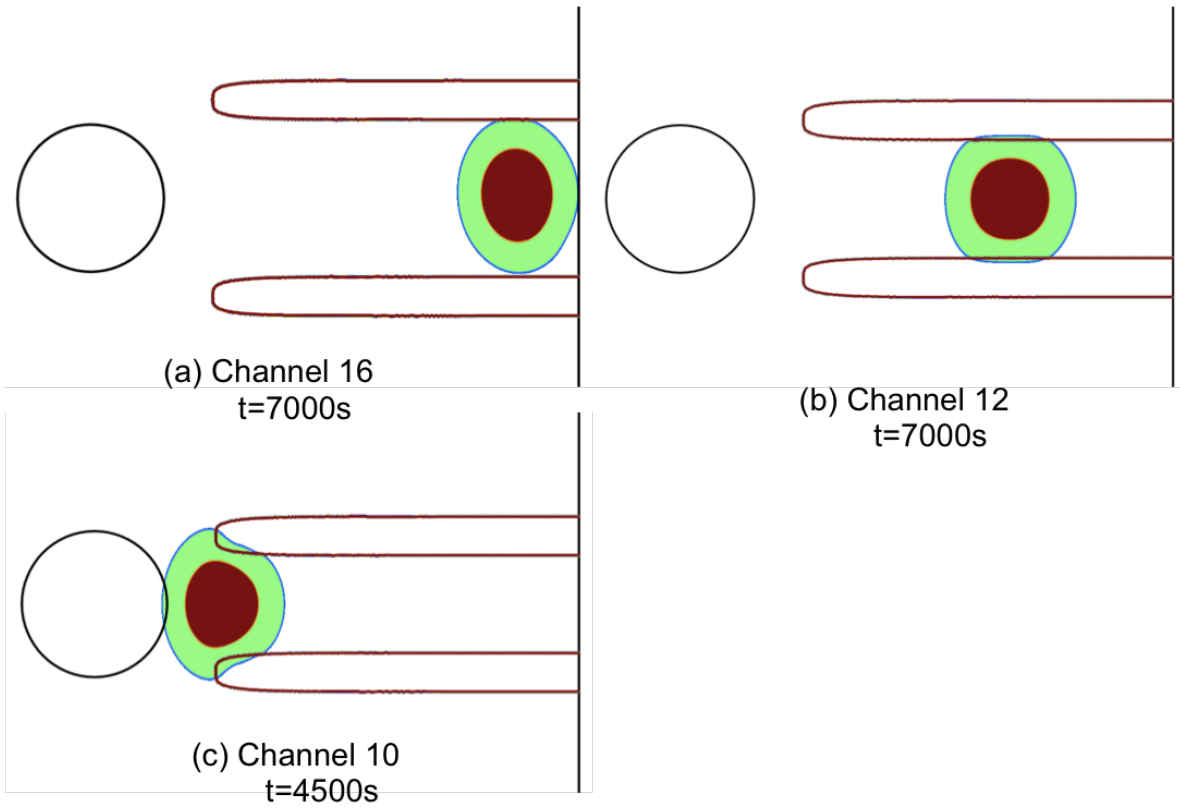

Figure 4.3: Snapshots of the permeative (a and b) and penetrating (c) cell during confined migration with a viscoelastoplastic nucleus

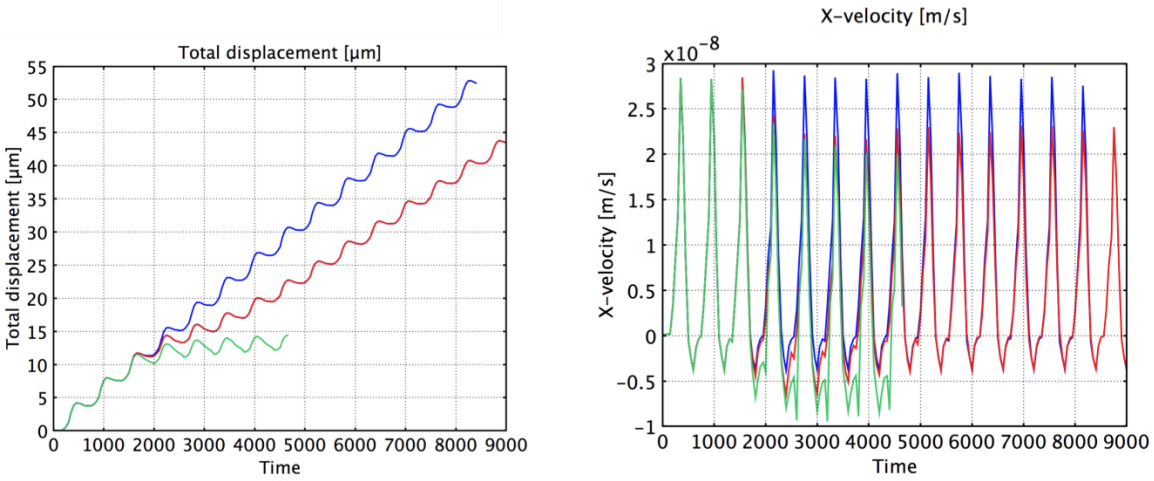

Figure 4.4: Total displacement of the cell (Left) and average cell velocity (Right) during confined migration in Channel 16 (blue), Channel 12 (red) and Channel 10 (green). Time is expressed in seconds.

4.3 Discussion

We implemented the viscoelastoplastic model of the nucleus from Chapter 3 in an existing confined migration model and compared our results to the ones from [Aubry et al., 2014] to see if the plasticity of the nucleus and the improvements from our model have a significant impact on cell confined migration. The previous study found the cell to have a permeative behaviour in channels with a diameter of 16 and 12 μm , an invasive behaviour in a channel of 7 μm diameter, and a penetrating one in a channel of $4\mu m$ diameter. In the first results, our model does not seem to show any invasive behaviour, but rather either a permeative one or a penetrating one for channels with aa diameter smaller smaller than 10 μm. Indeed, the cell manages to deform and migrate through sub-cellular channel, but the nucleus seems to be very limiting even before the channel dimensions become sub-nuclear. This comforts us on the influence the plasticity may have on cell migration in confined migration, and shows that our model might still be too simplified to be able to fully account for the cell behaviour in such environments. Indeed, experiments show that the cell is able to pass through sub-nuclear constrictions and this motivates us to push further our confined migration model. Another area of improvement would be to revise the mode of cell migration itself in confined environment, which will be the object of the following chapters.

5. Another mode of confined migration : chimneying

The model presented in Chapeter 3 reproduces an adhesion-based mode of migration. Nevetheless, another mode of migration is observed during 3D confined migration and particularly in cancer metastatic cells: bleb-based migration, or chimneying. Such mode of migration is fundamentally different since is does not require an adhesion with the substrate, but it is driven by actomyosin contraction of the rear edge of the cell which increases the hydrostatic pressure and hence leads to herniation of the membrane at the leading edge. As the cell is confined, the perpendicular forces that are exerted by the cell against the confining surface are sufficient to provide anchor points and to enable the cell to move forward. Chimneying is very often depicted in analogy with how one would climb a chimney. We decided to develop a model to mimic such migration mode. Here, the cell evolves in a pseudo-confined environment since it is seeded in a micro-channel and cannot spread freely as on a substrate, but it is not confined and squeezed to begin with.

In this chapter, we will first describe the different steps of the chimneying strategy and introduce a fully deterministic preliminary 1D model. Out of the four aspects from the adhesion-based migration model (see Chapter 4), there are three key aspects that drive our model:

- Newton's law, that provides the governing equations of the model.
- Active strains, that reflect the cell ability to generate a pulsatile movement triggered by intrinsic signals not considered here.
- Contact forces, which are of major importance in chimneying since they provide the anchoring the cell needs to move forward and not slide on the substrate.

Chimneying takes place in several steps. First, the cell rear extends until it reaches the walls of the channel (this is the initialisation phase). Once the contact occurs, the uropod builds on the walls and a perpendicular force arises, allowing the cell to anchor to the micro-channel walls. Then, the cell elongates and forward protrusions expand until contact with the micro-channel in ensured and similar perpendicular forces are developed. The cell being anchored at the front, the uropod can retract and the cell goes back to its initial length by pulling on its rear. At that point, the rear expands again until it touches the wall and the frontal protrusions can retract. Then, cycle then starts again. It is important to notice that, in such migration mode, the cell always keeps an anchor point to the micro-channel wall otherwise it would freely glide. It would be like telling a rock climber to stop exerting force against the walls of the chimney: he would most certainly fall down...

5.1 Models with active lateral and longitudinal strains

5.1.1 A priori synchronized model

We will present here the governing equations of the model. Throughout the whole study, the micro-channel is considered parallel to the x axis. In this model, the micro-channel geometry can vary and has a characteristic equation that depends on x. he cell geometry is quite basic and it is represented by three rectangles : one for the cell body, in the same direction as the channel, and two orthogonal ones for the uropod and the frontal blebs as depicted in Figure 5.1.

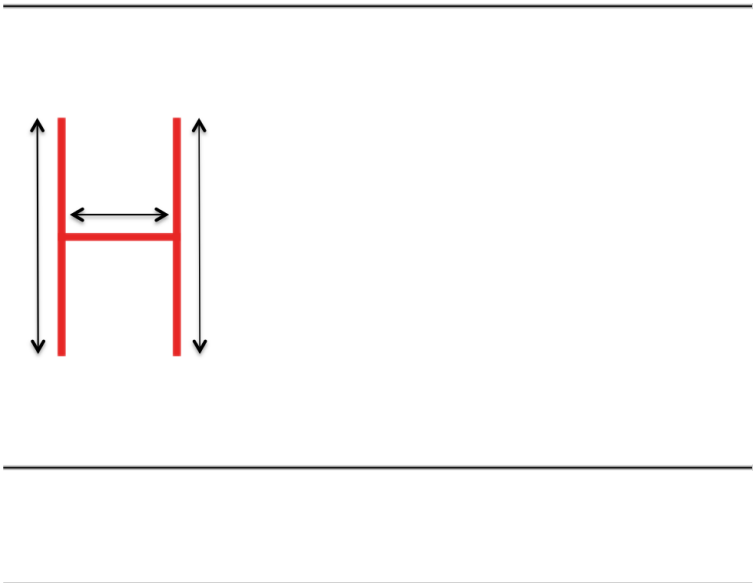

Figure 5.1: Simple geometry of the problem: the cell is represented in red inside the channel (in black). The black arrows feature the possible motion (extension and contraction) of the different regions of the cell (front, rear and body).

The contact force has been defined to slightly increase as the bleb or the uropod approaches the micro-channel wall, so that it is slowed down. However, the force sharply rises after contact has occurred (see Figure 5.2). Then, it reads :

$$F_c(x,y) = \begin{cases} T_n e^{k_n \frac{y-y_0(x)}{T_n}} & \text{if } y < y_0(x) \\ \frac{k_n^2}{2T_n} y^2 + (k_n - \frac{k_n^2}{T_n} y_0(x))y + (T_n - k_n y_0(x) + \frac{k_n^2}{2T_n} y_0^2(x)) & \text{if } y > y_0(x) \end{cases} \tag{5.1}$$

with T_n the nominal force, k_n the stiffness and $y_0(x)$ the distance between the bleb and the micro-channel wall.

The active deformations are then defined for the rear, the front and the cell body as follows :

$$\epsilon_{rear}(x,t) = y_{crit}(x)(\sin(\frac{t - \frac{T_a(x)}{4}}{T_a(x)}) + 1) \tag{5.2}$$

$$\epsilon_{front}(x,t) = \begin{cases} 0 & \text{if } 2\pi \frac{t - T_a(x+l_{cell})\frac{1}{2}}{T_a(x+l_{cell}} < 0 \\ \epsilon_{rear}(x + l_{cell}, t) & \text{if } 2\pi \frac{t - T_a(x+l_{cell})\frac{1}{2}}{T_a(x+l_{cell})} > 0 \end{cases} \tag{5.3}$$

$$\epsilon_{cellbody}(x,t) = \begin{cases} y_{crit}(x)\sin(2\pi \frac{t - \frac{T_a(x)}{2}}{T_a(x)}) & \text{if } \frac{\partial \epsilon_{front}(x,t)}{\partial t} > 0 \\ 0 & \text{if } \frac{\partial \epsilon_{front}(x,t)}{\partial t} < 0 \end{cases} \tag{5.4}$$

with l_{cell} the cell length along the x axis, t the time and $y_{crit}(x)$ the distance between the bleb and the micro-channel wall until a sufficient contact force is developed and ensures the anchoring of the cell. $T_a(x)$ is defined such that the velocity of the active deformation is constant and does not depend on the geometry of the channel: $T_a(x) = \lfloor 2\pi \frac{y_{crit}(x)}{v_{bleb}} \rfloor$, with v_{bleb} the average blebbing velocity.

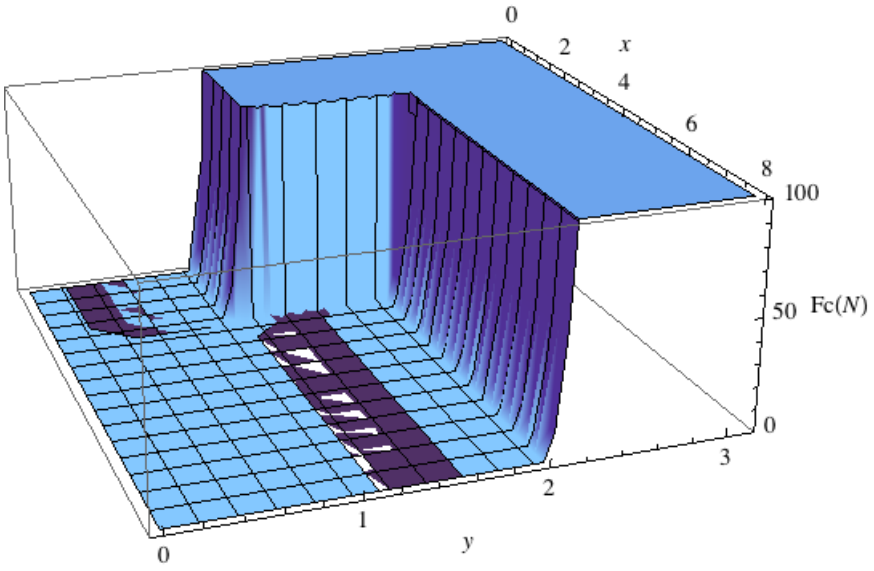

Figure 5.2: Representation of the contact force in the case of a channel with a step at x=2

During chimneying, we no longer need synchronization between active strains and adhesion forces since the anchoring of the cell is determined by the perpendicular contact forces. Hence, when the uropod is extended towards the wall, the cell rear is anchored, while when the frontal blebs are extended, the cell front is anchored.

5.1.2 Self-regulated model: confined migration

As a second approach, we decided to implement the chimneying mode of migration into a finite elements model to get a deeper insight of the cell behaviour during confined migration. The cell geometry was defined as by an initial rectangular shape with rounded corners. The contact forces and the active strains are applied at the front, the rear and the center of the cell, which are represented by caracteristic functions, and the channel is defined by an elliptic function, as in [Aubry et al., 2014] (see Figure 5.3). To simplify the calculations, the cell is considered to be an isotropic elastic material. The viscous forces exerted by the channel are the same as those used for the nucleus study in Chapter 2 (see also [Aubry et al., 2014] [Allena, 2014]).

This model is intrinsically different from the previous one, since the active strains inside the cell are self-regulated. In fact, the active strain of each part of the cell – rear, front and body – is defined using pulses that are integrated to generate the desired signal. Thus, an extension – or a retraction – is defined by the coupling of Heaviside functions. A series of conditions are used to mimic the cell 'decision process' during pseudo-confined migration (see Table B.1). In the following, the full definition of the cell motion is presented.

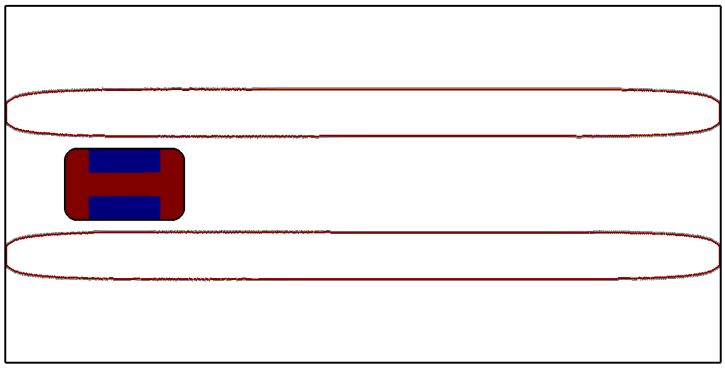

Figure 5.3: Geometry of the self-regulated finite model: cell and channel. The cell regions where active strains and contact forces are applied are represented in dark red.

Rear blebs

The motion of the rear blebs is regulated by a pulse P_{rear} which is divided into three phases, each defined by a Heaviside function. The phases are themselves determined by the combination of various conditions.

$$P_{rear} = h_{r,initialisation} + h_{r,extension} - h_{r,retraction} \tag{5.5}$$

- Initialisation: the rear blebs expand while the cell is not elongated (a), the frontal blebs are not extended (b) and while they have not reached the walls of the micro-channel (c).

$$\begin{aligned} h_{r,initialisation} &= c_{m,init} \times (1 - c_{f,ch}) \times (1 - c_{r,ch}) \\ &= a \times b \times c \end{aligned} \tag{5.6}$$

- Extension: the rear blebs will expand when the frontal blebs are pushing on the walls (a), while the cell is not elongated (b) and as long as they do not reach the channel walls (c).

$$\begin{aligned} h_{r,extension} &= c_{f,ch} \times c_{m,init} \times (1 - c_{r,ch}) \\ &= a \times b \times c \end{aligned} \tag{5.7}$$

- Retraction: the rears blebs will retract when the frontal ones reach the channel walls (a) and while the cell is elongated. This phase will stop when the cell is back to its initial length (b).

$$\begin{aligned} h_{r,retraction} &= c_{f,ch} \times (1 - c_{m,init}) \\ &= a \times b \end{aligned} \tag{5.8}$$

Frontal blebs

The motion of the frontal blebs is regulated by a pulse P_{front} which is divided into two phases, each defined by a Heaviside function.

$$P_{front} = h_{f,extension} - h_{f,retraction} \tag{5.9}$$

- Extension: the frontal blebs expand when the rear blebs are pushing on the walls (a), the frontal blebs are still expanding (b) and until they have not reached the channel walls (c).

$$\begin{aligned} h_{f,extension} &= c_{r,ch} \times c_{f,exp} \times (1 - c_{f,ch}) \\ &= a \times b \times c \end{aligned} \tag{5.10}$$

- Retraction: they retract when the rear blebs are pushing off the walls (a), the cell is not elongated (b) and until they have come back to their initial state (c).

$$\begin{aligned} h_{f,retraction} &= c_{r,ch} \times c_{m,init} \times (1 - c_{f,init}) \\ &= a \times b \times c \end{aligned} \tag{5.11}$$

Cell body

The cell elongates when the frontal blebs expand and it retracts with the rear blebs.

Name	Description
$c_{f,init}$	Condition that is true when the frontal blebs are in their initial state (not elongated)
$c_{f,ch}$	Condition that is true when the frontal blebs are pushing on the channel walls
$c_{f,exp}$	Condition that is true when the frontal blebs are expanding
$c_{r,ch}$	Condition that is true when the rear blebs are pushing on the channel walls
$c_{m,init}$	Condition that is true when the cell body is in its initial state (not elongated)

Table 5.1: Conditions used to define the self-regulated motion of the cell

5.2 Results

The numerical simulations have been run using Mathematica®9 and the finite elements software COMSOL Multiphysics®3.5a . The focus of these models being mainly on the implementation of a new migration mode, the cell was considered as an isotropic elastic material, with a Young modulus equal to 10 Pa and a Poisson ratio of 0.4. The cell geometry is a rectangle (10 μm long and 6 μm wide) with cornered angles. The active strains are applied to three part of the cell: the frontal and the rear parts, which are both 2 μm long and 6 μm wide, and the cell body, which is 6 μm long and 2 μm wide (see Figure 5.3). The cell density has been set to 1,000 kg/m^3 and the channel wall have been placed 1 μm away from the cell. The intensity of the active strain rate has been set to 0.1.

5.2.1 A priori synchronized model

For this model, we chose to focus our study on two different channels: a straight channel and a channel with a step. The successive phases of the simulations can be seen in Figure 5.4: in both cases, the cell behaved as expected and followed the steps of migration. Additionally, it was also able to adapt to the step present in the second type of channel and to expend its blebs further so they would go push on the channel walls.

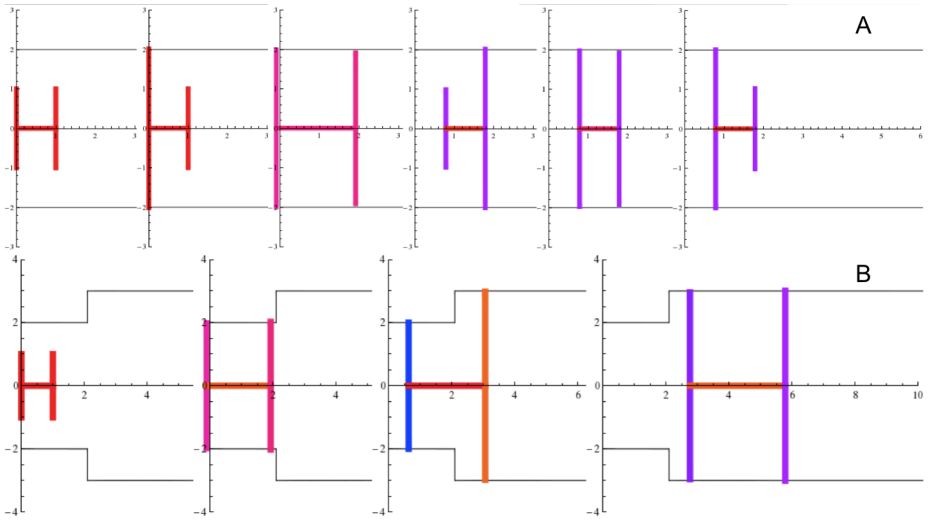

Figure 5.4: Successive phases of the deterministic chimneying migration in (A) a straight micro-channel and (B) a micro-channel with a step.

5.2.2 Self-regulated model: confined migration

For this finite elements simulation, we have studied the cell behaviour during pseudo-confined migration in a straight channel, where the cell active strains are no longer defined a priori, but are self-regulated depending on various conditions previously defined. The cell is able to generate a forward movement by cyclically pushing off the walls of the channel and creating anchor points to translocate (see Figure 5.6). As expected, the rear blebs expand and once they touch the channel (b), the frontal bleb as well as the cell body start protruding , while the rear is anchored to the channel. When the frontal blebs reach the channel (c), they anchor to the wall and the rear of the cell body retracts as well as the rear bleb (d). Then, then rear blebs expend until they touch the channel walls (e) and eventually, the frontal blebs slightly retract (f) and the cycle restarts. The displacement of the various regions of the cell is depicted in Figure 5.5 and the velocity of the cell rear is shown in Figure 5.7. The cell has an average migration velocity of 1-4 $\mu m/s$ that is calculated at the cell rear.

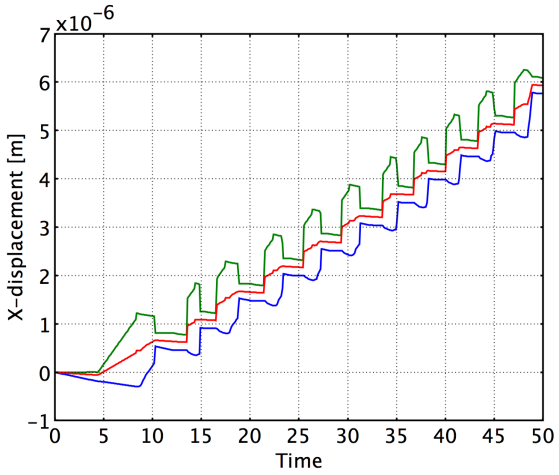

Figure 5.5: Total displacement of each cell region during pseudo-confined and self-regulated chimneying migration. The blue line stands for the cell rear, the green one for the cell body and the red one for the cell front.

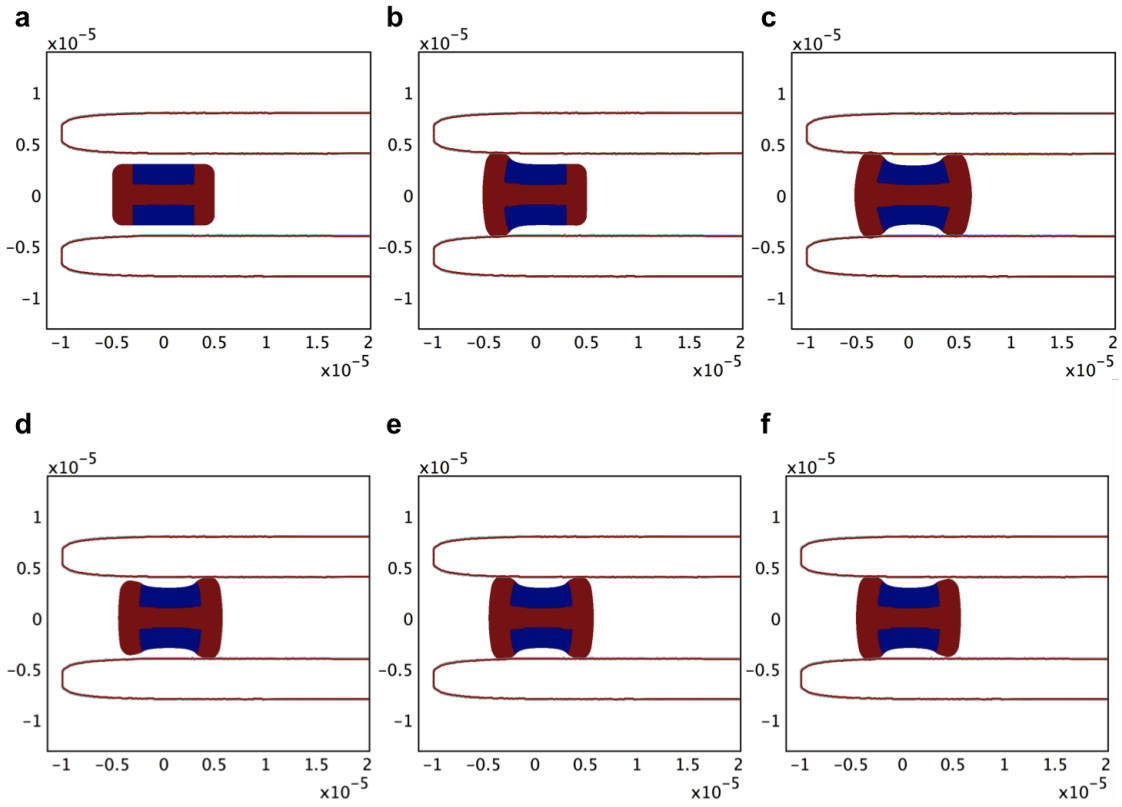

Figure 5.6: Successive phases of the self-regulated chimneying migration in a straight micro-channel. (a) Initial state of the cell; (b) extension of the rear blebs; (c) lateral extension of the cell simultaneous to the the frontal blebs extension; (d) rear blebs contraction; (e) rear blebs extension; (f) frontal blebs contraction.

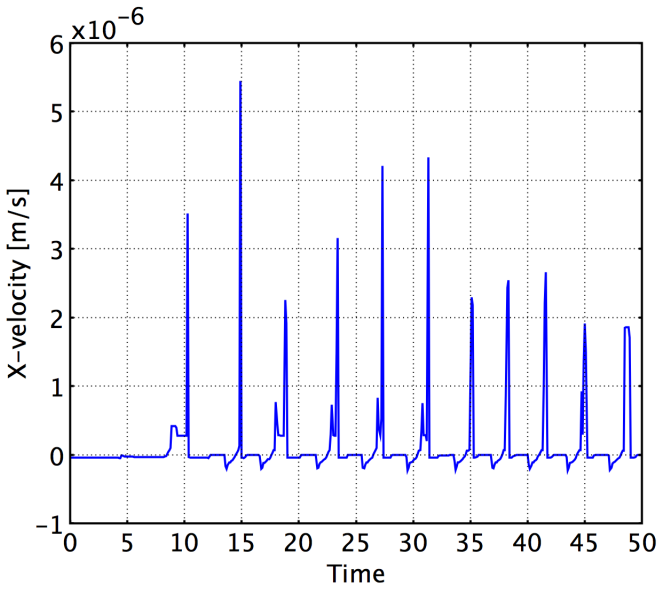

Figure 5.7: Average velocity of the cell during pseudo-confined self-regulated chimneying migration

5.3 Discussion

The deterministic model (Sec. 5.1.1) gave us a preliminary analysis and a good insight of how the cell should behave during chimneying migration. Nonetheless, this model is very limited since we fully determined the active strains as a function of the channel geometry. Hence, it is very useful as an intermediate tool, but we need to develop a more realistic model. That drove us to work on a migration model with self-determined active strains of the cell (Sec. 5.1.2). Here, the cell is able to 'feel' when the perpendicular force it applies on the wall by pushing against it is enough to anchor itself and keep steady. If this is the case, depending on its strain state –elongated cell body, expanded or retracted blebs–, it triggers the next motion phase, that in the end results in a forward movement. Our model can still be improved since we can see that the blebs do not completely retract before starting their next extension phase.

Pseudo-confined chimneying takes in the major properties of chimneying migration and successfully gets rid of the necessity for focal adhesions. However, chimneying seems to occur in rather fully confined environment and our previous model is thus a springboard to a more lifelike approach. Indeed, in such an approach, the rear blebs would disappear and the cell forward motion would be governed by the mere contraction of its rear. We started working on such an approach which is described in the next section. Our pseudo-confined migration model is nonetheless very interesting in that we introduced a self-regulated migration system: a cell that is able to feel its environment and to migrate consequently. This is the first step towards a more realistic model for confined migration in which the cell would be left to its own fate and would adapt its migration strategy according to its environment.

In this chapter, we tackled this issue of another mode of migration in which the cell does not need to form focal adhesions with the substrate anymore, but it pushed against the confining surfaces and generate a perpendicular force that will act as an anchor point. We developed two models mimicking the behaviour of a rock-climber in a chimney. In the first model, the synchronization between the active strains and the adhesion to the walls is entirely controlled by our inputs, and it results into a perfect cyclic movement of the cell that is fully deterministic. The aim of the second model was to introduce a self-regulation in the cell motion. The protrusion and contraction of each region of the cell is governed by a combination of strain conditions; then the cell current state regulates its migration. This latest model works fine but experimental observations show that the cell motion during chimneying differs slightly from the one we developed. The next chapter thus introduces a more lifelike model of chimneying.

6. A more lifelike chimneying model

The previous model relied on the extension and retraction of both rear and frontal bleb to push on the micro-channel walls and allow a forward movement of the cell. Experimentally, the cell appears not to have rear extensions but only a contraction at the rear which governs its migration. In this chapter we develop such a lifelike chimneying model and present our preliminary results.

6.1 Governing equations of the model

To be more realistic compared to experimental observations on cell confined migration, in this new model, the only active deformation that is needed is the contraction of the cell rear, as expressed in Equation 6.1. This increases the intracellular hydrostatic pressure, leading to herniation of the membrane at the leading edge and the nucleation of a bleb. Thanks to the confinement, the bleb itself become compressed when it touches the walls, and it is therefore anchored. Then the cycle will resume and a new bleb will form on top of the first one. Little by little, the cell is thus able to migrate forward.

$$\epsilon_{rear}(t) = \epsilon_0(-\sin(2\pi\frac{t-\frac{T_a}{4}}{T_a}) - 1) \tag{6.1}$$

with $\epsilon_0 = \frac{(r_{channel}-r_{bleb})}{4}$, $r_{channel}$ the inner radius of the channel and r_{bleb} the frontal bleb radius.

As for the previous model, we began by implementing a simple model in Mathematica ®. The cell is considered as an elastic material in which the formation of blebs at the leading edge is governed by the pressure increase from the rear contraction. The evolution of the rear-contraction-generated pressure $P_{fluid}(t)$ is described by Equation 6.2. The cell also feels a viscous forces from the channel as described in Equation 4.1. The forward migration is enabled by the force exerted by the cell pushing off the walls

$$m_{fluid}\frac{\mathrm{d}^2P_{fluid}(t)}{\mathrm{d}t^2} + \mu_{fluid}\frac{\mathrm{d}P_{fluid}(t)}{\mathrm{d}t} + P_{fluid}(t) = -k_{fluid}.y_r(t) \tag{6.2}$$

with m_{fluid} the very low mass of the fluid, μ_{fluid} the damping coefficient, and k_{fluid} the compressibility of the fluid. In this study, the cell geometry is defined by simple sticks,as in Section 4.1, and will be represented by a fitting polynomial but it is now fully confined in the channel (see Figure 6.1).

6.2 Results and Discussion

We present here some preliminary results from this study. The rear contraction sucessfully generates a pressure that governs the nucleation of a bleb at the cell front. Figure 6.2 illustrates the profiles of the cell behaviour during chimneying. Thanks to these pressure 'pulses', the cell migrates succesfully through the channel.

This model is very simplistic and would require some improvement. Indeed, it is still quite deterministic and it would be interesting to have a self-regulated model, as for pseudo-confined migration. Moreover, we observe that the cell rear has a net tendency to glide over the surface, while experimental observations do not highlight such a behaviour.

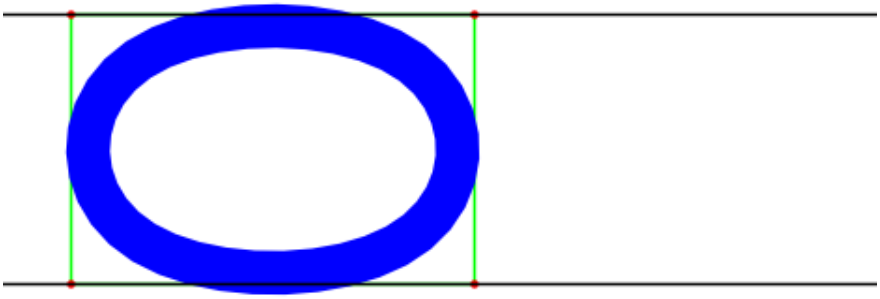

Figure 6.1: Simple geometry for the study of chimneying 2.0. The cell is represented in blue, the channel in black, and the red dots are the points for the polynome interpolation

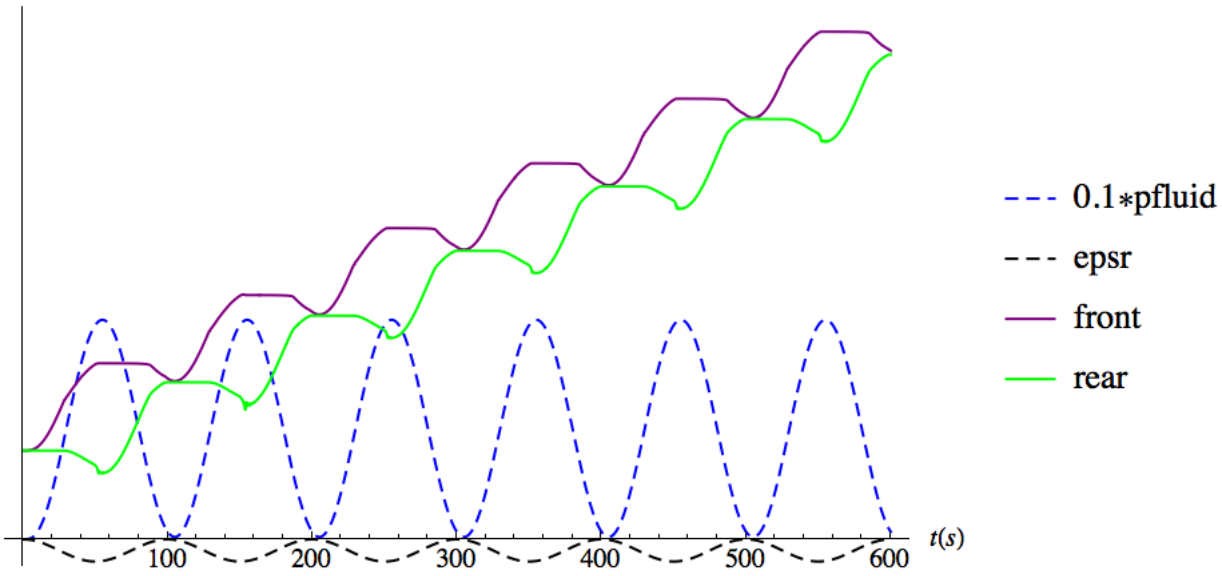

Figure 6.2: Profiles of the cell behaviour during chimneying. epsr is the contraction of the rear, pfluid is the pressure generated by such a contraction, and front and rear are respectively the motion of the cell front and cell rear along the channel axis.

Conclusion

This master thesis tackles various aspects of cell confined migration in order to gain a deeper understanding of this phenomenon that is so crucial to the development (embryogenesis) and survival (immune system) of a living organism, and that also rules so diseased processes like cancer metastasis. Our work is based on two main observations: some cells are able to break their lamina while migrating through sub-nuclear constrictions to ensure an easier translocation, and the prominent migration mode in 3D confined environment does not appear to be adhesion-based, but rather contraction-based. Based on these, we decided to work on the improvement of the model of the cell nucleus, and on the implementation of contraction-based confined migration, also referred to as chimneying.

In previous work, the nucleus was merely described as a viscoelastic material. Some cells ability to break their lamina could be a sign of a certain plasticity of the nucleus, which we decided to implement in the nucleus model since it had never been considered before. The cell nucleus is composed of two areas : the viscoelastic cytosol and the viscoelastoplastic surrounding lamina that each have different mechanical properties. The model was tested under compression in a 2D finite elements simulation and compared to experimental data to assess its validity. Although it still needs refinement, the results from the simulation are consistent enough to let us use this model onwards. Hence, we updated the previous confined migration model by using the viscoelastoplastic model of the nucleus and by using two different viscoelastic rheological models for the cell cortex and the cell cytosol. As a result, the rate-limiting role of the nucleus seemed to be enhanced, since the cell is now unable to pass through a sub-nuclear micro-channel. This might be the sign that there mere input of plasticity in the cell nucleus model is not enough to fully describe the cell behaviour during confined migration, and that the current model still has some improvement to go through. Moreover, the migration mode used here is adhesion-based, while cells in 3D confined migration rather use a contraction-based mode.

Our second axis of study thus focuses on implementing chimneying as a migration mode. Chimneying is sometimes simply described as a migration mode mimicking the behaviour of a rock-climber in a chimney, and sometimes described more in details. In the latter case, the governing process is said to be the contraction of the actomyosin network at the rear of the cell, which generates an overpressure inside the cytosol and comes to herniation of the cell membrane at its leading edge: a bleb is formed. As the cell in confined by its environment, forces are generated, perpendicular to the confining surfaces, that act as anchor points for the cell and ensure its forward movement. First, we developed a deterministic model in which the cell acts as a rock-climber in a chimney. This migration mode was then implanted in a 2D finite element model and was improved to become self-regulated: a set of conditions on the cell strain state governs each migration phase in the different cell regions (cell front, back and body). A more lifelike model is currently under development and already shows promising results for cell migration in a fully confined environment.

Confined cell migration has been a trending research topic in the past decades but only recently did mechanical models of such process start to be developed. This makes it a most interesting area since so much remains uncovered. This thesis aspires to shed some new light on the mechanics of cell confined migration and to open up new paths for further research.

A. Confined migration model

Biomech Model Mechanobiol
DOI 10.1007/s10237-014-0595-3

ORIGINAL PAPER

A computational mechanics approach to assess the link between cell morphology and forces during confined migration

D. Aubry · H. Thiam · M. Piel · R. Allena

Received: 12 December 2013 / Accepted: 12 May 2014

Abstract Confined migration plays a fundamental role during several biological phenomena such as embryogenesis, immunity and tumorogenesis. Here, we propose a two-dimensional mechanical model to simulate the migration of a HeLa cell through a micro-channel. As in our previous works, the cell is modelled as a continuum and a standard Maxwell model is used to describe the mechanical behaviour of both the cytoplasm (including active strains) and the nucleus. The cell cyclically protrudes and contracts and develops viscous forces to adhere to the substrate. The micro-channel is represented by two rigid walls, and it exerts an additional viscous force on the cell boundaries. We test four channels whose dimensions in terms of width are i) larger than the cell diameter, ii) sub-cellular, ii) sub-nuclear and iv) much smaller than the nucleus diameter. The main objective of the work is to assess the necessary conditions for the cell to enter into the channel and migrate through it. Therefore, we evaluate both the evolution of the cell morphology and the cell-channel and cell-substrate surface forces, and we show that there exists a link between the two, which is the essential parameter determining whether the cell is permeative, invasive or penetrating.

Keywords Confined cell migration · Continuum mechanics · Computational mechanics · Forces

1 Introduction

In our previous works (Allena and Aubry 2012; Allena 2013), we have presented numerical models which helped to understand the mechanisms controlling cell motility on two-dimensional (2D) flat surfaces. Nevertheless, during many biological processes such as embryogenesis, immunity and tumorogenesis, cell migration takes place in confined environments of tissues (Friedl and Wolf 2010). In these cases, cell locomotion is influenced by the presence of attractant molecules, but also by the morphology of the extracellular matrix (ECM). In fact, the surrounding tissues may vary in terms of heterogeneity, fibres density and organization. As shown both experimentally (Erler and Weaver 2009; Wolf et al. 2009; Egeblad et al. 2010; Friedl and Wolf 2010) and theoretically (Zaman et al. 2005, 2006, 2007; Scianna et al. 2013), the width of the ECM pores, the degree of ECM alignment as well as the ECM stiffness are fundamental parameters, which determine how and how much the ECM steers or inhibits the cell movement. Therefore, the cell needs to continuously adapt its shape and consequently its migratory behaviour. In tumorogenesis for instance, cancer cells develop an invasive behaviour, which allows them to enter and progressively invade healthy tissue as they are constantly exposed to biomechanical and biophysical stimuli. Such adaptation requires an internal reorganization of both the cytoskeleton and the embedded organelles, among which the nucleus is the stiffest and the most voluminous. Consequently, it has become essen-

Electronic supplementary material The online version of this article (doi:10.1007/s10237-014-0595-3) contains supplementary material, which is available to authorized users.

D. Aubry
Laboratoire MSSMat UMR CNRS 8579, Ecole Centrale Paris, 92295 Châtenay-Malabry, France

H. Thiam · M. Piel
Biologie systémique de la division et de la polarité cellulaire, Institut Curie UMR 144, 12 Rue Lhomond, 75005 Paris, France

R. Allena ( )
Arts et Metiers ParisTech, LBM, 151 Bd de l'hôpital, 75013 Paris, France
e-mail: Rachele.allena@ensam.eu

Published online: 04 June 2014

tial to quantitatively assess the cell ability to deform as well as which mechanical forces the cell has to develop in order to move forward within a confined micro-structure.

In the last few years, several experimental studies have tried to provide such data. Systems like collagen gels or lattices are commonly used to simulate cell migration in confined connective tissues (Wolf et al. 2009). Although very simplified, such systems are highly complex and difficult to control since many physical parameters (i.e. gel density and elasticity, local constrictions) may affect the global mobility of the cell and furthermore fail to reproduce spatial tracks or obstacles (Provenzano et al. 2008; Wolf et al. 2009; Egeblad et al. 2010). More recently, it has been possible to better control, vary and tune the geometrical characteristics of the patterned micro-structure using micro-laser techniques (Ilina et al. 2011) or photolithography (Heuzé et al. 2011). In the latter work, cells migrate through straight micro-channels made of silicone rubber (i.e. polydimethylsiloxane, PDMS), whose sub-cellular dimensions vary between 2 and 10 μm in width and highly depend on cell type. Such an approach has provided interesting results for cancer cells (Irimia and Toner 2009; Ronot et al. 2000), immune cells (Irimia et al. 2007; Faure-André et al. 2008) and neurons (Taylor et al. 2005). Micro-channels may be modulated in order to investigate specific biological problems such as trans-migration ability within a well-defined geometry or the influence of the substrate stiffness by letting channel material vary. Additionally, more complex geometries can be obtained to force the cell to take turns and explore its 2D confined environment.

From a numerical point of view, many models have been proposed to simulate single cell migration on 2D flat surfaces or in three-dimensional (3D) environment (Rangarajan and Zaman 2008). Such models have used different approaches resulting in force-based dynamics models (Zaman et al. 2005, 2006), stochastic models to simulate persistent random walks (Tranquillo and Lauffenburger 1987; Tranquillo et al. 1988; Stokes et al. 1991; Stokes and Lauffenburger 1991), models reproducing the movement of cancer cell spheroids (McElwain and Ponzo 1977; McElwain 1978; McElwain et al. 1979), Monte Carlo models (Zaman et al. 2007; Scianna and Preziosi 2013; Scianna et al. 2013) or purely mechanical models (Allena and Aubry 2012; Allena 2013). Active gel layers submitted to external forces have been used to represent acto-myosin cells migrating in a free (Recho and Truskinovsky 2013; Recho et al. 2013) or confined (Hawkins et al. 2009; Hawkins and Voituriez 2010) environment. Scianna and Preziosi (Scianna and Preziosi 2013) have presented a cellular potts model (CPM), which reproduces an experimental assay very similar to those used in (Taylor et al. 2005; Irimia et al. 2007; Faure-André et al. 2008; Irimia and Toner 2009; Rolli et al. 2010; Heuzé et al. 2011). In this model, the cell is modelled as a discrete physical unit, including the cytosol and the nucleus, while channels of different widths constitute the migration chamber. The authors have investigated the invasiveness of tumour cells by evaluating their displacement and velocity as well as their deformability, which seems to be strongly linked to the deformability of the nucleus. In (Tozluoğlu et al. 2013), a hybrid agent-based finite element model is proposed to evaluate the migration strategy of the cell in different environments such as confinement. The model is able to simulate both the protrusion–contraction and the membrane blebbing modes of migration. Therefore, the authors estimate the effects of the ECM geometry on the relationship between cell velocity, contractility and adhesion, and they also find interesting effects of membrane blebbing on cell velocity and morphology. Finally, in (Giverso et al.), an energetic continuum approach is employed to investigate the necessary condition for which a cell migrate through a cylindrical channel. They consider the nucleus either as an elastic membrane surrounding a liquid droplet or as an incompressible elastic material. By taking into account and balancing different forces exerted by and on the cell during confined movement, they are able to determine the minimal size of the cylindrical structure and they observe that cell ability to migrate through it depends on both nucleus stiffness and adhesion to ECM.

1.1 Objective of the present work

In the present paper, a finite element model that reproduces the experimental set-up used in (Heuzé et al. 2011) for HeLa cells is proposed, which is based on the following hypotheses:

- the 2D geometry represents a top view of the global structure, and a plane stress hypothesis has been made;
- as in (Giverso et al.), a purely mechanical approach is used to describe the cell behaviour. However, a different mathematical method is applied. In fact, the decomposition of the deformation gradient is employed to consider both the active (i.e. protrusion and contraction) and the elastic (i.e. strains generated by the interaction with the environment) strains undergone by the cell;
- contrary to previous works (Scianna and Preziosi 2013; Scianna et al. 2013; Tozluoğlu et al. 2013), the cell is modelled as a continuum. Nonetheless, both the cytoplasm and the nucleus have been originally represented through two characteristic functions, and a standard Maxwell model has been used to describe their viscoelastic behaviour (Allena and Aubry 2012; Allena 2013; Tozluoğlu et al. 2013);
- the cell is able to cyclically protrude and contract. Such active strains are triggered respectively by the polymerization and depolymerization of the actin filaments and are synchronized with the viscous adhesion forces between the cell and the substrate (Allena and Aubry 2012; Allena 2013);

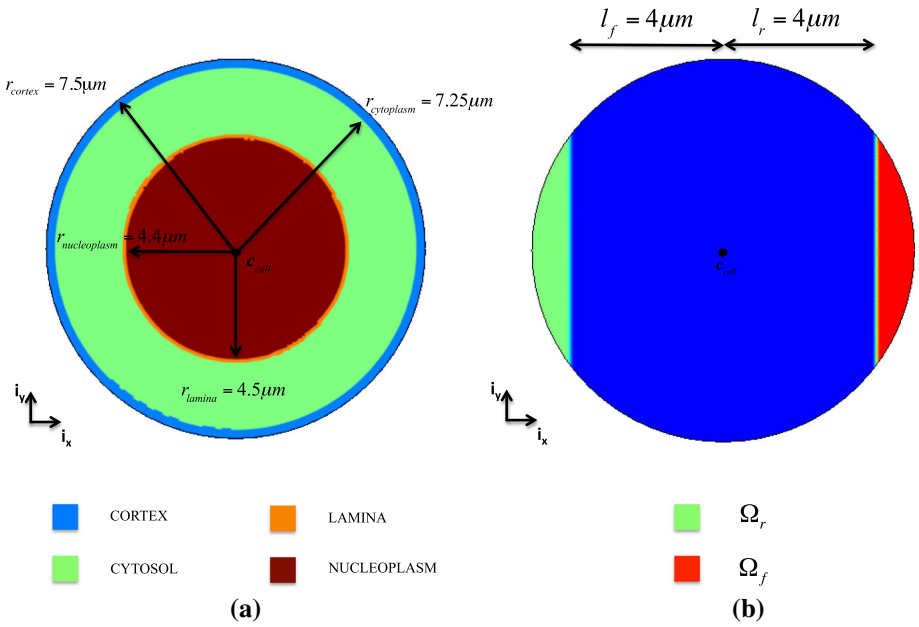

Fig. 1 Geometry of the cell (**a**) and frontal and rear adhesion surfaces (**b**)

– the micro-channel is represented by two rigid walls, which are described by two characteristic functions, and exerts an additional normal viscous force on the cell boundaries when contact condition is fulfilled.

The main objective of our work is to assess the necessary conditions for the cell to enter into the channel and migrate through it. In order to do so, we test four different channels whose dimensions in width are i) larger than the cell diameter, ii) sub-cellular, iii) sub-nuclear and iv) much smaller than the nucleus diameter. We analyse the evolution of the cell morphology by consistently comparing it with experimental observations, and we classify the cell behaviour according to the covered distance inside the channel. Additionally, we evaluate both the cell-substrate and the cell-channel surface forces during migration, and we find that there exists a link between such forces and the changes in cell shape, which may be essential in determining the invasive behaviour of the cell.

The paper is organized as follows: in Sect. 2, the geometry of the cell, the constitutive model and the mechanical approach are described. In Sect. 3, the results of the numerical simulations are presented. First, we analyse the cell behaviour (Sect. 3.1). Second, we evaluate the mechanical cell-substrate and cell-channel surface forces (Sect. 3.2), and we find the necessary conditions determining whether the cell is penetrating, invasive or permeative.

2 The model

In this section, we provide the general framework of the model. First, we describe the geometry of the cell including the cytoplasm and the nucleus. Second, we focus on the mechanics of the system. Specifically, we introduce the standard Maxwell models, which are used to reproduce the viscoelastic behaviour of the nucleus and the cytoplasm. Third, the intra-synchronization is presented. As in our previous works (Allena and Aubry 2012; Allena 2013), this represents the key ingredient of the cell movement. In fact, we show how the cyclic active strains (i.e. protrusion and contraction) are strongly coupled with the viscous forces generated by the cell to adhere to the substrate and necessary to efficiently move forward. Finally, we describe the geometry of the micro-channel and the associated viscous force exerted on the cell boundaries, which allows the cell to squeeze and pass (or not) through it.

2.1 Cell geometry

HeLa cells are human cells with a rather rounded initial shape and a diameter of about 15 µm (Ronot et al. 2000; Ngalim et al. 2013). For the numerical model, the geometry of the cell has been simplified by a circular domain Ω_{cell} of radius r_{cell} (Fig. 1a). Here, we consider two main components of the cell: the cytoplasm ($\Omega_{\text{cytoplasm}}$) and the nucleus ($\Omega_{\text{nucleus}}$) (Fig. 1a, Sect. 5.1). Additionally, the cell cyclically generates a frontal (Ω_f) and a rear (Ω_r) adhesion region in order to move forward (Allena and Aubry 2012; Allena 2013) (Fig. 1b, Sect. 5.1).

2.2 Constitutive model and mechanics of the cell

Both the nucleus and the cytoplasm are assumed to be viscoelastic materials, and their behaviour is described by two

standard Maxwell models (Larson 1998) (Sect. 5.2). On one hand, the nucleus is composed by the nuclear lamina Ω_{lamina} (the solid phase, Sects. 5.1 and 5.2), which surrounds the viscoelastic nucleoplasm $\Omega_{\text{nucleoplasm}}$ (the fluid phase, Sects. 5.1 and 5.2). On the other hand, the cytoplasm is essentially made of a solid phase represented by the cell cortex Ω_{cortex} (Sects. 5.1 and 5.3) and a fluid-like phase, the cytosol Ω_{cytosol} (Sects. 5.1 and 5.3) in which the organelles such as the actin filaments are embedded. As in our previous works (Allena and Aubry 2012; Allena 2013), we assume that the polymerization of the actin filaments inside the cytosol, which mostly occurs at the front of the cell (Schaub et al. 2007), generates the protrusive force at the leading edge, and their contraction due to binding of myosin generates the contractile stress at the rear of the cell (Mogilner 2009). Such active strains triggering the deformability of the cell are then described through a deformation tensor $\boldsymbol{F}_{\text{cytosol},a}$ (Sects. 2.3 and 5.3) in the fluid-like branch of the symbolic standard Maxwell model of the cytoplasm.

As described in (Allena and Aubry 2012; Allena 2013), the global equilibrium of the system is expressed as

$$\rho \boldsymbol{a} = \boldsymbol{Div}_{\boldsymbol{p}} \left(J \sigma \boldsymbol{F}^{-T} \right) + \boldsymbol{f}_{\text{adh}} + \boldsymbol{f}_{\text{channel}} \tag{1}$$

where ρ is the cell density, $\boldsymbol{a}$ is the acceleration, $\boldsymbol{Div}_{\boldsymbol{p}}$ is the divergence with respect to the initial position $\boldsymbol{p}$, J is the determinant of the deformation gradient $\boldsymbol{F}$ and $\boldsymbol{A}^{-T}$ denotes the inverse transpose of the matrix $\boldsymbol{A}$ (Holzapfel 2000; Taber 2004). $\boldsymbol{f}_{\text{adh}}$ and $\boldsymbol{f}_{\text{channel}}$ indicate, respectively, the viscous adhesion forces between the cell and the substrate (Sect. 2.3) and the viscous force exerted by the channel on the cell boundaries (Sect. 2.4). Here, all the body forces but the inertial effects are neglected (Gracheva and Othmer 2004; Allena and Aubry 2012; Allena 2013).

2.3 Intra-synchronization

To describe the oscillating movement of the cell, two main assumptions have been made:

1) the active strains of protrusion and contraction are only applied in the cytosol. In fact, as in our previous works (Allena and Aubry 2012; Allena 2013), we assume that the oscillatory movement of the cell is triggered by the periodic polymerization and depolymerization of the actin filaments, which are embedded in the cytosol. The former only occurs at the front of the cell, while the latter takes place from the front towards the rear of the cell. Therefore, although the nucleus does not undergo any active strain, it will interact with the surrounding cytosol apart from the protrusion phase (Friedl et al. 2011);
2) although the cell may form multiple pseudopodia (Allena 2013), here only one is generated in the direction of migration, which, to reproduce the experimental set-up where the cell is constrained into a micro-channel (Heuzé et al. 2011), corresponds to the horizontal axis $\boldsymbol{i}_x$.

Therefore, the solid active deformation tensor $\boldsymbol{F}_{\text{cytosol},a}$ reads

$$\boldsymbol{F}_{\text{cytosol},a} = \begin{cases} e_{a0} \sin\left(2\pi \frac{t}{T}\right) h_{\text{cytosol,front}} \boldsymbol{i}_x \otimes \boldsymbol{i}_x & \text{if } \sin\left(2\pi \frac{t}{T}\right) > 0 \\ \frac{e_{a0}}{2} \sin\left(2\pi \frac{t}{T}\right) h_{\text{cytosol}} \boldsymbol{i}_x \otimes \boldsymbol{i}_x & \text{if } \sin\left(2\pi \frac{t}{T}\right) < 0 \end{cases} \tag{2}$$

where e_{a0} is the amplitude of the active strain, t is time, T is the migration period, h_{cytosol} and $h_{\text{cytosol,front}}$ are two characteristic functions (Sect. 5.1) and $\otimes$ indicates the tensorial product.

As shown in (Allena and Aubry 2012), in order to be able to effectively migrate, the cell must adhere on the substrate otherwise it would only deform on place. Thus, an intra-synchronization is required which coordinates the cyclic protrusion–contraction deformations with the adhesion forces $\boldsymbol{f}_{\text{adh}}$ (Eq. 1) generated between the cell frontal and rear adhesion surfaces and the underneath substrate. As in previous works (Phillipson et al. 2006; Sakamoto et al. 2011; Allena and Aubry 2012; Allena 2013), such forces are assumed to be viscous and may be distinguished into a frontal ($\boldsymbol{f}_{\text{adh},f}$) and a rear ($\boldsymbol{f}_{\text{adh},r}$) force as follows

$$\begin{aligned} \boldsymbol{f}_{\text{adh},f}(\boldsymbol{n}_{\text{cell}}) &= -\mu_{\text{adh}} h_{\text{sync}} \left(-\frac{\partial e_a}{\partial t} \right) \boldsymbol{v} \quad \text{on}\Omega_f \\ \boldsymbol{f}_{\text{adh},r}(\boldsymbol{n}_{\text{cell}}) &= -\mu_{\text{adh}} h_{\text{sync}} \left(\frac{\partial e_a}{\partial t} \right) \boldsymbol{v} \quad \text{on}\Omega_r \end{aligned} \tag{3}$$

with $\boldsymbol{n}_{\text{cell}}$ the outward normal to the cell boundary, μ_{adh} the friction coefficient and $\boldsymbol{v}$ the velocity. The characteristic function h_{sync} is the key ingredient of the preceding equations since it couples the adhesion forces with the active strains, which results in the intra-synchronization mentioned above. Thus, we observe two main phases during the migratory movement of the cell: i) the protrusion and the adhesion at the rear edge; ii) the contraction and the adhesion at the frontal edge.

2.4 Micro-channel

Here, we want to reproduce the micro-channel-based assay presented in (Heuzé et al. 2011). Thus, the micro-channel domain Ω_{channel} is represented by two pseudo-elliptical rigid walls with no top roof (Sect. 5.4).

When the cell enters into the micro-channel, it is then submitted to a viscous force $\boldsymbol{f}_{\text{channel}}$ (Eq. 1), which can be distinguished into an upper ($\boldsymbol{f}_{\text{channel},uw_i}$) and a lower ($\boldsymbol{f}_{\text{channel},lw_i}$) force as follows

$$
\begin{aligned}
&\boldsymbol{f}_{\text{channel},uw_i}\left(\boldsymbol{n}_{uw,i}\right) \\
&\quad = -\mu_{\text{channel}} \frac{1}{\left(l_{uw,i}+1\right)^8+\alpha}\left(\frac{\partial \boldsymbol{u}}{\partial t}, \boldsymbol{n}_{uw,i}\right) n_{uw,i} \quad \text{on} \partial\Omega_{uw,i} \\
&\boldsymbol{f}_{\text{channel},lw_i}\left(\boldsymbol{n}_{lw,i}\right) \\
&\quad = -\mu_{\text{channel}} \frac{1}{\left(l_{lw,i}+1\right)^8+\alpha}\left(\frac{\partial \boldsymbol{u}}{\partial t}, \boldsymbol{n}_{lw,i}\right) \boldsymbol{n}_{lw,i} \quad \text{on} \partial\Omega_{lw,i}
\end{aligned}
\tag{4}
$$

where μ_{channel} is the viscosity of the micro-channel, $l_{uw,i}$ and $l_{lw,i}$ are two level set functions (Sect. 5.4), α is a constant and $\boldsymbol{n}_{uw,i}$ and $\boldsymbol{n}_{lw,i}$ are the outward normal to the boundaries $\partial\Omega_{uw,i}$ and $\partial\Omega_{lw,i}$ of the upper and lower wall, respectively, which are here originally calculated (Sect. 5.4) (the subscript 'i' indicates the channel number as explained in Sect. 3.1 and 5.4). Finally, (***a,b***) defines the scalar product between two vectors.

3 Results

The numerical simulations have been run using the finite element software COMSOL Multiphysics® 3.5a. As described in Sect. 2.2, the viscoelastic behaviour of the cell has been taken into account. The components of the cytoplasm and the nucleus have been implicitly described by specific characteristic functions (Sect. 5.1) in order to be able to define the parameters of the standard Maxwell models. The radius r_{cortex}, r_{cytosol}, r_{lamina} and $r_{\text{nucleoplasm}}$ of the HeLa cell have been fixed to 7.5, 7.25, 4.5 and 4.4 μm, respectively. Then, the cell cortex and the nuclear lamina have a thickness t_{cortex} and t_{lamina} of 0.25 μm (Pesen and Hoh 2005; Tinevez et al. 2009; Jiang and Sun 2013) and 0.1 μm (Righolt et al. 2010), respectively. The nominal values of the Young moduli $E_{\text{cortex},0}$ of the cell cortex and $E_{\text{cytosol},0}$ of the cytosol have been chosen equal to 100 and 10 Pa (Crick and Hughes 1950). For the nucleus, assuming that its stiffness is mostly provided by the nuclear lamina, we have set $E_{\text{lamina},0}$ and $E_{\text{nucleoplasm},0}$ to 3,000 Pa (Caille et al. 2002; Dahl et al. 2008) and 25 Pa (Vaziri et al. 2006), respectively. According to a simple spatial homogenization approach (Christensen 1991; Larson 1998), such moduli have then been recalculated according to the surface occupied by each component in the cell to obtain E_{cortex}, E_{cytosol}, E_{lamina} and $E_{\text{nucleoplasm}}$ (Table 1). Since we consider here that the cell cortex and the nuclear lamina are rather elastic, while the cytosol and the nucleoplasm are rather viscoelastic, the Poisson's ratios ν_{cortex} and ν_{lamina} have been set to 0.3, while ν_{cytosol} and $\nu_{\text{nucleoplasm}}$ to 0.4. The viscosities μ_{cytosol} and $\mu_{\text{nucleoplasm}}$ are equal to 3×10^5 Pa-s (Bausch et al. 1999; Drury and Dembo 2001). The cell density ρ has been set to 1,000 kg/m^3 (Fukui et al. 2000), and the viscous friction coefficient μ_{adh} is equal 10^8Pa-s/m. Finally, the intensity of the active strain e_{a0} and the migration period T have been chosen equal to 0.2 and 600 s, respectively, in order to obtain an average migration velocity of the order of magnitude of the one experimentally observed for HeLa cells (Ronot et al. 2000; Ngalim et al. 2013).

All the parameters of the model have been reported in Table 1.

3.1 Cell behaviour and morphology

As described in Sect. 2.4, the channel is represented by two pseudo-elliptical walls ($l_{uw,i}$ and $l_{lw,i}$), whose semi-axes a and b are 30 and 2 μm long, respectively.

For the simulations, only two-thirds of the total length of the channel are considered, which corresponds to 40 μm.

By letting the position of the upper and lower walls centres $\boldsymbol{c}_{uw,i}$ and $\boldsymbol{c}_{lw,i}$ vary, we have tested four channels with different width as follows:

- *channel 16* has a width $W_{c,1}$ of 16 μm, which is larger than the cell diameter with $\boldsymbol{c}_{uw,16}$ (42.5, 10 μm) and $\boldsymbol{c}_{lw,16}$ (42.5 μm, −10 μm);
- *channel 12* has an intermediate width $W_{c,2}$ of 12 μm, which is smaller than the cell diameter and bigger than the nucleus diameter, with $\boldsymbol{c}_{uw,12}$ (42.5, 8 μm) and $\boldsymbol{c}_{lw,12}$ (42.5, −8 μm);
- *channel 7* has a width $W_{c,3}$ of 7μm, which is slightly smaller than the nucleus diameter with $\boldsymbol{c}_{uw,7}$ (42.5, 5.5 μm) and $\boldsymbol{c}_{lw,7}$ (42.5, −5.5 μm);
- *channel 4* has a width $W_{c,4}$ of 4μm, which is much smaller than the nucleus diameter with $\boldsymbol{c}_{uw,4}$ (42.5, 4 μm) and $\boldsymbol{c}_{lw,4}$ (42, −4 μm).

For the first set of simulations, the viscous friction coefficient μ_{channel} and the constant α have been set equal to 10^{10} Pa-s/m and 0.1, respectively.

We have studied the cell behaviour for each of the previous configurations by analysing specific aspects of the confined movement, and the main results are listed in Table 2.

First, we have evaluated the efficiency of the migration in terms of covered distance. In Fig. 3, the total displacement of the frontal edge of the cell is reported for the four simulations. Then, as previously proposed by (Rolli et al. 2010; Scianna et al. 2013), we can classify the cell as permeative, invasive or penetrating. The permeative behaviour is observable for *channel 16* and *channel 12* (Fig. 2a, b) where the cell reaches the other side of the channel by covering a distance of 38 μm in 9,000 s (blue and red lines in Fig. 3, and Movie 1 and Movie 2, respectively). The invasive behaviour occurs when the cell enters into the channel, but it is not able to achieve the other side (Fig. 2c). This is the case of *channel 7* where the cell only migrates over 25 μm in 6,000 s (green line in Fig. 3 and Movie 3). Finally, the cell is penetrating (Fig. 2d)

Table 1 Main geometrical and material parameters of the model

Parameter	Description	Value (unit)	References
r_{cell}	Cell radius	7.5 μm	
r_{cortex}	Cortex radius	7.5 μm	
r_{cytosol}	Cytosol radius	7.25 μm	
r_{lamina}	Lamina radius	4.5 μm	
$r_{\text{nucleoplasm}}$	Nucleoplasm radius	4.4 μm	
t_{cortex}	Cortex thickness	0.25 μm	Pesen and Hoh (2005), Tinevez et al. (2009), Jiang and Sun (2013)
t_{lamina}	Lamina thickness	0.1 μm	Righolt et al. (2010)
l_f	Distance cell centre—boundary of frontal adhesion region	4 μm	
l_r	Distance cell centre—boundary of rear adhesion region	4 μm	
Ω_{cell}	Initial cell area	176.6 μm^2	
Ω_{cortex}	Initial cortex area	11.6 μm^2	
Ω_{cytosol}	Initial cytosol area	101.4 μm^2	
$\Omega_{\text{cytoplasm}}$	Initial cytoplasm area	113 μm^2	
Ω_{lamina}	Initial lamina area	2.8 μm^2	
$\Omega_{\text{nucleoplasm}}$	Initial nucleoplasm area	60.8 μm^2	
Ω_{nucleus}	Initial nucleus area	63.6 μm^2	
Ω_f	Initial frontal adhesion region area	31 μm^2	
Ω_r	Initial rear adhesion region area	31 μm^2	
$E_{\text{cortex},0}$	Nominal cortex Young modulus	100 Pa	
$E_{\text{cytosol},0}$	Nominal cytosol Young modulus	10 Pa	Crick and Hughes (1950)
$E_{\text{lamina},0}$	Nominal lamina Young modulus	3,000 Pa	Caille et al. (2002), Dahl et al. (2008)
$E_{\text{nucleoplasm},0}$	Nominal nucleoplasm Young modulus	25 Pa	Vaziri et al. (2006)
E_{cortex}	Equivalent cortex Young modulus	15 Pa	
E_{cytosol}	Equivalent cytosol Young modulus	8 Pa	
E_{lamina}	Equivalent lamina Young modulus	196 Pa	
$E_{\text{nucleoplasm}}$	Equivalent nucleoplasm Young modulus	23 Pa	
ν_{cortex}	Cortex Poisson ratio	0.3	
ν_{cytosol}	Cytosol Poisson ratio	0.4	
ν_{lamina}	Lamina Poisson ratio	0.3	
$\nu_{\text{nucleoplasm}}$	Nucleoplasm Poisson ratio	0.4	
μ_{cytosol}	Cytosol viscosity	3×10^5 Pa-s	Bausch et al. (1999), Drury and Dembo (2001)
$\mu_{\text{nucleoplasm}}$	Nucleoplasm viscosity	3×10^5 Pa-s	Bausch et al. (1999), Drury and Dembo (2001)
ρ	Cell density	1,000 kg/m^3	Fukui et al. (2000)
e_{a0}	Amplitude of the active strain	0.8	
T	Migration period	600 s	
μ_{adh}	Cell friction coefficient	10^8 Pa-s/m	
a	Semi-axis of the pseudo-elliptical walls	30 μm	

Table 1 continued

Parameter	Description	Value (unit)	References
b	Semi-axis of the pseudo-elliptical walls	2 μm	
x_0	x-coordinate of the pseudo-elliptical walls centre	42.5 μm	
$y_{uw0,i}$	y-coordinate of the upper pseudo-elliptical wall centre	$y_{uw0,1}$: 10 $y_{uw0,2}$: 8 $y_{uw0,3}$: 6 $y_{uw0,4}$: 4 μm	
$y_{lw0,i}$	y-coordinate of the lower pseudo-elliptical wall centre	$y_{lw0,1}$: −10 $y_{lw0,2}$: −8 $y_{lw0,3}$: −6 $y_{lw0,4}$: −4 μm	
μ_{channel}	Channel viscous friction coefficient	10^{10} Pa-s/m	
α		0.1	
$W_{c,16}$	Width of *channel 1*	16 μm	
$W_{c,12}$	Width of *channel 3*	12 μm	
$W_{c,7}$	Width of *channel 3*	8 μm	
$W_{c,4}$	Width of *channel 4*	4 μm	

Table 2 Main numerical results for the different channels

	Channel 16	Channel 12	Channel 7	Channel 4
Displacement (μm)	38	38	25	7.5
Protrusion average velocity (μm/s)	0.0055	0.0051	0.0055	0.0053
Contraction average velocity (μm/s)	0.0102	0.0122	0.0118	0.0115
t_{contact} (s)	–	1,950	1,250	1,220
$t_{\text{penetration}}$ (s)	3,900	4,600	4,610	–
T_{entry} (s)	–	2,650	3,360	–
Maximal ratio cell area/nucleus area	3.29	2.89	2.25	3.29
Minimal ratio cell area/nucleus area	2.11	1.93	1.35	2.11
t_{regime1} (s)	–	1,800	1,250	1,230
t_{regime2} (s)	–	2,450	1,350	1,250
t_{regime3} (s)	–	2,600	1,850	–

when only part of the body (or nothing) penetrates within the channel as it takes place for *channel 4* (purple line in Fig. 3 and Movie 4) where the total displacement is only equal to 7.5 μm.

In Fig. 4, the trend of the cell average velocity is represented. As a general remark, the velocity during the contraction phase is slightly higher than during the contraction phase, since the former only involves the frontal portion of the cytoplasm (see Sect. 2.3). While the average protrusion velocity remains rather constant for all the channels (roughly $5 \cdot 10^{-3}$ μm/s), the average contraction velocity varies between a minimal value of about $10^{-2}\mu$m/s for channel 16 (blue line Fig. 4) and a maximal value of $1.2 \cdot 10^{-2}$ μm/s for channel 12 (red line Fig. 4). Additionally, for *channel 7* (green line Fig. 4), we observe a peak of the velocity up to $1.3 \cdot 10^{-2}$ μm/s at the entrance of the channel, while afterwards the cell acquires again a constant velocity. Such values are of the same order of magnitude of those experimentally observed for HeLa cells (Ronot et al. 2000; Ngalim et al. 2013).

Second, for each configuration, we have quantified the entry time (T_{entry}), which has been defined by Lautenschläger et al. (Lautenschlager et al. 2009) as the time interval between the first contact of the cell with the channel walls (t_{contact}) and the complete penetration of the cell body within the channel ($t_{\text{penetration}}$). For *channel 16* and *channel 4*, such a parameter cannot be evaluated since the cell either does not enter in contact with the channel (*channel 16*) or does not migrate through it (*channel 4*). For *channel 12* and *channel 7*, we found 2,650 and 3,360 s respectively, which confirms that the smaller the channel, the more the difficult is for the cell to get in. In fact, the contact cell channel occurs earlier for *channel 7* than for *channel 12* ($t_{\text{contact}} = 1{,}250$ s versus $t_{\text{contact}} = 1{,}950$ s), while $t_{\text{penetration}}$ is almost the same

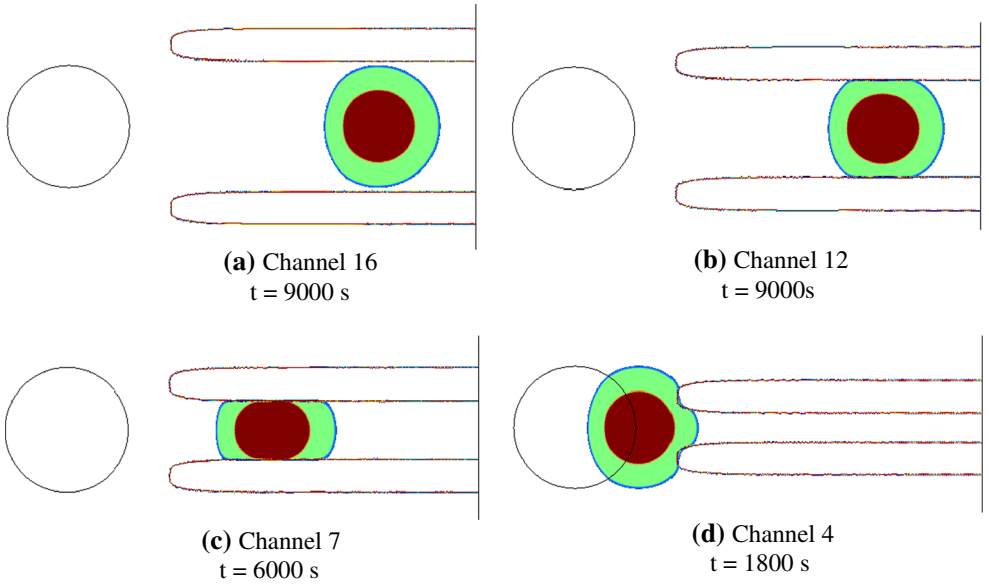

Fig. 2 Snaphots of the permeative (**a** and **b**), invasive (**c**) and penetrating (**d**) cell

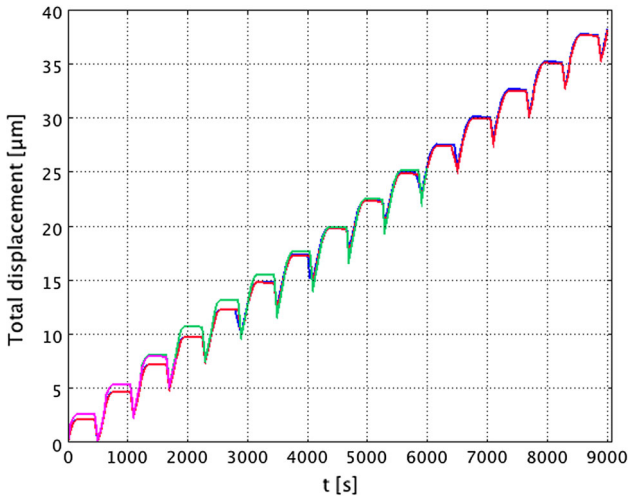

Fig. 3 Total displacement of the cell for *channel 16* (*blue line*), *channel 12* (*red line*), *channel 7* (*green line*) and *channel 4* (*purple line*)

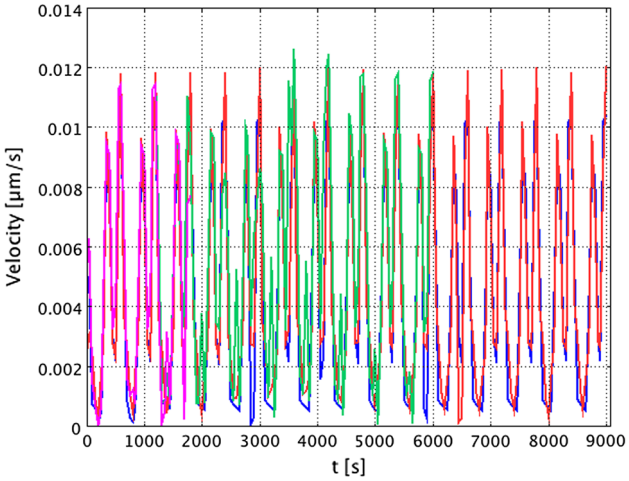

Fig. 4 Migration average velocity of the cell for *channel 16* (*blue line*), *channel 12* (*red line*), *channel 7* (*green line*) and *channel 4* (*purple line*)

for both channels ($t_{\text{penetration}} = 4{,}610\,s$ versus $t_{\text{penetration}} = 4{,}600$ s).

Third, we have evaluated the ratio between the total cell area and the nucleus area. At the initial configuration, such ratio is equal to 2.8, but it undergoes an oscillatory variation due to the protrusion–contraction movement of the cell. In the case of *channel 16* (Fig. 5, blue line), it varies between a maximal value of 3.3 during protrusion and a minimal value of 2.1 during contraction. Here, such values are the same at the end of each phase during the whole simulation since the cell overall deformation is not perturbed by the contact with channel. For *channel 12* instead, we observe a decrease of the maximal value of the ratio to 2.9 once the cell has completely entered the channel ($t_{\text{penetration}} = 4{,}600$ s, Fig. 5, red line), while the minimal value decreases to 1.9. Such drop is mainly due to a bigger shrinkage of the cell cytoplasm rather than of the nucleus due to the subcellular dimensions of the channel. However, in the case of *channel 7* (Fig. 5, green line), both cytoplasm and nucleus contribute to the progressive decrease of the ratio. In fact, the nucleus must squeeze too to move forward since the channel has sub-nuclear dimensions. Then, the maximal and minimal values of the ratio at $t_{\text{penetration}} = 4{,}610$ s decrease down to 2.25 and 1.35, respectively. For *channel 4* (Fig. 5, purple line), the ratio evolution is the same as for *channel 16* since the cell is not able to penetrate the channel and neither cytoplasm nor nucleus do not undergo large deformation.

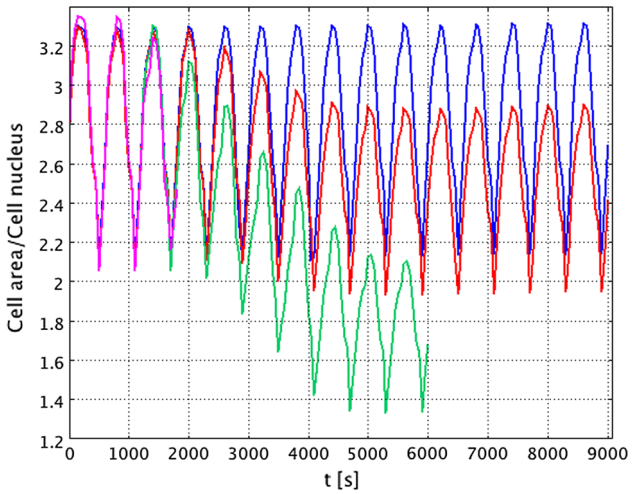

Fig. 5 Ratio between the cell area and the nucleus area for *channel 16* (*blue line*), *channel 12* (*red line*), *channel 7* (*green line*) and *channel 4* (*purple line*)

Finally, we have analysed the morphology of the cell relative to the channel, which can actually be divided into three regimes. The first regime is observed when the length L_p of the cell protrusion into the channel is smaller than half the width of the channel $W_{c,i}$ ($2L_p/W_{c,i} < 1$), and it has been indicated as t_{regime1}. The second regime occurs when $2L_p/W_{c,i} = 1$, and the protrusion is hemicircular with radius equal to $W_{c,I}$ (t_{regime2}). Finally, the third regime is obtained when $2L_p/W_{c,i} > 1$ (t_{regime3}). At this point, the first half of the protrusion is rectangular of length $W_{c,i}$ and the second half is hemicircular of radius L_c.

In the case of *channel 16*, the migration mode and the morphology of the cell do not change and are very similar to those observed for cell migrating over flat surfaces (Allena and Aubry 2012; Allena 2013). In fact, there is no contact between the cell cortex and the channel walls, and thus, the cell body is not perturbed during its movement. This is not the case for *channel 12* and *channel 7* where the cell needs to squeeze in order to enter the channel. For *channel 12* , regime 1 is observed at $t_{\text{regime1}} = 1{,}800$ s, while L_p becomes equal to $W_{c,2}/2$ at $t_{\text{regime2}} = 2{,}450$ s. Starting from $t_{\text{regime3}} = 2{,}600$ s, regime 3 is achieved and the protrusion is clearly half rectangular and half hemicircular. For *channel 7* (Fig. 6), steps occur earlier. In fact, regime 1 and regime 2 are reached at $t_{\text{regime1}} = 1{,}250$ s and $t_{\text{regime2}} = 1{,}350$ s, respectively, while regime 3 starts at $t_{\text{regime3}} = 1{,}850$ s. For *channel 4* instead, only regime 1 and 2 observed at $t_{\text{regime1}} = 1{,}230$ s and $t_{\text{regime2}} = 1{,}250$ s, respectively. The reason why regime 3 is not achieved is mainly due to the fact that, despite the cell tries to enter the channel by protruding and contracting, the force $\boldsymbol{f}_{\text{channel}}$ exerted by the channel walls on the cell boundaries is too high. This means that reaching regime 3 is a necessary, but not sufficient condition for the cell to be invasive. In fact, a second necessary condition need to be satisfied, that is, the cell-channel surface force $\boldsymbol{f}_{\text{channel}}$ at t_{regime3} must be low enough for the cell to enter.

We have also been able to experimentally observe such changes in morphology for two types of cells using a micro-channel-based essay as proposed in (Heuzé et al. 2011). Figure 7a–d shows the successive steps (top view) of bone marrow-derived dendritic cells (BDMCs) migration through a 5μm (Fig. 7a–b) and 1.5μm (Fig. 7c, d) wide micro-channel. It is possible to clearly distinguish the three regimes undergone by the whole cell body (Fig. 7b, d) and by the stained nucleus (Fig. 7a, c). Figure 7e shows instead a sagittal view of the successive steps of a HeLa cell migrating through a 20 μm wide micro-channel. We observe the deformation undergone by the stained nucleus along the z axis. In fact, in this specific case, the cell is confined in the x–y plane,

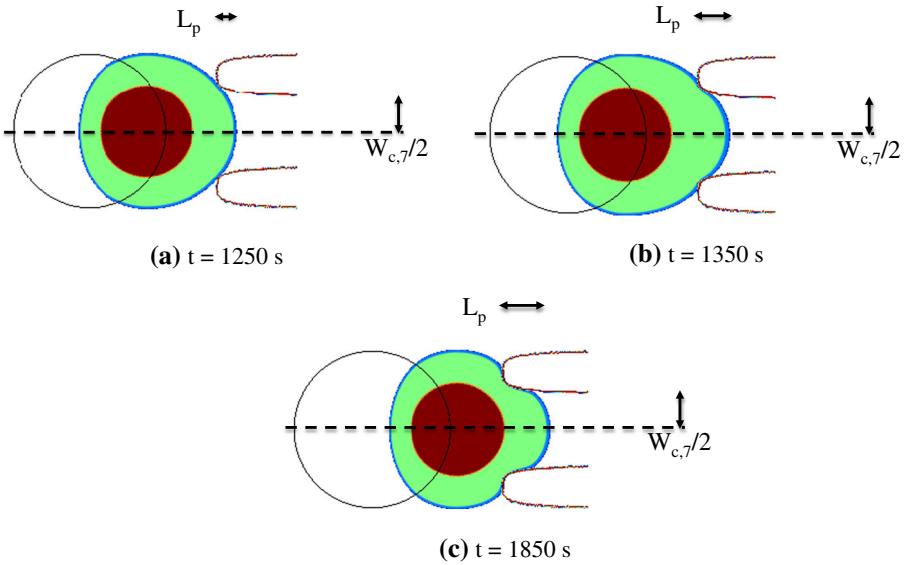

Fig. 6 The three regimes of the cell morphology during the migration through *channel 7*

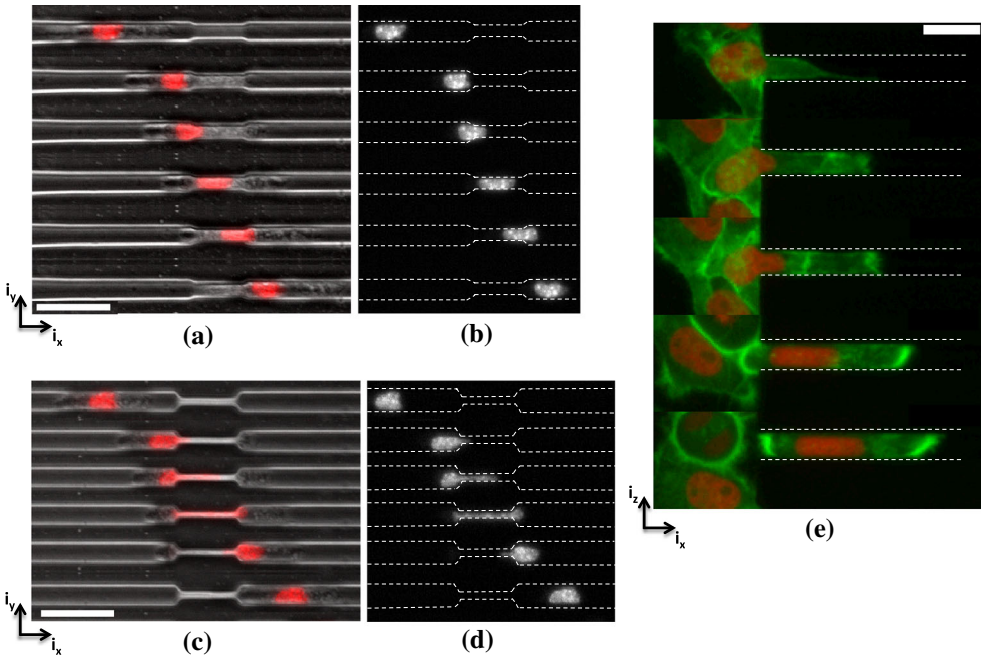

Fig. 7 (**a**:**d**) Top view of successive steps of a bone marrow-derived dendritic cell (BMDC) migration (from the *left* to the *right*) through a 5μm **a**–**b** and 1.5μm **c**–**d** wide micro-channels. Nuclear staining with Hoechst (**a** and **c**) (*scale bar*: 30μm) **e** Sagittal view of successive steps of a HeLa cell entering (from the *left* to the *right*) a 20μm wide micro-channel (HeLa Histone2B-mcherry (nucleus), MyrPalm-GFP (plasma membrane), *scale bar*: 15μm)

Table 3 Values of the mechanical forces for the different channels

	Channel 16	Channel 12	Channel 7	Channel 4
Maximal frontal cell-substrate surface force (Pa)	10	10	10	10
Maximal rear cell-substrate surface force (Pa)	4	4	4	4
Maximal cell-channel surface force at t_{contact} (Pa)	–	3.3	3.1	7.2
Maximal cell-channel surface force at $t_{\text{penetration}}$ (Pa)	–	3.3	3.9	–
Average cell-substrate surface force between t_{contact} and $t_{\text{penetration}}$ (Pa)	–	3.3	3.3	3.3
Average cell-channel surface force between t_{contact} and $t_{\text{penetration}}$ (Pa)	–	2.5	3.2	$t_{\text{contact}} - t_{\text{regime2}}$ 4.5
Absolute maximal cell-channel surface force (Pa)	–	4.2	6.2	8.6

but also in the x–z plane. Although such an aspect has not been numerically considered so far, we are currently working to improve the model in order to have a three-dimensional representation of the cell and the micro-channel and therefore being able to implement this further confinement

3.2 Mechanical forces

In this section, we try to evaluate the cell-substrate and cell-channel surface forces, in particular during the time interval between t_{contact} and $t_{\text{penetration}}$ in which t_{regime3} is included. The main values are summarized in Table 3.

Some general remarks may be pointed out:

- given the asymmetry of the active strain (Sect. 2.3) and the equation expressing the cell-substrate surface forces (Eq. 3), we found 10 and 4 Pa, respectively, at the front and rear edge of the cell. Additionally, such values do not change from one configuration;
- the cell-channel surface force increases as the channel width $W_{c,i}$ decreases (maximal absolute value of 4.25,

6.25 and 8.5 Pa for *channel 12, channel 7* and *channel 4* , respectively);

- as mentioned in Sect. 3.1, the necessary condition for the cell to be invasive is that the average cell-channel surface force at t_{regime3} must be lower than the average cell-substrate surface force at the same time point. This allows the cell to pull enough to penetrate within the channel without being obstructed by the channel. Since t_{regime3} is included in the time interval between t_{contact} and $t_{\text{penetration}}$, we have calculated the average cell-channel surface force during this period. For *channel 12* and *channel 7*, we have found an average value for the cell-channel surface force of about 2.5 Pa and 3.2, respectively, which is lower than the average cell-substrate surface force of 3.3 Pa. As a result, the cell is able to enter the channel. For *channel 4*, since the cell-channel surface force between t_{contact} and $t_{\text{penetration}}$ cannot be calculated, we have evaluated it between t_{contact} and t_{regime2} finding an average value of 4.5 Pa and a maximal value of 8.6 Pa, which is twice the cell-substrate surface force. Therefore, the cell is stuck at the entrance of the channel and shows a penetrating behaviour;
- once the cell has completely penetrated into the channel, the upper and lower central boundaries of the cell come very close or directly in contact with the nucleus, which is the stiffest component of the system. Then, a higher cell-channel surface force is necessary at this specific region to maintain the cell squeezing during the whole migration process and in order for the cell to be permeative. This is the case for *channel 12* for which the cell is able to reach the opposite end of the channel (Movie 5). However, for *channel 7*, the cell-channel surface force is slightly higher at the rear of the cell. Thus, the cell is slowed down and shows a penetrating behaviour (Movie 6).

For *channel 16*, only the cell-substrate surface force can be evaluated while the cell-channel surface force is null since no contact between the cell boundaries and the channel walls occurs.

4 Conclusions

In this paper, we have proposed a 2D mechanical model to simulate the migration of HeLa cell under confinement. The model reproduces the set-up used in a micro-channel assay as presented in (Heuzé et al. 2011). As in our previous works (Allena and Aubry 2012; Allena 2013), the cell is modelled as continuum and a standard Maxwell model is used to describe the mechanical behaviour of the cytoplasm (including active strains) and the nucleus. The cell is able to cyclically develop protrusion–contraction strains, which are synchronized with the adhesion forces between the cell and the substrate. By approaching the channel, which is represented here by two pseudo-elliptical rigid walls, the cell is submitted to an additional viscous force. We have tested four channels whose dimensions in terms of width are larger than the cell diameter (*channel 16*), sub-cellular (*channel 12*), sub-nuclear (*channel 7*) and much smaller than the nucleus diameter (*channel 4*). We have analysed the cell behaviour and classified it as permeative (*channel 16* and *channel 12*), invasive (*channel 7*) or penetrating (*channel 4*) according to the distance covered by the cell inside the channel. From a morphological point of view, we have identified three different regimes in relation to the ratio between the cell protrusion length in the channel and the width of the channel. Additionally, we have evaluated the evolution of the cell shape and the cell-substrate and cell-channel surface forces between the first contact between the cell and the channel (t_{contact}) and the complete penetration of the cell body within the channel ($t_{\text{penetration}}$).

Therefore, we have been able to define the necessary conditions in order for the cell to be invasive or permeative. In the first case, two main conditions must be satisfied: i) regime 3 (i.e. cell protrusion length in the channel larger than half the channel width) has to be achieved, and ii) simultaneously, the cell-substrate surface force must be higher than the cell-channel surface force so that the cell is able to pull on the substrate and enter into the channel. For the second behaviour to occur, a further condition must be satisfied, that is, the cell-channel surface force during the whole migration has to be maximal along the upper and lower central boundaries of the cell. Those boundaries may come very close or directly in contact with the cell nucleus, which is the stiffest component of the system. Then, a larger force is required to maintain the squeezed cell shape.

Despite the consistent results shown in the present paper, our model still presents some limitations. Firstly, the geometry is 2D, which does not allow considering a top-roofed micro-channel and the cell deformation in the third direction. Secondly, the active strains of protrusion and contraction have been defined through a sinusoidal function, which may lead to a rather stable periodic deformation of the cytoplasm and consequently of the nucleus. In order to control the effects of such a phenomenon, some stochastic active input close to cell perception may be introduced and improve the global movement. Finally, so far all the cell components have been considered as viscoelastic materials. However, the nucleus may be able to adapt its deformation to the forces exerted by the micro-channel on the cell boundaries. Therefore, a viscoplastic behaviour with restoration (Mandel 1972; Lubliner 2008) would probably be more appropriate. We are currently working on this aspect in order to be able to investigate the ability of the cell to penetrate micro-channels with significant sub-nuclear dimensions.

5 Appendix

5.1 Geometry of the cell

For any spatial point $\boldsymbol{p}$, the four components of the cell body (the cortex Ω_{cortex}, the cytosol Ω_{cytosol}, the lamina Ω_{lamina} and the nucleoplasm $\Omega_{\text{nucleoplasm}}$) are described through characteristic functions (i.e. composition of a Heaviside and a level set function (Allena 2013) as follows

$$h_{\text{cortex}}(\boldsymbol{p}) = \begin{cases} 1 & \text{if} r^2_{\text{cytoplasm}} < \|\boldsymbol{p} - \boldsymbol{c}_{\text{cell}}\| < r^2_{\text{cortex}} \\ 0 & \text{otherwise} \end{cases} \tag{5}$$

$$h_{\text{cytosol}}(\boldsymbol{p}) = \begin{cases} 1 & \text{if} r^2_{\text{lamina}} < \|\boldsymbol{p} - \boldsymbol{c}_{\text{cell}}\| < r^2_{\text{cytosol}} \\ 0 & \text{otherwise} \end{cases} \tag{6}$$

$$h_{\text{lamina}}(\boldsymbol{p}) = \begin{cases} 1 & \text{if} r^2_{\text{nucleoplasm}} < \|\boldsymbol{p} - \boldsymbol{c}_{\text{cell}}\| < r^2_{\text{lamina}} \\ 0 & \text{otherwise} \end{cases} \tag{7}$$

$$h_{\text{nucleoplasm}}(\boldsymbol{p}) = \begin{cases} 1 & \text{if } \|\boldsymbol{p} - \boldsymbol{c}_{\text{cell}}\| < r^2_{\text{nucleoplasm}} \\ 0 & \text{otherwise} \end{cases} \tag{8}$$

where $\boldsymbol{p} = \boldsymbol{x} - \boldsymbol{u}$, with $\boldsymbol{x}$ and $\boldsymbol{u}$ being, respectively, the actual position and the displacement, $\boldsymbol{c}_{\text{cell}}$ is the cell centre and r_{cortex}, r_{cytosol}, r_{lamina} and $r_{\text{nucleoplasm}}$ are the external radius of the cell cortex, the cytosol, the nuclear lamina and nucleoplasm, respectively (Fig. 1a). Therefore, the cytoplasm $\Omega_{\text{cytoplasm}}$ and the nucleus Ω_{nucleus} domains are defined by the following characteristic functions

$$\begin{aligned} h_{\text{cytoplasm}}(\boldsymbol{p}) &= h_{\text{cortex}}(\boldsymbol{p}) + h_{\text{cytosol}}(\boldsymbol{p}) \\ h_{\text{nucleus}}(\boldsymbol{p}) &= h_{\text{lamina}}(p) + h_{\text{nucleoplasm}}(\boldsymbol{p}) \end{aligned} \tag{9}$$

The frontal portion of cytosol where the polymerization of the actin filaments takes place is described as follows

$$h_{\text{cytosol,front}}(\boldsymbol{p}) = \begin{cases} h_{\text{cytosol}} & if \boldsymbol{p} > \boldsymbol{c}_{\text{cell}} \\ 0 & \text{otherwise} \end{cases} \tag{10}$$

The frontal (Ω_f) and rear (Ω_r) adhesion regions are also defined by two characteristic functions as

$$\begin{aligned} h_f(\boldsymbol{p}) &= \begin{cases} 1 & (\boldsymbol{p} - \boldsymbol{c}_{\text{cell}}, \boldsymbol{i}_x) > l_f \\ 0 & \text{otherwise} \end{cases} \\ h_r(\boldsymbol{p}) &= \begin{cases} 1 & (\boldsymbol{p} - \boldsymbol{c}_{\text{cell}}, \boldsymbol{i}_x) < -l_r \\ 0 & \text{otherwise} \end{cases} \end{aligned} \tag{11}$$

with l_f and l_r the distances of $\boldsymbol{c}_{\text{cell}}$ from the boundaries of Ω_f and Ω_r, respectively, (Fig. 1b). As soon as the cell moves, the argument $\boldsymbol{p}$ is replaced by $\boldsymbol{x}$-$\boldsymbol{u}$, with $\boldsymbol{x}$ the actual spatial position and $\boldsymbol{u}$ the displacement.

5.2 Nucleus constitutive law

As mentioned in Sect. 2.2, the nucleus is described through a viscoelastic constitutive equation based on a standard Maxwell model including a solid phase (i.e. the lamina) and a fluid phase (i.e. the nucleoplasm) (Fig. 8).

The Cauchy stress $\boldsymbol{\sigma}_{\text{nucleus}}$ and the deformation tensor $\boldsymbol{F}_{\text{nucleus}}$ in the nucleus are defined by

$$\begin{aligned} \boldsymbol{\sigma}_{\text{nucleus}} &= \boldsymbol{\sigma}_{\text{lamina}} + \boldsymbol{\sigma}_{\text{nucleoplasm}} \\ \boldsymbol{F}_{\text{nucleus}} &= \boldsymbol{D}_p\boldsymbol{u} + \boldsymbol{I} = \boldsymbol{F}_{\text{lamina}} = \boldsymbol{F}_{\text{nucleoplasm}} \end{aligned} \tag{12}$$

where $\boldsymbol{D_p u} = \sum_{m=1}^{3} \frac{\partial \boldsymbol{u}}{\partial p_m} \otimes \boldsymbol{i}_m$, with $\boldsymbol{u}$ the displacement and $\boldsymbol{I}$ the identity matrix (Holzapfel 2000; Taber 2004), and $\boldsymbol{F}_{\text{nucleoplasm}} = \boldsymbol{F}_{\text{nucleoplasm},e}\boldsymbol{F}_{\text{nucleoplasm},v}$. The solid part of the stress $\boldsymbol{\sigma}_{\text{lamina}}$ in the lamina reads

$$\boldsymbol{\sigma}_{\text{lamina}} = \frac{1}{J_{\text{lamina}}} \boldsymbol{F}_{\text{lamina}} \boldsymbol{S}_{\text{lamina}} \boldsymbol{F}^T_{\text{lamina}} \tag{13}$$

where J_{lamina} is the determinant of $\boldsymbol{F}_{\text{lamina}}$ and $\boldsymbol{S}_{\text{lamina}}$ is the second Piola–Kirchoff stress tensor, which is computed as an isotropic hyperelastic Saint Venant material as follows

$$\boldsymbol{S}_{\text{lamina}} = \lambda_{\text{lamina}} Tr\left(\boldsymbol{E}_{\text{lamina}}\right) \boldsymbol{I} + 2\mu_{\text{lamina}} \boldsymbol{E}_{\text{lamina}} \tag{14}$$

with λ_{lamina}, μ_{lamina} and $\boldsymbol{E}_{\text{lamina}}$ the Lame's coefficients and the Green-Lagrange strain tensor of the solid phase, respectively.

The fluid part of the stress $\boldsymbol{\sigma}_{\text{nucleoplasm}}$ in the nucleoplasm can be expressed as

$$\boldsymbol{\sigma}_{\text{nucleoplasm}} = 2\mu_{\text{nucleoplasm}} \boldsymbol{D}_{\text{nucleoplasm,v}} \tag{15}$$

with $\mu_{\text{nucleoplasm}}$, the viscosity of the nucleoplasm and the eulerian strain rate $\boldsymbol{D}_{\text{nucleoplasm},v}$ is computed from the strain gradient velocity as

$$\begin{aligned} 2\boldsymbol{D}_{\text{nucleoplasm},v} &= \dot{\boldsymbol{F}}_{\text{nucleoplasm},v} \boldsymbol{F}^{-1}_{\text{nucleoplasm},v} \\ &\quad + \boldsymbol{F}^{-T}_{\text{nucleoplasm},v} \dot{\boldsymbol{F}}^{T}_{\text{nucleoplasm},v} \end{aligned} \tag{16}$$

5.3 Cytoplasm constitutive law

The cytoplasm is composed by two phases: i) a solid phase represented by the cell cortex and ii) a fluid phase represented by the viscous cytosol with the embedded organelles such as the actin filaments that undergo the active strains (Fig. 8). It is assumed that the Cauchy stress $\boldsymbol{\sigma}_{\text{cytoplasm}}$ and the deformation tensor $\boldsymbol{F}_{\text{cytoplasm}}$ read

$$\begin{aligned} \boldsymbol{\sigma}_{\text{cytoplasm}} &= \boldsymbol{\sigma}_{\text{cortex}} + \boldsymbol{\sigma}_{\text{cytosol}} \\ \boldsymbol{F}_{\text{cytoplasm}} &= \boldsymbol{F}_{\text{cortex}} = \boldsymbol{F}_{\text{cytosol}} \end{aligned} \tag{17}$$

Additionally, the fluid deformation tensor $\boldsymbol{F}_{\text{cytosol}}$ is multiplicatively decomposed as follows

$$\boldsymbol{F}_{\text{cytosol}} = \boldsymbol{F}_{\text{cytosol},v} \boldsymbol{F}_{\text{cytosol},e} \boldsymbol{F}_{\text{cytosol},a} \tag{18}$$

where e and v stand for elastic and viscous, respectively.

The solid stress $\boldsymbol{\sigma}_{\text{cortex}}$ in the organelles can be written as

$$\boldsymbol{\sigma}_{\text{cortex}} = \frac{1}{J_{\text{cortex}}} \boldsymbol{F}_{\text{cortex}} \boldsymbol{S}_{\text{cortex}} \boldsymbol{F}^T_{\text{cortex}} \tag{19}$$

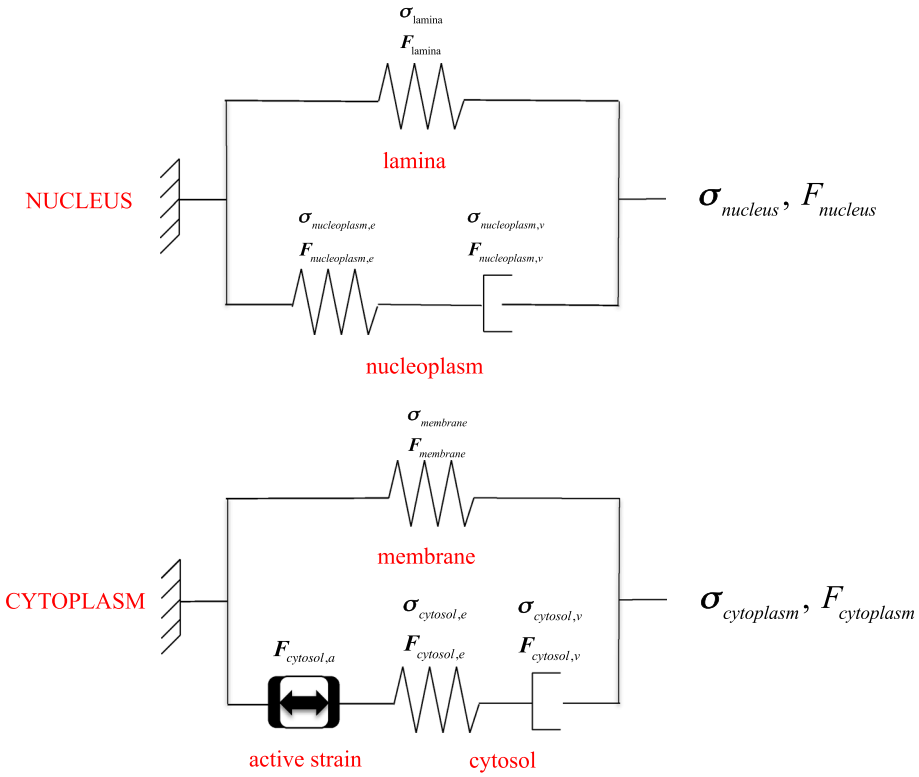

Fig. 8 Symbolic schemas for the standard Maxwell models used to describe the nucleus (*top*) and the cytoplasm (*bottom*) behaviours

with J_{cortex} the determinant of $\boldsymbol{F}_{\text{cortex}}$ and $\boldsymbol{S}_{\text{cortex}}$ the second Piola–Kirchoff stress tensor, which, similarly to the nucleus (Sect. 5.2), is defined as an isotropic hyperplastic Saint Venant material as follows

$$S_{\text{cortex}} = \lambda_{\text{cortex}} Tr\left(\boldsymbol{E}_{\text{cortex}}\right) \boldsymbol{I} + 2\boldsymbol{\mu}_{\text{cortex}} \boldsymbol{E}_{\text{cortex}} \tag{20}$$

where λ_{cortex}, μ_{cortex} and $\boldsymbol{E}_{\text{cortex}}$ the Lame's coefficients and the Green-Lagrange strain tensor of the solid phase, respectively.

Finally, the fluid stress $\boldsymbol{\sigma}_{\text{cytosol}}$ in the cytosol reads

$$\boldsymbol{\sigma}_{\text{cytosol}} = 2\mu_{\text{cytosol}} \boldsymbol{D}_{\text{cytosol},v} \tag{21}$$

with μ_{cytosol} the viscosity of the cytosol and $\boldsymbol{D}_{\text{cytosol},v}$ the eulerian strain rate expressed as follows

$$2\boldsymbol{D}_{\text{cytosol},v} = \dot{\boldsymbol{F}}_{\text{cytosol},v} \boldsymbol{F}^{-1}_{\text{cytosol},v} + \boldsymbol{F}^{-T}_{\text{cytosol},v} \dot{\boldsymbol{F}}^{T}_{\text{cytosol},v} \tag{22}$$

5.4 Micro-channel geometry

As mentioned in Sect. 2.4, the micro-channel domain Ω_{channel} is modelled as two pseudo-elliptical rigid walls: a upper one (Ω_{uw}) and a lower one (Ω_{lw}). They are described through two characteristic functions as follows

$$\begin{aligned} h_{uw,i}\left(\boldsymbol{p}\right) &= \begin{cases} 1 & \text{if} l_{uw,i} < 1 \\ 0 & \text{otherwise} \end{cases} \\ h_{lw,i}\left(\boldsymbol{p}\right) &= \begin{cases} 1 & \text{if} l_{lw,i} < 1 \\ 0 & \text{otherwise} \end{cases} \end{aligned} \tag{23}$$

where the subscript 'i' indicates the number of the channel, and $l_{uw,i}$ and l_{lw} are two level set functions expressed as

$$\begin{aligned} l_{uw,i} &= \left(\frac{x - x_0}{a}\right)^4 + \left(\frac{y - y_{uw0,i}}{b}\right)^4 \\ l_{lw,i} &= \left(\frac{x - x_0}{a}\right)^4 + \left(\frac{y + y_{lw0,i}}{b}\right)^4 \end{aligned} \tag{24}$$

with a and b are the semi-axes of the pseudo-elliptical walls with centres $\boldsymbol{c}_{uw,i}\left(x_0, y_{uw0,i}\right)$ and $\boldsymbol{c}_{lw,i}\left(x_0, y_{lw0,i}\right)$. Thus, the micro-channel is the composition of the two previous characteristic functions as follows

$$\Omega_{\text{channel}} = h_{uw,i}\left(\boldsymbol{p}\right) + h_{lw,i}\left(\boldsymbol{p}\right) \tag{25}$$

The c outward normals $\boldsymbol{n}_{uw}$ and $\boldsymbol{n}_{lw}$ to the boundary $\partial\Omega_{uw}$ and $\partial\Omega_{lw}$, respectively, given by

$$\begin{aligned} \boldsymbol{n}_{uw,i} &= h'\left(l_{uw,i}\right) \frac{\nabla l_{uw,i}}{\left\|\nabla l_{uw,i}\right\|} \\ \boldsymbol{n}_{lw,i} &= h'\left(l_{lw,i}\right) \frac{\nabla l_{lw,i}}{\left\|\nabla l_{lw,i}\right\|} \end{aligned} \tag{26}$$

where h' indicates the Dirac function.

References

Allena R (2013) Cell migration with multiple pseudopodia: temporal and spatial sensing models. Bull Math Biol 75:288–316. doi:10.1007/s11538-012-9806-1

Allena R, Aubry D (2012) "Run-and-tumble" or "look-and-run"? A mechanical model to explore the behavior of a migrating amoeboid cell. J Theor Biol 306:15–31. doi:10.1016/j.jtbi.2012.03.041

Bausch AR, Möller W, Sackmann E (1999) Measurement of local viscoelasticity and forces in living cells by magnetic tweezers. Biophys J 76:573–579

Caille N, Thoumine O, Tardy Y, Meister J-J (2002) Contribution of the nucleus to the mechanical properties of endothelial cells. J Biomech 35:177–187

Christensen RM (1991) Mechanics of composite materials. Krieger Publishing Company, NY

Crick FHC, Hughes AFW (1950) The physical properties of cytoplasm. Exp Cell Res 1:37–80. doi:10.1016/0014-4827(50)90048-6

Dahl KN, Ribeiro AJS, Lammerding J (2008) Nuclear shape, mechanics, and mechanotransduction. Circ Res 102:1307–1318. doi:10.1161/CIRCRESAHA.108.173989

Drury JL, Dembo M (2001) Aspiration of human neutrophils: effects of shear thinning and cortical dissipation. Biophys J 81:3166–3177

Egeblad M, Rasch MG, Weaver VM (2010) Dynamic interplay between the collagen scaffold and tumor evolution. Curr Opin Cell Biol 22:697–706. doi:10.1016/j.ceb.2010.08.015

Erler JT, Weaver VM (2009) Three-dimensional context regulation of metastasis. Clin Exp Metastas 26:35–49. doi:10.1007/s10585-008-9209-8

Faure-André G, Vargas P, Yuseff M-I et al (2008) Regulation of dendritic cell migration by CD74, the MHC class II-associated invariant chain. Science 322:1705–1710. doi:10.1126/science.1159894

Friedl P, Wolf K (2010) Plasticity of cell migration: a multiscale tuning model. J Cell Biol 188:11–19. doi:10.1083/jcb.200909003

Friedl P, Wolf K, Lammerding J (2011) Nuclear mechanics during cell migration. Curr Opin Cell Biol 23:55–64. doi:10.1016/j.ceb.2010.10.015

Fukui Y, Uyeda TQP, Kitayama C, Inoué S (2000) How well can an amoeba climb? PNAS 97:10020–10025. doi:10.1073/pnas.97.18.10020

Giverso C, Grillo A, Preziosi L, Influence of nucleus deformability on cell entry into cylindrical structures. Biomech Model Mechanobiol, pp 1–22. doi:10.1007/s10237-013-0510-3

Gracheva ME, Othmer HG (2004) A continuum model of motility in ameboid cells. Bull Math Biol 66:167–193. doi:10.1016/j.bulm.2003.08.007

Hawkins RJ, Piel M, Faure-Andre G et al (2009) Pushing off the walls: a mechanism of cell motility in confinement. Phys Rev Lett 102:058103. doi:10.1103/PhysRevLett.102.058103

Hawkins RJ, Voituriez R (2010) Mechanisms of cell motion in confined geometries. Math Model Nat Phenom 5:84–105. doi:10.1051/mmnp/20105104

Heuzé ML, Collin O, Terriac E et al (2011) Cell migration in confinement: a micro-channel-based assay. Methods Mol Biol 769:415–434. doi:10.1007/978-1-61779-207-6_28

Holzapfel GA (2000) Nonlinear solid mechanics: a continuum approach for engineering, 1st edn. Wiley, London

Ilina O, Bakker G-J, Vasaturo A et al (2011) Two-photon laser-generated microtracks in 3D collagen lattices: principles of MMP-dependent and -independent collective cancer cell invasion. Phys Biol 8:015010. doi:10.1088/1478-3975/8/1/015010

Irimia D, Charras G, Agrawal N et al (2007) Polar stimulation and constrained cell migration in microfluidic channels. Lab Chip 7:1783–1790. doi:10.1039/b710524j

Irimia D, Toner M (2009) Spontaneous migration of cancer cells under conditions of mechanical confinement. Integr Biol (Camb) 1:506–512. doi:10.1039/b908595e

Jiang H, Sun SX (2013) Cellular pressure and volume regulation and implications for cell mechanics. Biophys J 105:609–619. doi:10.1016/j.bpj.2013.06.021

Larson RG (1998) The structure and rheology of complex fluids. Oxford University Press, USA

Lautenschlager F, Paschke S, Schinkinger S et al (2009) The regulatory role of cell mechanics for migration of differentiating myeloid cells. Proc Natl Acad Sci 106:15696–15701. doi:10.1073/pnas.0811261106

Lubliner J (2008) Plasticity theory. Dover Publications, New York

Mandel J (1972) Plasticité classique et viscoplasticité: course held at the Department of Mechanics of Solids, September-October, 1971. Springer, Berlin

McElwain DLS (1978) A re-examination of oxygen diffusion in a spherical cell with michaelis-menten oxygen uptake kinetics. J Theor Biol 71:255–263. doi:10.1016/0022-5193(78)90270-9

McElwain DLS, Callcott R, Morris LE (1979) A model of vascular compression in solid tumours. J Theor Biol 78:405–415. doi:10.1016/0022-5193(79)90339-4

McElwain DLS, Ponzo PJ (1977) A model for the growth of a solid tumor with non-uniform oxygen consumption. Math Biosci 35:267–279. doi:10.1016/0025-5564(77)90028-1

Mogilner A (2009) Mathematics of cell motility: have we got its number? J Math Biol 58:105–134. doi:10.1007/s00285-008-0182-2

Ngalim SH, Magenau A, Zhu Y et al (2013) Creating adhesive and soluble gradients for imaging cell migration with fluorescence microscopy. J Vis Exp. doi:10.3791/50310

Pesen D, Hoh JH (2005) Micromechanical architecture of the endothelial cell cortex. Biophys J 88:670–679. doi:10.1529/biophysj.104.049965

Phillipson M, Heit B, Colarusso P et al (2006) Intraluminal crawling of neutrophils to emigration sites: a molecularly distinct process from adhesion in the recruitment cascade. J Exp Med 203:2569–2575. doi:10.1084/jem.20060925

Provenzano PP, Inman DR, Eliceiri KW et al (2008) Collagen density promotes mammary tumor initiation and progression. BMC Med 6:11. doi:10.1186/1741-7015-6-11

Rangarajan R, Zaman MH (2008) Modeling cell migration in 3D. Cell Adhes Migr 2:106–109

Recho P, Putelat T, Truskinovsky L (2013) Contraction-driven cell motility. Phys Rev Lett 111:108102. doi:10.1103/PhysRevLett.111.108102

Recho P, Truskinovsky L (2013) An asymmetry between pushing and pulling for crawling cells. arXiv:1302.4002 [cond-mat, physics:physics, q-bio]

Righolt CH, Raz V, Vermolen BJ et al (2010) Molecular image analysis: quantitative description and classification of the nuclear lamina in human mesenchymal stem cells. Int J Mol Imaging. doi:10.1155/2011/723283

Rolli CG, Seufferlein T, Kemkemer R, Spatz JP (2010) Impact of tumor cell cytoskeleton organization on invasiveness and migration: a microchannel-based approach. PLoS ONE 5:e8726. doi:10.1371/journal.pone.0008726

Ronot X, Doisy A, Tracqui P (2000) Quantitative study of dynamic behavior of cell monolayers during in vitro wound healing by optical flow analysis. Cytometry 41:19–30

Sakamoto Y, Prudhomme S, Zaman MH (2011) Viscoelastic gel-strip model for the simulation of migrating cells. Ann Biomed Eng 39:2735–2749. doi:10.1007/s10439-011-0360-z

Schaub S, Bohnet S, Laurent VM et al (2007) Comparative maps of motion and assembly of filamentous actin and myosin II in migrating cells. Mol Biol Cell 18:3723–3732. doi:10.1091/mbc.E06-09-0859

Scianna M, Preziosi L (2013) Modeling the influence of nucleus elasticity on cell invasion in fiber networks and microchannels. J Theor Biol 317:394–406. doi:10.1016/j.jtbi.2012.11.003

Scianna M, Preziosi L, Wolf K (2013) A cellular potts model simulating cell migration on and in matrix environments. Math Biosci Eng 10:235–261

Stokes CL, Lauffenburger DA (1991) Analysis of the roles of microvessel endothelial cell random motility and chemotaxis in angiogenesis. J Theor Biol 152:377–403. doi:10.1016/S0022-5193(05)80201-2

Stokes CL, Lauffenburger DA, Williams SK (1991) Migration of individual microvessel endothelial cells: stochastic model and parameter measurement. J Cell Sci 99(Pt 2):419–430

Taber LA (2004) Nonlinear theory of elasticity: applications in biomechanics. World Scientific Pub Co Inc., Singapore

Taylor AM, Blurton-Jones M, Rhee SW et al (2005) A microfluidic culture platform for CNS axonal injury, regeneration and transport. Nat Methods 2:599–605. doi:10.1038/nmeth777

Tinevez J-Y, Schulze U, Salbreux G, et al. (2009) Role of cortical tension in bleb growth. PNAS pnas.0903353106. doi:10.1073/pnas.0903353106

Tozluoğlu M, Tournier AL, Jenkins RP et al (2013) Matrix geometry determines optimal cancer cell migration strategy and modulates response to interventions. Nat Cell Biol 15:751–762. doi:10.1038/ncb2775

Tranquillo RT, Lauffenburger DA (1987) Stochastic model of leukocyte chemosensory movement. J Math Biol 25:229–262

Tranquillo RT, Lauffenburger DA, Zigmond SH (1988) A stochastic model for leukocyte random motility and chemotaxis based on receptor binding fluctuations. J Cell Biol 106:303–309

Vaziri A, Lee H, Mofrad MRK (2006) Deformation of the cell nucleus under indentation: mechanics and mechanisms. J Mater Res 21:2126–2135. doi:10.1557/jmr.2006.0262

Wolf K, Alexander S, Schacht V et al (2009) Collagen-based cell migration models in vitro and in vivo. Semin Cell Dev Biol 20:931–941. doi:10.1016/j.semcdb.2009.08.005

Zaman MH, Kamm RD, Matsudaira P, Lauffenburger DA (2005) Computational model for cell migration in three-dimensional matrices. Biophys J 89:1389–1397. doi:10.1529/biophysj.105.060723

Zaman MH, Matsudaira P, Lauffenburger DA (2007) Understanding effects of matrix protease and matrix organization on directional persistence and translational speed in three-dimensional cell migration. Ann Biomed Eng 35:91–100. doi:10.1007/s10439-006-9205-6

Zaman MH, Trapani LM, Sieminski AL et al (2006) Migration of tumor cells in 3D matrices is governed by matrix stiffness along with cell-matrix adhesion and proteolysis. Proc Natl Acad Sci USA 103:10889–10894. doi:10.1073/pnas.0604460103

B. Detailed equations

B.1 Mechanical constitutive laws

The major constitutive laws of the model are described in Appendix A. However, the rheological models used in our simulations being slightly different, the basic constitutive laws for each cell region will be described here. The nucleoplasm and the cell cortex are described by the very same rheological model: only the mechanical parameters vary. Figure B.1 sets the rheological model used for the nucleoplasm (b) – which is the same as for the cell cortex – and for the lamina (a). The model used for the cytosol is depicted in Figure B.2.

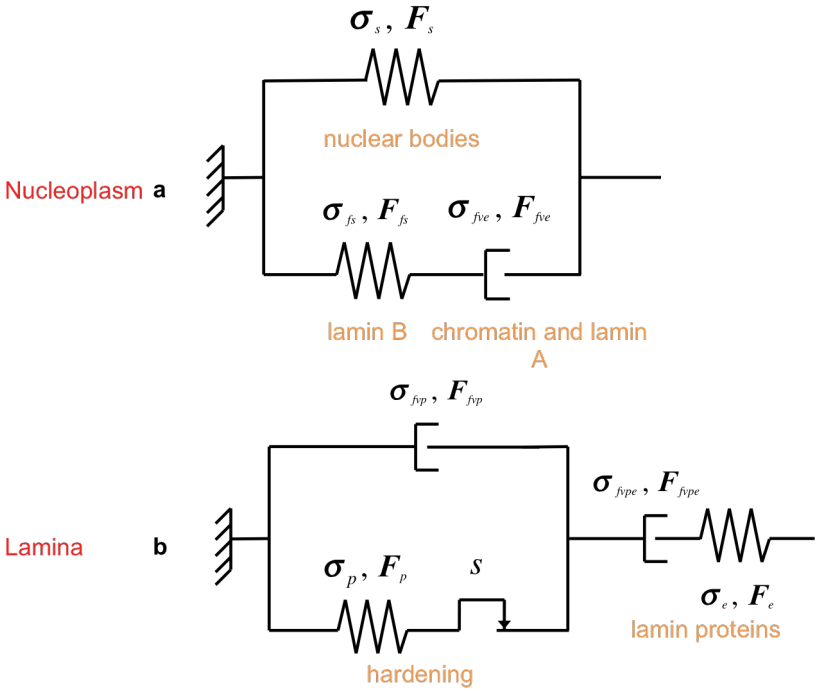

Figure B.1: Rheological models used to describe the nucleoplasm (**a**) and the lamina (**b**) behaviour

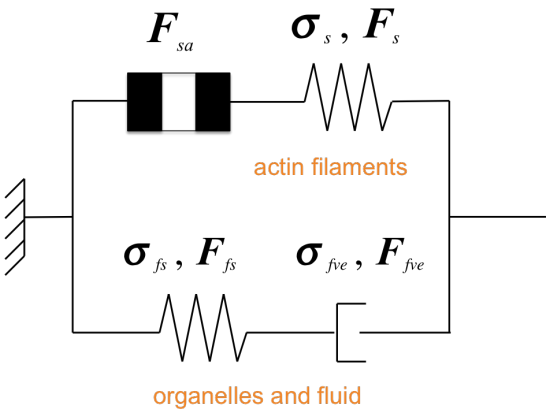

Figure B.2: Rheological model for the cytosol, comprising active deformation in the actin filaments.

In all our model, we use the definition of stress with the Lamé coefficients:

$$\boldsymbol{\sigma} = 2\mu\boldsymbol{\epsilon} + \lambda tr(\boldsymbol{\epsilon})\boldsymbol{I} \tag{B.1}$$

where $tr(\boldsymbol{A})$ defines the trace of the matrix $\boldsymbol{A}$ and with the Lamé coefficients defined as:

$$\lambda = \frac{E\nu}{(1-2\nu)(1+\nu)}$$
$$\mu = \frac{E}{2(1+\nu)}$$

where E is the Young modulus and ν is the Poisson ratio.

To model the stain in the dashpots, we use the deviatoric stress tensor that is defined, in 2D, as

$$\boldsymbol{\sigma^D} = \boldsymbol{\sigma} - \frac{1}{2}tr(\boldsymbol{\sigma}) \tag{B.2}$$

B.1.1 Viscoelastic constitutive laws

Using the notations from the rheological model, the basic equations governing our model is

$$\boldsymbol{\sigma}_{ve} = \boldsymbol{\sigma}_s + \boldsymbol{\sigma}_{fs} \tag{B.3}$$
$$\boldsymbol{\sigma}_s = \lambda_s(\boldsymbol{\epsilon} - \boldsymbol{\epsilon}_{cytosol,a}) + 2\mu_s(\boldsymbol{\epsilon} - \boldsymbol{\epsilon}_{cytosol,a}) \tag{B.4}$$
$$\boldsymbol{\sigma}_{fs} = \lambda_{fs}(\boldsymbol{\epsilon} - \boldsymbol{\epsilon}_{fve}) + 2\mu_{fs}(\boldsymbol{\epsilon} - \boldsymbol{\epsilon}_{fve}) \tag{B.5}$$

where $\boldsymbol{\epsilon}_{cytosol,a}$ is the active strain tensor defined as in Equation 4.2 and $\boldsymbol{\epsilon}_{fve}$ is the strain from the dashpot which is defined as follows.

$$\frac{\partial \boldsymbol{\epsilon}_{fve}}{\partial t} = \frac{\boldsymbol{\sigma^D}_{fs}}{\mu_{fve}} \tag{B.6}$$

where $\boldsymbol{\sigma^D}_{fs}$ is the deviatoric stress tensor and μ_{fve} is the viscosity of the dashpot.

B.1.2 Lamina constitutive laws

In the lamina, the constitutive laws are more complex since we introduced a plasticity. Then it reads:

$$\boldsymbol{\sigma}_{vep} = \boldsymbol{\sigma}_e = \lambda_e(\boldsymbol{\epsilon} - \boldsymbol{\epsilon}_{fvp} - \boldsymbol{\epsilon}_{fvpe}) + 2\mu_e(\boldsymbol{\epsilon} - \boldsymbol{\epsilon}_{fvp} - \boldsymbol{\epsilon}_{fvpe}) \tag{B.7}$$

where $\boldsymbol{\epsilon}_{fvpe}$ and $\boldsymbol{\epsilon}_{fvp}$ are defined as:

$$\frac{\partial \boldsymbol{\epsilon}_{fvpe}}{\partial t} = \frac{\boldsymbol{\sigma^D}_{vep}}{\mu_{fvpe}} \tag{B.8}$$

$$\frac{\partial \boldsymbol{\epsilon}_{fvp}}{\partial t} = \begin{cases} \frac{(mises-s)^2}{\mu_{fvp}} \frac{\boldsymbol{\sigma^D}_{vep}}{\sqrt{2mises}} & \text{if } mises \geq s \\ 0 & \text{if } mises < s \end{cases} \tag{B.9}$$

and mises refers to the mises criterion, which is defined by:

$$mises = \frac{1}{2}tr(\boldsymbol{\sigma^D}_p^2) \tag{B.10}$$

B.2 Self-governed chimneying migration mode

As detailed in Chapter 5, various conditions regulate the cell migration. These conditions are expressed by Heaviside functions as follows:

Name	**Description**	**Analytical expression**
$c_{f,init}$	Condition that is true when the frontal blebs are in their initial state (not elongated)	$h(-\epsilon_{lat,f} + 3 \times 10^{-12})$
$c_{f,ch}$	Condition that is true when the frontal blebs are pushing on the channel walls	$h(A_{ch,f} - 1 \times 10^{-13})$
$c_{f,exp}$	Condition that is true when the frontal blebs are expanding	$h(v_{blebbing,f})$
$c_{r,ch}$	Condition that is true when the rear blebs are pushing on the channel walls	$h(A_{ch,r} - 1 \times 10^{-13})$
$c_{m,init}$	Condition that is true when the cell body is in its initial state (not elongated)	$h(-\epsilon_{long,b} + 1 \times 10^{-12})$

Table B.1: Analytical expressions of the conditions used to define the self-regulated motion of the cell

where $\epsilon_{lat,f}$ is the lateral extension of the frontal bleb, $A_{ch,f}$ and $A_{ch,r}$ are the overlap area of the frontal and rear blebs respectively over the channel, $v_{blebbing,f}$ is the lateral velocity of the frontal bleb, and $\epsilon_{long,b}$ is the longitudinal extension of the cell body.

List of Tables

List of Figures

Bibliography

[Alberts B., 2002] Alberts B., Johnson A., L. J. R. M. R. K. W. P. (2002). *Molecular Biology of the Cell*. Garland Science.

[Allena, 2013] Allena, R. (2013). Cell migration with multiple pseudopodia: Temporal and spatial sensing models. *Bulletin of Mathematical Biology*, 75(2):288–316.

[Allena, 2014] Allena, R. (2014). Mechanical modelling of confined cell migration across constricted-curved micro-channels. *Molecular & cellular biomechanics: MCB*, 11(3):185–208.

[Allena and Aubry, 2012] Allena, R. and Aubry, D. (2012). A purely mechanical model to explore amoeboid cell migration. *Computer Methods in Biomechanics and Biomedical Engineering*, 15:14–16.

[Allena et al., 2013] Allena, R., Aubry, D., and Sharpe, J. (2013). On the mechanical interplay between intra- and inter-synchronization during collective cell migration: A numerical investigation. *Bulletin of Mathematical Biology*, 75(12):2575–2599.

[Aubry et al., 2014] Aubry, D., Thiam, H., Piel, M., and Allena, R. (2014). A computational mechanics approach to assess the link between cell morphology and forces during confined migration. *Biomechanics and Modeling in Mechanobiology*, 14(1):143–157.

[Caille et al., 2002] Caille, N., Thoumine, O., Tardy, Y., and Meister, J.-J. (2002). Contribution of the nucleus to the mechanical properties of endothelial cells. *Journal of Biomechanics*, 35(2):177–187.

[Charras and Paluch, 2008] Charras, G. and Paluch, E. (2008). Blebs lead the way: how to migrate without lamellipodia. *Nature Reviews Molecular Cell Biology*, 9(9):730–736.

[Columbia University Medical Center, 2009] Columbia University Medical Center (2009). Brain tumors: Gaining on a formidable foe. `http://www.cumc.columbia.edu/psjournal/archive/winter_2009/brain.html`. [Online; accessed 07-April-2015].

[Dahl et al., 2008] Dahl, K. N., Ribeiro, A. J. S., and Lammerding, J. (2008). Nuclear shape, mechanics, and mechanotransduction. *Circulation Research*, 102(11):1307–1318.

[Davidson et al., 2014] Davidson, P. M., Denais, C., Bakshi, M. C., and Lammerding, J. (2014). Nuclear deformability constitutes a rate-limiting step during cell migration in 3-d environments. *Cellular and Molecular Bioengineering*, 7(3):293–306.

[Deguchi et al., 2005] Deguchi, S., Maeda, K., Ohashi, T., and Sato, M. (2005). Flow-induced hardening of endothelial nucleus as an intracellular stress-bearing organelle. *Journal of Biomechanics*, 38(9):1751–1759.

[Deshpande, 2006] Deshpande, McMeeking, E. (2006). A bio-chemo-mechanical model for cell contractility. *Proceedings of the National Academy of Sciences*, 103(38):14015–14020.

[Friedl et al., 2011] Friedl, P., Wolf, K., and Lammerding, J. (2011). Nuclear mechanics during cell migration. *Current Opinion in Cell Biology*, 23(1):55–64.

[Geng et al., 2011] Geng, T., Zhan, Y., Wang, J., and Lu, C. (2011). Transfection of cells using flow-through electroporation based on constant voltage. *Nature Protocols*, 6(8):1192–1208.

[Goldman Lab, 2014] Goldman Lab (2014). About lamins. `http://labs.feinberg.northwestern.edu/goldman/intro_lamins.htm`. [Online; accessed 05-March-2015].

[Guilak et al., 2000] Guilak, F., Tedrow, J. R., and Burgkart, R. (2000). Viscoelastic properties of the cell nucleus. *Biochemical and Biophysical Research Communications*, 269(3):781–786.

[Hawkins et al., 2009] Hawkins, R. J., Piel, M., Faure-Andre, G., Lennon-Dumenil, A. M., Joanny, J. F., Prost, J., and Voituriez, R. (2009). Pushing off the walls: A mechanism of cell motility in confinement. *Physical Review Letters*, 102(5):058103.

[Lammerding, 2011] Lammerding, J. (2011). Mechanics of the nucleus. *Comprehensive Physiology*, 1(2):783–807.

[Lim et al., 2013] Lim, F. Y., Koon, Y. L., and Chiam, K.-H. (2013). A computational model of amoeboid cell migration. *Computer Methods in Biomechanics and Biomedical Engineering*, 16(10):1085–1095.

[Lorentzen et al., 2011] Lorentzen, A., Bamber, J., Sadok, A., Elson-Schwab, I., and Marshall, C. J. (2011). An ezrin-rich, rigid uropod-like structure directs movement of amoeboid blebbing cells. *Journal of Cell Science*, 124(8):1256–1267.

[Lämmermann and Sixt, 2009] Lämmermann, T. and Sixt, M. (2009). Mechanical modes of 'amoeboid' cell migration. *Current Opinion in Cell Biology*, 21(5):636–644.

[Malawista et al., 2000] Malawista, S. E., de Boisfleury Chevance, A., and Boxer, L. A. (2000). Random locomotion and chemotaxis of human blood polymorphonuclear leukocytes from a patient with leukocyte adhesion deficiency-1: Normal displacement in close quarters via chimneying. *Cell Motility and the Cytoskeleton*, 46(3):183–189.

[MBI - National University of Singapore, 2014] MBI - National University of Singapore (2014). Nucleus - MBInfo wiki. `http://www.mechanobio.info/topics/cellular-organization/go-0005634`. [Online; accessed 03-March-2015].

[Mélina L Heuzé, 2011] Mélina L Heuzé, O. C. (2011). Cell migration in confinement: a micro-channel-based assay. *Methods in molecular biology (Clifton, N.J.)*, 769:415–34.

[Nava et al., 2014] Nava, M. M., Raimondi, M. T., and Pietrabissa, R. (2014). Bio-chemo-mechanical models for nuclear deformation in adherent eukaryotic cells. *Biomechanics and Modeling in Mechanobiology*, 13(5):929–943.

[Pablo Vargas, 2014] Pablo Vargas, E. T. (2014). Study of Cell Migration in Microfabricated Channels. *Journal of visualized experiments : JoVE*, (84).

[Pajerowski et al., 2007] Pajerowski, J. D., Dahl, K. N., Zhong, F. L., Sammak, P. J., and Discher, D. E. (2007). Physical plasticity of the nucleus in stem cell differentiation. *Proceedings of the National Academy of Sciences of the United States of America*, 104(40):15619–15624.

[Paluch and Raz, 2013] Paluch, E. K. and Raz, E. (2013). The role and regulation of blebs in cell migration. *Current Opinion in Cell Biology*, 25(5):582–590.

[Patricia M Davidson, 2013] Patricia M Davidson, J. L. (2013). Broken nuclei - lamins, nuclear mechanics, and disease. *Trends in cell biology*.

[Pederson and Marko, 2014] Pederson, T. and Marko, J. F. (2014). Nuclear physics (of the cell, not the atom). *Molecular Biology of the Cell*, 25(22):3466–3469.

[Rowat et al., 2005] Rowat, A., Foster, L., Nielsen, M., Weiss, M., and Ipsen, J. (2005). Characterization of the elastic properties of the nuclear envelope. *Journal of the Royal Society Interface*, 2(2):63–69.

[Rowat et al., 2006] Rowat, A. C., Lammerding, J., and Ipsen, J. H. (2006). Mechanical properties of the cell nucleus and the effect of emerin deficiency. *Biophysical Journal*, 91(12):4649–4664.

[Swift and Discher, 2014] Swift, J. and Discher, D. E. (2014). The nuclear lamina is mechano-responsive to ECM elasticity in mature tissue. *Journal of Cell Science*, page jcs.149203.

[Ujihara et al., 2011] Ujihara, Y., Nakamura, M., and Wada, S. (2011). *A Mechanical Cell Model and Its Application to Cellular Biomechanics*. INTECH Open Access Publisher.

[Vaziri et al., 2007] Vaziri, A., Gopinath, A., and Deshpande, V. S. (2007). Continuum-based computational models for cell and nuclear mechanics. *Journal of the Mechanics of Materials and Structures*, 2:1169–1192.

[Wilson et al., 2013] Wilson, K., Lewalle, A., Fritzsche, M., Thorogate, R., Duke, T., and Charras, G. (2013). Mechanisms of leading edge protrusion in interstitial migration. *Nature Communications*, 4.